# CLASSIFICATION OF CORTICAL TMS LOCATIONS ACCORDING TO MULTIPLE UPPER LIMB MUSCLE RESPONSES

Vesa Onnia

Master`s Thesis in Biomechanics
Faculty of Sport and Health Sciences
University of Jyväskylä
Autumn 2023

**FOREWORD**

This thesis was conducted at Functional Brain Laboratory of Faculty of Sport and Health Sciences at University of Jyväskylä.

I would like to thank associate professor PhD Harri Piitulainen for interesting topic and his patience when supervising me through this project. I also want to thank MSc Joona Juurakko who did an enormous amount of work when guiding me into the magical world of TMS measurements. With Joona I had many scientific and not so scientific discussions which helped me a lot to finish this thesis. Also, Chief Laboratory Technician Sakari Vekki deserves big thanks. Sakari always helped without asking with problems related to measuring equipment and software.

I would also like to thank all those who dared to become test subjects for this study. Without them this work would not have been possible.

Last but not least, I would like to thank my family: my wife, my parents, my wife's parents and my sister's family for their support. My dear wife in particular deserves the biggest thanks. She patiently fed me and took care of our home so that I could concentrate intensely on my studies and this thesis. So, this degree is as much of her achievement as mine.

Jyväskylä 5.8.2023

Vesa Onnia

## TIIVISTELMÄ

Onnia, V. 2023. Useiden yläraajan lihasvasteiden luokittelu kortikaalisten TMS-lokaatioiden mukaan. Jyväskylän yliopisto. Biomekaniikan pro gradu –tutkielma. 116 sivua, 1 liite.

**Johdanto.** Motorisen aivokuoren alueita on aiemmin kartoitettu siltä kannalta, että yksittäisillä lihaksilla on aivokuorella edustusalueita, joista niitä kontrolloidaan. Vähitellen on ymmärretty, että tällaiset edustusalueet ovat päällekkäisiä. Tämän on oletettu olevan osoitus lihasten välisistä synergioista, sekä motorisen aivokuoren toiminnallisista alueista, joista toimintoja ohjataan. Motorisen aivokuoren kartoitukseen liittyvä tutkimus onkin menossa toiminnalliseen suuntaan ns. toimintakarttojen löytämiseksi. Tällaisessa tutkimuksessa olisi edullista, jos tahdonalaisen liikkeen perusteella mitattuja tekijöitä voitaisiin liittää spesifeihin motorisen aivokuoren lokaatioihin. Tämä vaatisi esimerkiksi mahdollisuutta liittää transkraniaalisen magneettisen stimulaation (TMS) indusoimat motoriset herätepotentiaalit (MEP) tahdonalaisesta liikkeestä tallennettuun elektromyografiaan (EMG). Ennen tätä pitäisi tietää, kuinka tarkasti motorisen aivokuoren eri alueet voidaan erottaa toisistaan näiltä alueilta stimuloitujen MEP–signaalien perusteella. Tätä tarkoitusta varten tämä opinnäytetyö käsittelee useista TMS–menetelmää käyttäen stimuloiduista yläraajan lihaksista tallennettujen MEP–vasteiden luokittelua niitä vastaavien aivokuoren sijaintien mukaisiin luokkiin. Myös erilaisten lihasyhdistelmien vaikutusta luokittelutarkkuuteen tutkittiin.

**Menetelmät.** Tutkimuksen tulokset saavutettiin mittaamalla seitsemää vapaaehtoista koehenkilöä, joista jokainen osallistui yhteen mittausistuntoon. Abductor pollicis breviksen, flexor carpi radialiksen ja biceps brachiin pitkän pään hotspot–pisteitä stimuloitiin TMS-sekvensseillä intensiteetillä, joka oli 120% lepotilan motorisesta kynnyksestä (rMT). Ärsykkeiden aiheuttamat MEP–vasteet mitattiin 16 yläraajan lihaksesta. Saatua MEP–raakadataa käytettiin monikerroksisten perseptroniverkko– (MLP) luokittimien rakentamiseen ja testaamiseen. Luokittelutarkkuuden perusteella arvioitiin luokittelun tehokkuutta ja eri lihasyhdistelmien kykyä erotella MEP–vasteet hotspot–lokaatioiden muodostamiin luokkiin.

**Tulokset.** Korkeimpien luokittelutarkkuuksien mediaani oli 0.91 stimulusintensiteetillä ja vastaava parhaiden luokittelutulosten antaneiden lihasyhdistelmäkokojen mediaani oli 7. Tilastollisesti merkitsevästi korkeimman luokitustarkkuuden antaneet lihasyhdistelmät olivat yksilöllisiä sekä yhdistelmän koon että yhdistelmään sisältyvien lihasten suhteen.

**Johtopäätökset.** Luokittelu onnistuu hyvin, kun luokkina toimivat lihasten hotspot–pisteet motorisella aivokuorella valitaan tässä tutkimuksessa esitetyllä tavalla. Yksittäisten lihasyhdistelmien, jotka antoivat korkeimman luokitustarkkuuden, arvioitiin olevan osoitus hermo–lihaskontrollin yksilöllisyydestä, vaikka näillä ei olekaan yhtä selvää yhteyttä lihassynergioihin, kuin aikaisemmissa tutkimuksissa päällekkäisistä lihasten edustusalueista on arvioitu. Lisätutkimuksia tarvitaan sen selvittämiseksi, kuinka lähellä toisiaan motorisen aivokuoren stimuloidut pisteet voivat olla, jotta luokittelu edelleen onnistuisi.



Avainsanat: sensorimotorinen kontrolli, transkraniaalinen magneettistimulaatio, motorinen herätepotentiaali, luokittelu, monikerroksinen perseptroniverkko, toiminnallinen aivokuoren kartoitus

## ABSTRACT

Onnia, V. 2023. Classification of cortical TMS locations according to multiple upper limb muscle responses. University of Jyväskylä. Master's thesis in Biomechanics. 116 pages, 1 appendix.

**Introduction.** In the cerebral cortex, areas of the motor cortex have previously been mapped from the point of view that individual muscles have specific areas in the cortex from which they are controlled. It has gradually been understood that the muscle representation areas on the cortex overlap. This has been assumed to indicate individual synergies between muscles and that the motor cortex contains functional areas from which complex actions are controlled. Thus, research related to the mapping of the motor cortex is going in a functional direction aiming to find so–called action maps. For this kind of research, it would be advantageous if different factors measured from voluntary movement could be connected to specific locations of the motor cortex. This would require, for example, to be able to connect motor evoked potentials (MEP) induced by transcranial magnetic stimulation (TMS) to the electromyography (EMG) recorded from voluntary movement. Before this, one should know how accurately different areas of the motor cortex can be separated from each other based on the MEP signals stimulated from these areas. For this purpose, this thesis deals with the classification of cortical stimulus locations according to MEP patterns recorded from multiple upper–limb muscles induced by TMS. The effect of different muscle combinations on classification accuracy was also investigated.

**Methods.** Results in this study were achieved by measuring seven volunteers, who participated in one measurement session. The hotspot locations of the abductor pollicis brevis, flexor carpi radialis and biceps brachii's long head were stimulated by TMS sequences at 120% of resting motor threshold (rMT) stimulus intensity. The MEPs elicited by the stimuli were recorded in 16 muscles of the upper limb. The obtained raw MEP data was used to build and test multilayer perceptron (MLP) classifiers. Based on the classification accuracy, the effectiveness of the classification and the ability of different muscle combinations to separate MEP patterns into the classes formed by the hotspot locations were evaluated.

**Results.** The median of the highest estimated mean classification accuracy was 0.91 and the corresponding median of combination size was 7. The muscle combinations that gave statistically significantly the highest classification accuracy were unique in terms of both the combination size and the muscles included in the combination.

**Conclusion.** The classification succeeds well when the muscle hotspots on the motor cortex, which act as classes, are selected as presented in this study. Individual muscle combinations giving the highest classification accuracies were assumed to indicate the individual versatility of neuromuscular control, although there is not as clear connection to muscle synergies as previous studies have established. Further studies are needed to clarify how close to each other the stimulated points of the motor cortex can be for the classification to be successful.

Key words: sensorimotor control, transcranial magnetic stimulation, motor evoked potential, classification, multilayer perceptron, functional brain mapping

**ABBREVIATIONS**

| | |
|---|---|
| AD | deltoid anterior |
| ADM | abductor digiti minimi |
| aMT | active motor threshold |
| APB | abductor pollicis brevis |
| ATP | adenosinetriphosphate |
| A/D | analog/digital |
| B | brachioradialis |
| BBs | biceps brachii short head |
| BBl | biceps brachii long head |
| $C_i$ | $i^{th}$ class |
| CMAP | compound muscle action potential |
| CoG | center of gravity |
| $D$ | number of inputs or length of the input vector |
| $E$ | error function |
| $e$ | exponential function |
| ECU | extensor carpi ulnaris |
| EDC | extensor digitorum communis |
| EMG | electromyografia |
| FCU | flexor carpi ulnaris |
| FCR | flexor carpi radialis |
| FDI | $1^{st}$ dorsal interosseus |
| FDS | flexor digitorum superficialis |
| FEM | finite element method |
| $f_i$ | activation function of the $i^{th}$ unit in the network |
| $H$ | hypotheses class, also amount of hidden units |
| $h$ | set of hypotheses belonging to hypothesis class |
| ICC | interclass correlation coefficient |
| ISI | interstimulus interval |
| $K$ | amount of classes |
| LD | deltoid lateral |
| LDA | linear discriminant analysis |

| | |
|---|---|
| lmTMS | landmark navigated transcranial magnetic stimulation |
| MEP | motor evoked potential |
| MLP | multilayer perceptron |
| MRI | magnetic resonance imaging |
| MT | motor threshold |
| mV | milliVolt |
| MVC | maximum voluntary contraction |
| M1 | primary motor cortex |
| nTMS | neuronavigated transcranial magnetic stimulation |
| rMT | resting motor threshold |
| sEMG | surface electromyografia |
| p | probability under the assumption of no effect or no difference in statistical test |
| PCA | principal component analysis |
| PD | deltoid posterior |
| $\boldsymbol{r}$ | class label vector |
| $r_i$ | $i^{\text{th}}$ component of the class label vector |
| S1 | primary sensory cortex |
| TBlat | triceps brachii lateral head |
| TBmed | triceps brachii medial head |
| TES | transcranial electrical stimulation |
| TMS | transcranial magnetic stimulation |
| UT | upper threshold |
| $\boldsymbol{w}$ | weight vector |
| $w_{ij}$ | weight connecting unit $i$ to unit $j$ |
| $X$ | training data set |
| $\boldsymbol{x}$ | training data or input vector |
| $x_i$ | $i^{\text{th}}$ input or $i^{\text{th}}$ component of training data vector |
| $y_i$ | $i^{\text{th}}$ component of the output vector |
| $\boldsymbol{z}$ | output vector of the hidden layer |
| $z_i$ | output of the $i^{\text{th}}$ unit in the hidden layer |
| α | statistical significance level |
| µV | microVolt |
| ρ | Spearman's correlation coefficient |

**CONTENTS**

# 1 INTRODUCTION

Our physical body is our interface to the world we are living in. It is therefore understandable that all structures of the nervous system are to some extent related to the regulation of interaction of the thick and thin filaments in muscle cells being the final output of the motor system. Thus, it is also understandable why the cooperation of these systems is very complex and understanding it is still a challenge and the subject of continuous research.

In the cerebral cortex, areas of the motor cortex have previously been mapped from the point of view that individual muscles have a specific area or areas in the cortex from which they are controlled, e.g., Wassermann et al. (1992). With the development of knowledge and technology, it has gradually been understood that the muscle representation areas on the cortex overlap (Melgari et al. 2008; Tardelli et al. 2022). This has been assumed to indicate individual synergies between muscles. These studies have generally used transcranial magnetic stimulation (TMS) to activate cortical neurons and electromyography (EMG) to measure the muscle activity resulting from this activation, shown as motor evoked potentials (MEP). Since then, research results have been obtained according to which it can be assumed that the motor cortex contains functional areas from which not only individual muscles are controlled, but complex actions (Brecht et al. 2004; Graziano et al. 2002; Graziano 2016; Harrison et al. 2012). Currently, research related to the mapping of the motor cortex is going in a functional direction, where the aim is to find so–called action maps.

For this kind of functional organization of the motor cortex to be effectively studied in humans, it would be advantageous if different factors measured from voluntary movement could be connected to areas of the motor cortex. So far, stimulus locations on the cortex have been directly connected to the responses they produce. When using TMS, these responses are usually MEPs and difficult to associate with voluntary actions. To connect factors measured from voluntary movement, e.g., EMG signals, to specific points in the motor cortex, it should be possible to develop methods that could predict the locations of the motor cortex involved in the control of voluntary actions. This would require to be able to connect the MEPs induced by TMS to the EMG signals measured from voluntary movement. This could happen by developing similarity measures for MEP and EMG signals, through which the cortical origin of the signal measured from voluntary movement could be predicted. Before this, one should get a clear picture of how accurately different areas of the motor cortex can be separated from each

other based on the MEP signals stimulated from these areas. This thesis represents such research. It deals with the classification of cortical stimulus locations according to their corresponding MEP patterns induced by TMS.

To the author's knowledge, a similar classification has not been made, or at least the results have not been published. In previous classification studies, EMG signals have been classified into categories according to different pathologies or voluntary movements performed by the subject (Hudgins et al. 1993; Kocer 2010; Phinyomark 2013). However, the EMG signal is continuous, whereas the MEP signals induced by TMS are transient. In addition to this, the activation of corticocortical and corticospinal circuits induced by TMS is external and artificial compared to the activation of the same structures by natural voluntary movement. For these reasons, a setup was created in this study, with which it was possible to investigate, on a rough level, whether it is possible to classify stimulus locations in the motor cortex according to the corresponding MEP patterns recorded from several muscles of the upper limb. At the same time, the effect of different muscle combinations on classification accuracy were also investigated. The results of this work can be used in the future when functional mapping studies of the motor cortex are planned.

The starting point of this kind of research is to understand how MEPs recorded in the musculature induced by TMS are generated and what kind of neural systems are influencing this. Therefore, Chapter 2 deals with sensorimotor control to the extent necessary, and Chapter 3 deals with the principles of TMS. Chapter 4 discusses the functional research of the motor cortex and the factors that influence the design of research settings. Chapter 5 deals with EMG, which is the method used in this study to record muscle activity. Chapter 6 focuses on classification and especially multilayer perceptron (MLP), the classifier structure used in this work. In Chapter 7, this study and research questions are justified and presented. Chapter 8 presents the methods used in the research and Chapter 9 gives the results. Chapters 10 and 11 provide the discussion and conclusions of the results, respectively.

# 2 SENSORIMOTOR CONTROL

Motor control of the muscles results from the operation of a hierarchical control system. The higher levels of this hierarchy create global plans and goals, while the lower levels are responsible for implementing those goals. This hierarchy is also represented by the division of motion regulation into voluntary, rhythmic, and reflexive control. Of these, voluntary movement occurs as a result of conscious regulation, whereas reflex control is a stereotypical response to specific stimuli. Rhythmic or cyclic regulation contains both voluntary and involuntary components. (Kandel et al. 2021, 715) This division is partly artificial. In our own opinion, our movement may be entirely based on our own decision, when in fact no voluntary act could happen smoothly if its components were not implemented as a result of the functions of an involuntary control system. Based on conscious goals, higher levels of sensorimotor control create motor plans and commands that lower levels of the system adapt to complex muscle synergies appropriate to the current state of the environment and the system itself. Thus, the same motor command from higher levels of the hierarchy may produce different variations of movements depending on the current context. (Scott 2016) In this way, the sensorimotor control system is capable of creating meaningful movement in the current context. When motor responses are induced by TMS, knowledge of the regulatory system is important to understand which factors influence the responses measured from the musculature, i.e., in the case of this work, the input to the classifier. Therefore, this chapter presents the known structure and function of the sensorimotor control system.

## 2.1 Bioelectrochemical signals as information carriers

The following Chapters 2.2–2.5 describe the body's sensorimotor system, which receives various stimuli, processes them, and produces responses based on them, which can be, for example, movements caused by muscle activity. In order for this to happen, there must be some mechanism to transport the information. In our nervous system, this is the bioelectrochemical signals, whose operating principles are roughly explained below.

The function of bioelectrochemical signals is based on $K^+$, $Cl^-$, $Na^+$ and $Ca^{2+}$ ions and corresponding membrane proteins, ion channels, on the cell membrane. These channels maintain and change the ion concentration differences across the cell membrane, thus controlling the voltage across the membrane. Such channels exist in receptor cells specialized

for the reception of various stimuli, such as mechanical, auditory, visual, or chemical stimuli, in nerve-nerve and nerve-muscle junctions, and in nerve fibers. In the case of receptor cells, a specific stimulus changes the state of the ion channels, creating a receptor potential, while in nerve-nerve and nerve-muscle junctions various neurotransmitters transported from cell to cell affect the function of the channels, creating a so-called synaptic potential. (Kandel et al. 2021, 191–198; Purves et al. 2018, 33–34, 61) Both of these potentials are local and do not travel very far. They just announce something happening at their origin. In addition to these, there is a third form of bioelectrochemical activity on the cell membrane, an action potential, which carries the signal over long distances along the membrane. In the action potential, the action of ion channels causes an all-or-none type of potential difference propagating in a certain direction along the nerve fiber having a certain amplitude. Thus, the message is not encoded in the amplitude of the action potential but in the frequency of them. (Kandel et al. 2021, 211–212; Purves et al. 2018, 34–35, 55–60) It is also noteworthy that in the nervous system, the messages conveyed by the action potentials are interpreted according to the path along which the signal travels. Two exactly same action potential patterns conducted along two trajectories can result in very different interpretations. (Kandel et al. 2021, 68; Purves et al. 2018, 16)

It is also worth noting that the signals delivered can change the membrane potential in nerve-nerve and nerve-muscle junctions in a more negative or more positive direction depending on the receptors (ion channels) of the receiving cell. In the former case the connection is called an inhibitory coupling and, in the latter, an excitatory coupling. Thus, the signal might remain the same, but the connection between the transmitting and receiving cell determines the effect of the signal on the receiver. An action potential is generated in a receiving nerve or muscle cell at a given time point if the sum of inhibitory and excitatory potential changes exceeds a threshold value. In this way, the neuron–neuron and neuron–muscle connections form circuits whose outputs integrate with signals traveling in pathways. The pathways, in turn, connect larger network entities to each other, creating a regulatory system that makes the body function to achieve a particular goal. (Kandel et al. 2021, 68, 74; Purves et al. 2018, 99–101)

### 2.2 Cortical structures

The highest-level functions representing the sensorimotor control system are located in the cerebral cortex surrounding the sub-cortical parts of the brain, which, in turn, are located as an extension of the spinal cord, see Figure 1. The cerebral cortex can be divided into different areas

according to the functions performed by each area. Roughly divided, these regions are the frontal, parietal, temporal and occipital lobe. (Kandel et al. 2021, 10–16) Although all cortical areas are involved in motor control somehow, only areas most closely related to this are discussed in this section. These areas are the primary motor cortex and pre-motor area of the frontal lobe, and the superior and posterior areas of the parietal lobe.

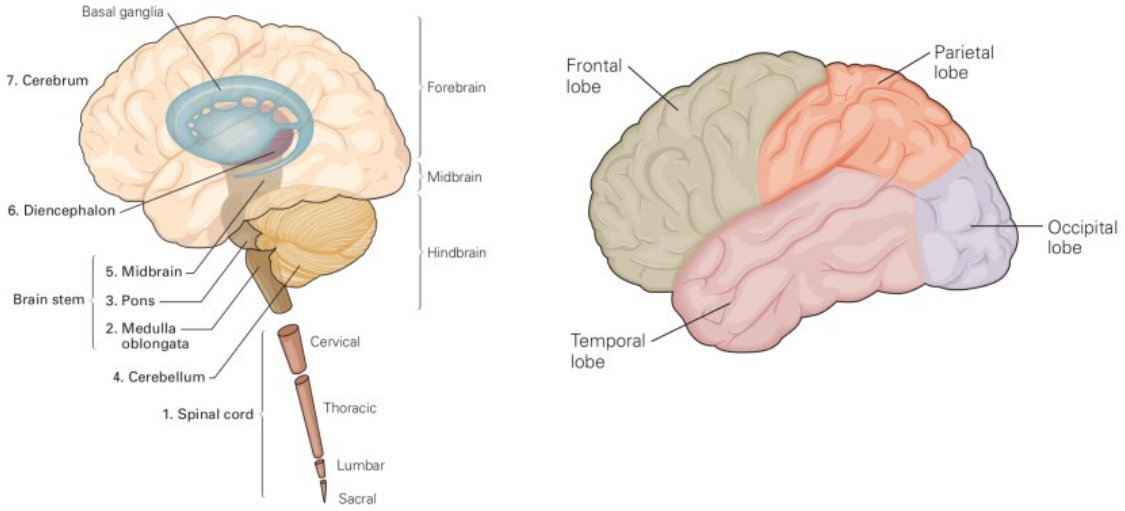


FIGURE 1. (Left) The divisions of the central nervous system. (Right) Major lobes of the cerebral cortex. (Adapted from Kandel et al. 2021)

The primary sensory cortex (S1) as well as other areas of the superior parietal lobe receive sensory information from the skin and muscle receptors. Here, the sensory information received from different areas of the body form a somatotopic map representing different parts of the body, see Figure 2. Other areas of the superior parietal lobe integrate information about individual joints and the position of body segments relative to the rest of the body. Regions of the superior parietal cortex are major sources of proprioceptive and tactile information transmitted to other areas of the brain. In the posterior parietal cortex, in turn, multiple sensory sources are combined, including visual and vestibular signals. The neurons here are therefore often multimodal. In this area, representations of the environment and the body itself and their interrelationships are formed. (Kandel et al. 2021, 84, 824) This information is essential when planning activities appropriate to the current state of the body and the environment. Thus, the functional regions of the posterior parietal cortex as well as S1 connect with the motor areas of the frontal lobe. (Borich et al. 2015; Chao et al. 2015; Kandel et al. 2021, 823–827; Kertzman et al. 1997)

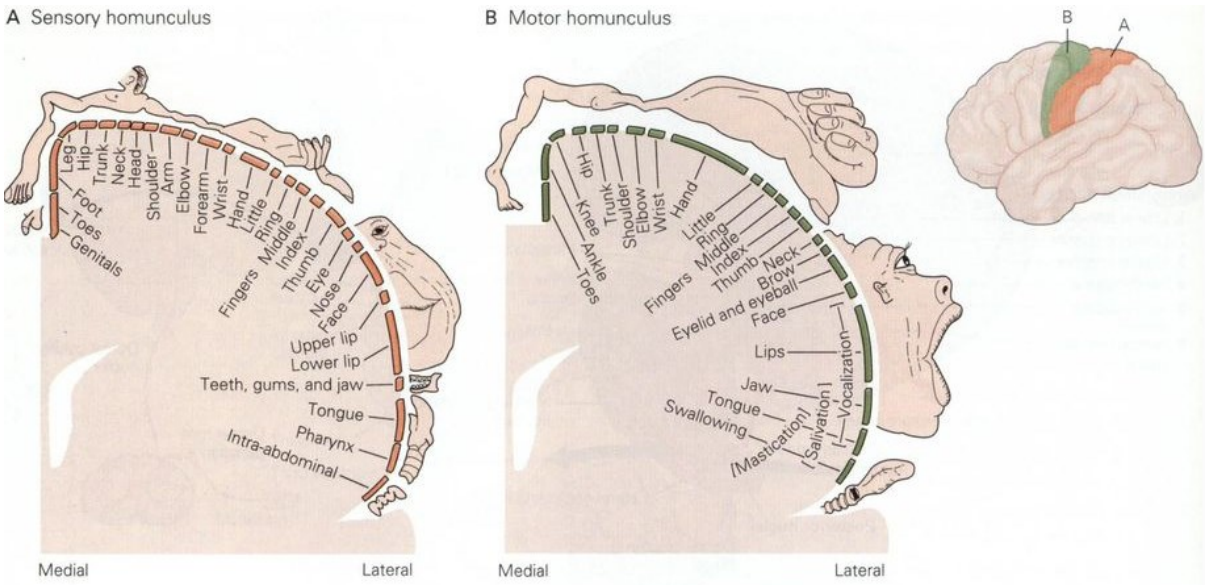


FIGURE 2. Somatotopic maps of the primary sensory (left A) and motor (right B) cortex. (From Kandel et al. 2021)

In the frontal lobe, in turn, movement is planned, and motor commands are transmitted along the pyramidal pathway to the brainstem and spinal cord. These parts of the pyramidal pathway are called the corticobulbar and corticospinal pathways, respectively. (Kandel et al. 2021, 819–821, 828–836) It should be noted that pyramidal pathway includes also tracts originating from somatosensory areas in the parietal lobe (Moreno–López et al. 2016; Kandel et al. 2021, 819–821). The pre-motor regions located in the frontal lobe are functionally divided into different regions (Lorey et al. 2014). Neurons in these regions have been interpreted as participating in changes in action, plan, and strategy, as well as in the organization of movement cycles. Many of the neurons in these areas respond to a specific sensory stimulus before the corresponding movement. (Thut et al. 2000; Kandel et al. 2021, 828 835)

On the posterior side of the pre-motor cortex is the primary motor cortex (M1). Neurons here, like neurons at S1, form a fine-grained somatotopic map so that those areas of the body where more precise control of movement is required are more represented, see Figure 2. (Kandel et al. 2021, 841) Most of M1's upper motoneurons projecting into the spinal cord and brainstem innervate the lower motoneurons through the spinal interneurons, but some of the neurons at M1 form monosynaptic connections with the lower motoneurons (Kandel et al. 2021, 841; Quallo et al. 2012). M1 plays an important role in the generation of motor commands and thus in the regulation of spinal activity (e.g., regulation of the timing and intensity of muscle activity) (Kandel et al. 2021, 841–852; Sergio et al. 2005).

## 2.3 Subcortical structures

In the context of motor control, subcortical structures perform tasks related to action selection, signal flow regulation, movement fine-tuning as well as regulation of balance, posture, and locomotion. They also take part in cognitive functions. This section reviews the role of these structures underlying the cerebral cortex, see Figure 1.

### 2.3.1 Basal ganglia

Before executing the motor commands, the appropriate actions for the situation must be chosen. According to the current understanding, such tasks are carried out by the basal ganglia. These are a group of sub-cortical structures consisting of three parts: the input (caudate, putamen, and substantia nigra pars compacta) and output nuclei (substantia nigra pars reticulata and internal globus pallidus) and one internal nucleus (external globus pallidus). (Humphries et al. 2006; Kandel et al. 2021, 933–935; Redgrave et al. 1999) Inputs and outputs of basal ganglia are illustrated in Figure 3.

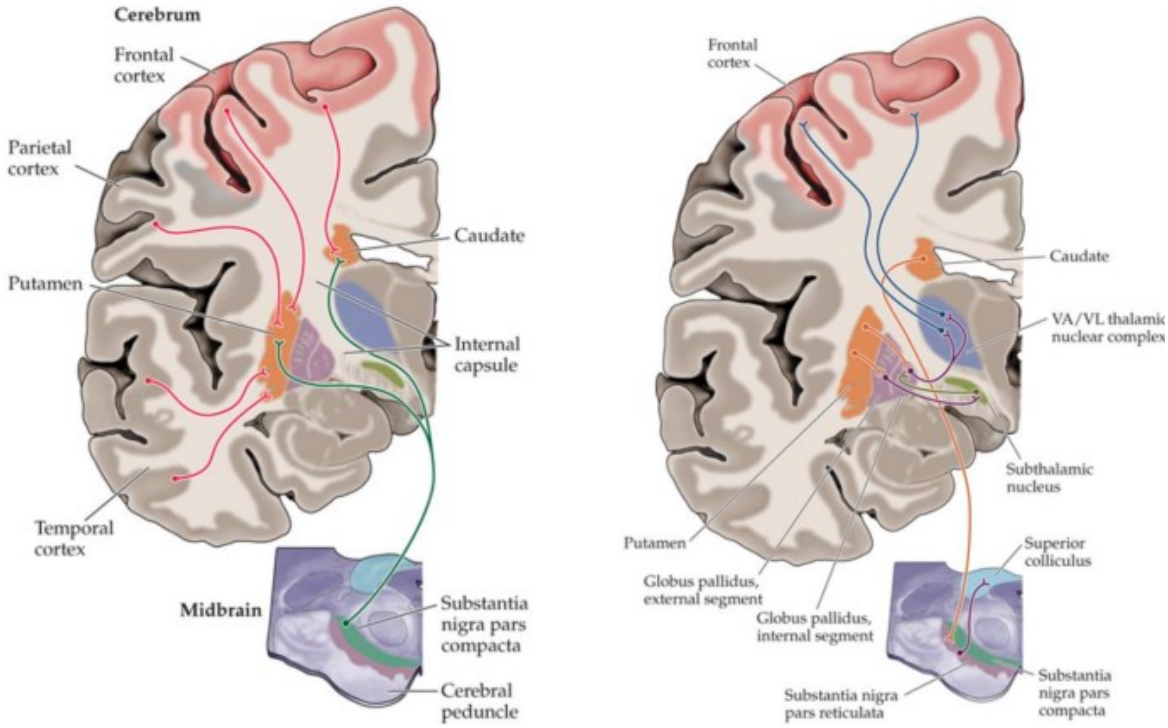


FIGURE 3. Anatomical organization of the inputs to the basal ganglia (left), and outputs as well as internal nucleus of the basal ganglia (right). (From Purves et al. 2018)

The basal ganglia receive their input from the cerebral cortex, the limbic area and through the thalamus from the brainstem. The inputs are thought to represent options for different behaviors that, in the current context, compete for what would be the best. The basal ganglia transmit their output to the brainstem and, through the thalamus, to the cortical areas that originally produced the input. Outputs are often collateral, mediating multiple brain structures working together toward a certain goal. The structures of the basal ganglia form, together with the structures of the cortex, brainstem, and the thalamus, so called reentrant circuits, which correspond to different behavioral options. (Kandel et al. 2021, 937–940; Redgrave et al. 1999) Any part of these circuits can receive regulatory signals from outside the circuit that determine which circuit will be the winner. When the winning behavior leads to the achievement of the goal, this produces a sensitizing reward signal to some part of the reentrant circuit increasing the probability of the behavior to occur in the future. (Kandel et al. 2021, 942–946; Redrgave et al. 1999)

### 2.3.2 Thalamus

The thalamus, already mentioned, is a structure located in the diencephalon, see Figure 1, containing more than 50 nuclei. It relays signals from sensory receptors to the primary sensory areas of the cortex as well as motor signals from the basal ganglia and cerebellum to the motor areas of the cortex. (Kandel et al. 2021, 82–84; Kim et al. 2017) In addition to these, the thalamus receives signals from several other areas in the brain and spinal cord and relays them to the cortex and brainstem (Kandel et al. 2021, 82–84; Latchoumane et al. 2017; Ren et al. 2018; Rovó et al. 2012; Varela et al. 2014; Zhao et al. 2021). It acts not only as a relay of signals, but also regulates their flow, preventing and enhancing the transmission of information in a manner appropriate to the current context (Kandel et al. 2021, 82–84; Schmitt et al. 2017; Whitmire et al. 2016). It is also important to note that the thalamus receives feedback signals from the areas of the cortex that are the target of its outputs, as well as regulatory signals from the brainstem. These are thought to regulate the thalamic processes themselves. (Crandall et al. 2015; Kandel et al. 2021, 82–84; Whitmire et al. 2016)

### 2.3.3 Cerebellum

The cerebellum comprises only 10% of the brain in terms of volume but contains more than half of the neurons in the brain (Kandel et al. 2021, 908). The structure receives its input from

different parts of the brain and spinal cord, passing its output back to the brain (Bonassi et al. 2021; Xue et al. 2021). Like basal ganglia, the same microcircuit structure is repeated from input to output, from which it has been concluded that the cerebellum performs the same computational procedures on different inputs (Kandel et al. 2021, 918–922; Kolkman et al. 2011). Neurons in the cerebellum form a complex network, which has been interpreted to compare the predicted sensory information from movement with the actual measured information using internal models. According to the comparison the structure provides an error signal that can be used to adjust motion and models. The output of the cerebellum anticipates the actions required to achieve the goal for smooth motion. (Brooks & Cullen 2013; Popa et al. 2012) Through its networks, the cerebellum regulates balance and eye movements, control posture and locomotion, and participates in the planning and execution of movement as well as cognitive functions. (Benagiano et al. 2017; Dietrichs 2008; Kandel et al. 2021, 911–917; Poppele et al. 2003)

### 2.3.4 Brainstem

The brainstem, located between the spinal cord and the diencephalon, consists of the midbrain, pons, and medulla, see Figure 1 (Kandel et al. 2021, 12). Its nuclei are involved in the regulation of a wide range of functions, including sensory and motor systems, as well as systems related to alertness, motivational state, and learning (Kandel et al. 2021, 977–978). In terms of motor functions, the nuclei of the brainstem are important in controlling stereotypic and reflex functions related to balance, postural regulation, and locomotion as well as head and eye movements through the vestibulospinal, reticulospinal and colliculospinal pathways. (Purves et al. 2018, 374–379) In addition to these, the brainstem controls breathing, heart rate, and emotionally related facial reflex expressions (Kam et al. 2013; Kandel et al. 2021, 992–998; Kihara et al. 2001). It also controls anticipatory postural responses via cortico–reticulospinal pathway (Fregosi et al. 2017). Furthermore, the nuclei of the brainstem deliver regulatory signals, as already noted, to the thalamus, and interact with the basal ganglia and cerebellum to control muscle synergies.

## 2.4 Spinal structures

Nerve pathways in the spinal cord carry information between peripheral and central nervous system structures. The ascending pathways formed by spinal cord neurons provide afferent

information from sensory receptors and associated primary sensory neurons. They also carry information about the current state of the circuits formed by spinal cord neurons. These signals are delivered to cortical and sub-cortical structures. (Kandel et al. 2021, 74–81; Purves et al. 2018, 190) The descending pathways, in turn, transmit efferent signals from cortical and sub-cortical structures either directly through monosynaptic connections or polysynaptically via interneurons to lower motoneurons in the spinal cord and brainstem (Kandel et al. 2021, 76, 89; Purves et al. 337–340). Furthermore, neurons in the spinal cord are not only signal carriers but also participate in the processing of information through both simpler reflex circuits and much more complex neuronal circuits. The following sections explain these structures and their functional significance in motor control.

### 2.4.1 Spinal circuits

Signals transmitted to muscles by lower motor neurons are the result of the complex computational processes of a peripheral and central nervous system. At its simplest, this means involuntary reflex regulation and, at its most complex, the voluntary activity generated by the integration of multi–sensory information and prior experiences. Between these two extremes are rhythmic and stereotyped movements controlled by spinal circuits. (Kandel et al. 2021, 761–762, 816; Purves et al. 2018, 337–338) Reflexes are involuntary muscle contractions that occur in response to a sensory stimulus that elicits an afferent signal in a sensory nerve fiber that is linked to motoneurons of the same muscle, an agonist, and its synergist through synaptic connections in the spinal cord. The same sensory nerve fiber is also connected to the antagonist muscle via inhibitory interneurons, causing its activity to be attenuated through reciprocal inhibition. Between the sensory nerve fiber and motoneuron there can be one (monosynaptic) or more (polysynaptic) synaptic connections. Each synaptic connection allows such reflex arch to be regulated by other neural circuits and thus giving possibility for more diverse adaptation of the reflex function, while at the same time making the reflex action slower. (Kandel et al. 2021, 762–773; Purves et al. 2018, 346–352) In addition, the spinal cord also contains so called central pattern generator circuits formed by excitatory and inhibitory couplings between different spinal interneurons that regulate stereotypic and rhythmic muscle synergies. These circuits consist of separate parts that independently generate the rhythm and spatiotemporal motion pattern and can be separately controlled by both sensory afferent and supraspinal efferent signals. (Kandel et al. 2021, 790–795, 799–809; Purves et al. 2018, 352–356, Rybak et al. 2006)

### 2.4.2 Lower motoneurons and sensory fibers

There are two different types of lower motoneurons: α– and γ–motoneurons. α–motoneurons innervate the actual muscle, or extrafusal, fibers, causing the activation of contractile elements and thus the intended tension (Kandel et al. 2021, 764–765). γ–motoneurons, in turn, innervate the intrafusal fibers in the muscle spindles located between extrafusal fibers. Muscle spindles are sensory organs that respond to changes in muscle length and the activity of γ–motoneurons regulates the sensitivity of spindles to changes in muscle length. Lengthening or shortening of the muscle causes the intrafusal fibers also lengthen or shorten, resulting in increase or decrease in the activity of the sensory fibers connected to the intrafusal fibers. These signals are used to regulate the activity of α–motoneurons through both mono– and polysynaptic couplings to control the desired muscle tension level by reflexive manner as described earlier. Both α– and γ–motoneurons receive regulatory projections from descending efferent pathways to balance muscle function. (Kandel et al. 2021, 762–769, 773–779; Purves et al. 2018, 341, 346–352) In addition to this regulatory system, the activity of α-motoneurons is controlled by inhibitory and excitatory signals from sensory receptors in the joints, skin, and tendons. It should be noted that these connections also receive regulatory signals from the descending pathways to adjust the intensity of the sensory feedback at any given time. (Kandel et al. 2021, 769–773)

## 2.5 Skeletal muscles

Finally, as a result of the cooperation of the separate and interconnected sensorimotor systems described in the previous sections, the action potential reaches the presynaptic terminal of the lower motoneuron (see Figure 4), causing voltage sensitive $Ca^{2+}$ channels to open, allowing $Ca^{2+}$ ions to flow through. This triggers a chain of intracellular events, as a result of which neurotransmitter is released into the synaptic cleft, where it diffuses into the postsynaptic membrane of the muscle cell. Here, it binds to postsynaptic receptors, opening their $Na^{+}$ and $K^{+}$ ion-permeable channels, causing a change in the potential difference across the cell membrane in the depolarizing direction. If this change is large enough, it produces an action potential conducting along the muscle cell membrane and finally muscle contraction due to cross-bridge cycle between thick and thin filaments of the muscle fiber. This process in which the action potential is transferred from the motoneuron axon to the muscle cell membrane is called neuromuscular transmission. (Kandel et al. 2021, 255–269, 747–750) Muscle contractions result from the contraction of several muscle fibers. The currents flowing across

the cell membrane of several muscle cells induced by action potentials add up in the tissues, creating a compound muscle action potential (CMAP) that can be measured from the skin surface using EMG. (Kandel et al. 2021, 738–739)

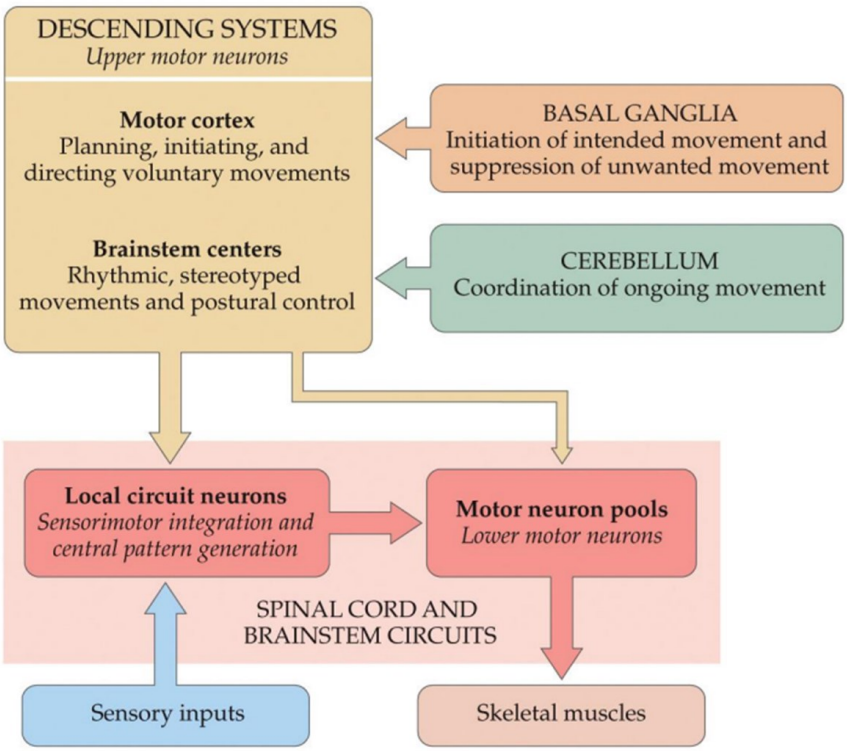


FIGURE 4. Main components of the sensorimotor regulatory system. (From Purves et al. 2018)

Physical movement is practically the only way we can communicate with our environment. This communication is represented by a response resulting from the action of the complex sensorimotor system described in this chapter. From a certain point of view, this response reflects the complexity of our living environment, as it must adapt to very different and ever–changing situations. When such a system is stimulated, e.g., with TMS, and when the resulting muscle activity is measured, e.g., with EMG, it is good to keep in mind the system behind the measured values and its complex structure because all parts of it might to some extent have effect in recorded responses.

# 3 TRANSCRANIAL MAGNETIC STIMULATION

Understanding how TMS works requires knowledge from physical principles and physiological phenomena connected to this method. In addition, when used to scientific research, stimulation is nothing without measurements. We need to measure responses of the stimulation somehow if we want to get information to make conclusions about those responses. In this chapter a brief history of TMS is given first. After that basic physical and physiological principles of the method are described in the extent needed to understand TMS when used for recording responses of muscles. Also, the generation of MEP is discussed in this chapter.

## 3.1 Brief history

In 1980, Merton & Morton introduced a transcranial electrical stimulation (TES) that could be used to stimulate brain areas through the intact scalp. That method utilizes a high-voltage electric shock to stimulate a targeted brain area. By using their method Merton & Morton (1980) proved that it is possible to induce action potentials to lower motor neurons by stimulating the motor cortex. However, electrical stimulation activates pain fibers in the scalp being a limitation with TES (Hallett 2000). An answer for this problem came from Barker et al. (1985) when they introduced almost pain free TMS, which is a contactless and non–invasive technique used to study the excitability of the human cortex. In this method pulse of current is generated by a high-voltage capacitor discharge system and led through a flat coil (Figure 5). Barker et al. (1985) demonstrated that muscle action potentials could be induced as a response to a single stimulus from the coil placed on the scalp over the primary motor cortex and assumed that this happened because the rapid, time–varying magnetic field caused the current in the tissues.

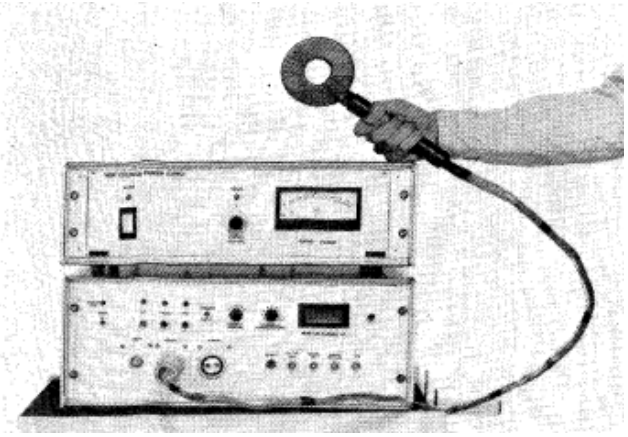

FIGURE 5. Transcranial magnetic stimulator device (From Barker et al. 1985).

TMS introduced produces a magnetic field induced current flow in the brain. This externally induced current flow, or electric field, can have temporary excitatory or inhibitory effects on targeted areas of the cortex caused by depolarization or hyperpolarization of cortical neurons. (Petrov et al. 2017) The method has been used to generate a muscle twitch or to inhibit movement when targeting motor cortex, or to produce visual phosphenes or scotomas by targeting occipital cortex. TMS has become a widely used stimulation method in many areas of brain research. Because it can be used to modify brain functions, TMS has been used in clinical context in different therapies. (Hallett 2000)

### 3.2 Physical principles of TMS

In TMS, a capacitor is used to store electric charge which is discharged and led through the coil generating a time varying magnetic field. The magnetic field induces the electric field according to Faraday's law of electromagnetic induction. The magnitude of the induced electric field in the brain is proportional to the time rate of change of the magnetic field. When using TMS the rate of change of the current in the magnetic coil determines the rate of the change of the magnetic field. (Rossi et al. 2009) Lines of flux in the magnetic field are perpendicular to the plane determined by the coil (Figure 6) and to the electric field which, in the case of a homogenous medium, induces the current to flow in loops that are oriented parallel to the plane determined by the coil and have an opposite direction compared to the electrical current in the coil. (Groppa et al. 2012†; Hallett 2000)

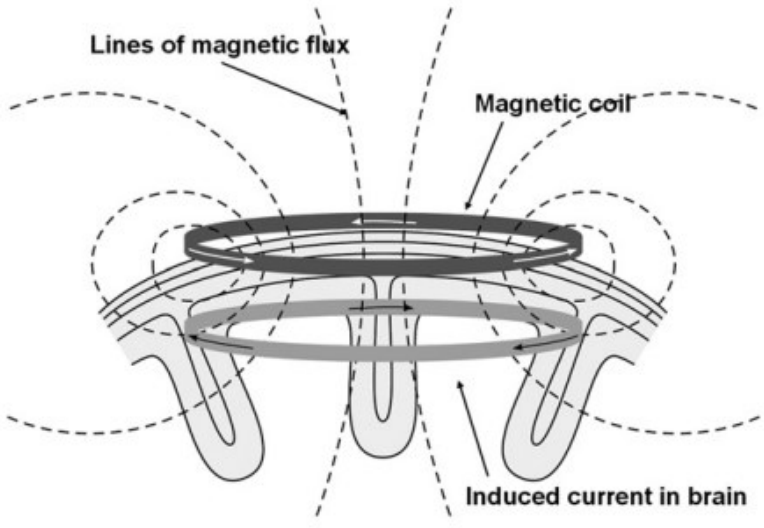


FIGURE 6. The current in the brain is induced by the current flow in the magnetic coil. (From Hallett 2007)

Coil design is an important factor as it affects the stimulation depth, intensity and focality. When circular coil is used induced current loops near the circumference of the coil are the strongest and become weaker near the center of the coil (Figure 7). (Hallett 2000) For the circular coil, the stimulation area in the brain is large but depth is low causing poor focal accuracy (Cohen et al. 1990). The intensity of the induced current decreases as a function of distance from the coil, which means that for the stimulation of the deeper targets, higher stimulation intensity levels are needed (Rossini et al. 2015). Even if TMS is used with the highest intensity level, the stimulus is unable to activate deeper neural structures, such as the medial part of the temporal lobes, thalamus, or basal ganglia (Groppa et al. 2012†).

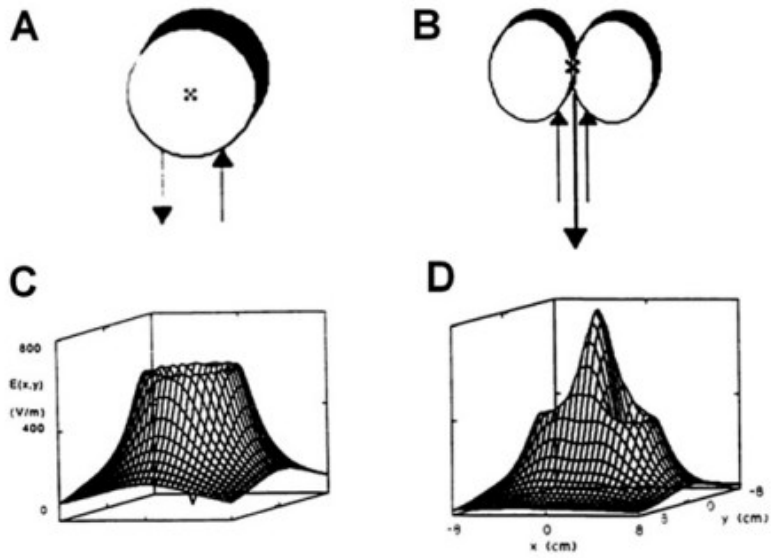


FIGURE 7. Intensity of the electric field is related to the shape of the magnetic coil. A and B illustrate round and figure–of–eight coils, respectively. C and D illustrate intensities of the electric fields induced by A and B, respectively. (From Hallett et al. 2007)

More focal stimulation can be achieved by using coils with a smaller diameter, but this advantage comes with price. The electric field generated by smaller diameter coils decays faster in depth. Thus, larger coils produce larger electric field in deeper targets, but fields are less focal and vice versa for smaller diameter coils. Targeted depth can be increased by increasing the current through the coil also when using smaller diameter, but this results in an increase of the activated brain volume decreasing the focal accuracy. (Deng et al. 2014) More focal stimulation is achieved also by using figure–of–eight–shaped coil (Cohen et al. 1991; Ueno & Matsuda 1992). In this coil configuration, which has become the most popular TMS coil type, there are two overlapping circular coils with opposing current directions generating more focal

maximal stimulation point at the intersection area of the coils (Figure 7). (Rastogi et al. 2019; Ueno & Matsuda 1992) In addition, Cohen et al. (1990) found out that the focality of the figure–of–eight coil can be increased by the coil construction where angle between two coils is more than 180°. Moreover, Roth et al. (2002) addressed the problem of the small depth by studying several types of coils and found out that with so called Hesed coil (H–coil) configuration deeper brain structures could be stimulated without increasing the stimulation intensity above the undesirable side effects. More recent study about coil configuration comes from Rastogi et al. (2019) who introduced the multicoil configuration called the triple–halo coil which is capable to stimulate brain regions at a depth of 10 cm with more than seven times stronger magnetic field if compared with the figure–of–eight coil. However, all TMS coil configurations have the same problem: deeper targets are stimulated with lower intensity than more superficial targets. (Rastogi et al. 2019)

The waveform of the current passing through the coil is also an important factor. The configuration of the current flowing in the magnetic coil has a monophasic or biphasic/polyphasic waveform (Figure 8). The integral of the electric field induced by these different waveforms over the duration of the magnetic pulse is zero. This means that the elicited current in one direction is balanced by the same amount of current in the opposite direction. (Groppa et al. 2012†; Kammer et al. 2001)

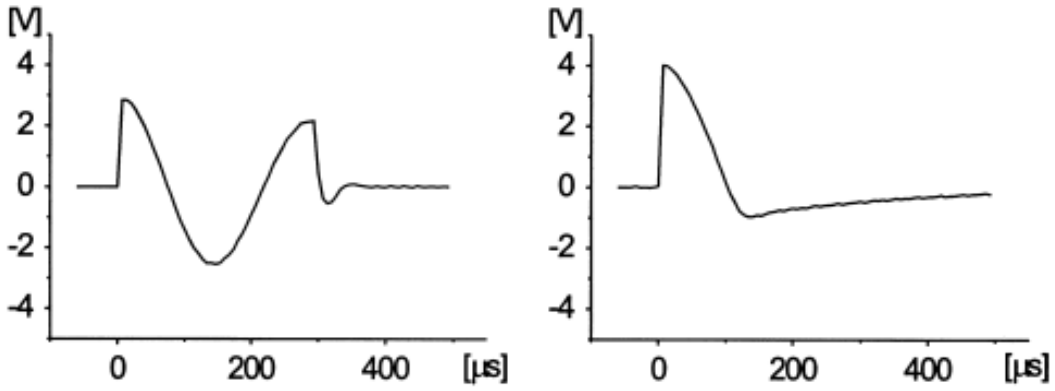


FIGURE 8. Biphasic (on the left) and monophasic (on the right) waveforms. (Kammer et al 2001)

In the case of the monophasic pulse the initial phase of the current is strong and a lower and temporally longer return current follows that. (Groppa et al. 2012†; Kammer et al. 2001) From those two phases of the current, only the stronger initial phase generates current flow in the

brain (Groppa et al. 2012†). The biphasic configuration differs from the monophasic so that there is a clear change in the current direction twice or more during a pulse: an initial positive current is followed by a reversed negative current which in turn is followed by a rising current. (Kammer et al. 2001) Physiologically significant currents in the brain are induced by these two or more phases. However, the second phase is more effective in the case of the biphasic current as it has the largest amplitude and the longest duration. Also differing neural structures are stimulated in the cortex because of opposing direction of the current to the initial phase. (Groppa et al. 2012†; Maccabee et al. 1998; Sommer et al. 2018)

### 3.3 Physiological principles of TMS

When stimulating cortical neurons, induced current flow in the tissue must produce depolarizing ion flow in cortical axon's membrane strong enough to trigger an action potential. Two factors, the spatial derivative (the spatial relationship between the stimulated axons and the current induced in tissues) and the temporal derivative (the rate of the change of the induced magnetic field) of the induced electrical field, determine the location where the membrane depolarization occurs the most effectively. At that location the derivatives are maximal. When the TMS coil is in tangential orientation to the head, a generated magnetic field penetrates the skull with minimum attenuation inducing the current in conductive intra-cranial tissues. When a medium has a homogenous conductivity, the current runs in parallel to the TMS coil, as explained in the previous section. However, the human brain tissue is not homogenous and elicited currents are distorted due to local differences in conductivity. (Groppa et al. 2012†) It has been found out that sensitivity of cortical neurons to the TMS pulse is the highest at locations of axonal bending (Maccabee et al. 1993). Modeling studies have shown that induced currents are strongest in the crown of the gyrus and depend on the coil angle and orientation with respect to the curvature of individual gyrus. It seems that TMS pulse activates cortical interneurons in the gyral crown, lip of the sulcus or slightly deeper and these, in turn, project to the corticospinal tract (Opitz et al. 2013; Laakso et al. 2014). Also, sub-cortical white matter may play some role as it includes axons of cortico-cortical loop fibers having possible effect to the corticospinal output neurons (Laakso et al. 2014).

Triggered action potentials in cortical axons are conducted to other neurons transsynaptically creating signal propagation via cortical, subcortical, and spinal paths. (Groppa et al. 2012††) A single TMS stimulation has been shown to elicit a series of descending volleys of excitation in

the corticospinal pathways by using epidural invasive recordings during anesthesia by Burke et al. (1993) and in conscious humans by Nakamura et al. (1997). These volleys travelling along the corticospinal tract induces neurotransmitter, glutamate, release summing up temporally and spatially in cortico-motoneuronal synapses causing a depolarization at the postsynaptic cell membrane. If descending volleys are strong enough to induce depolarization exceeding the threshold level for firing, they elicit action potentials in the peripheral motor nerve and the spinal motoneurons. These propagate through the neuromuscular junction and elicit, in turn, action potentials in muscle cell membrane, recorded as MEPs (Figure 9), and further activation of the contractile elements in the muscle cell. (Groppa et al. 2012†; Groppa et al. 2012††)

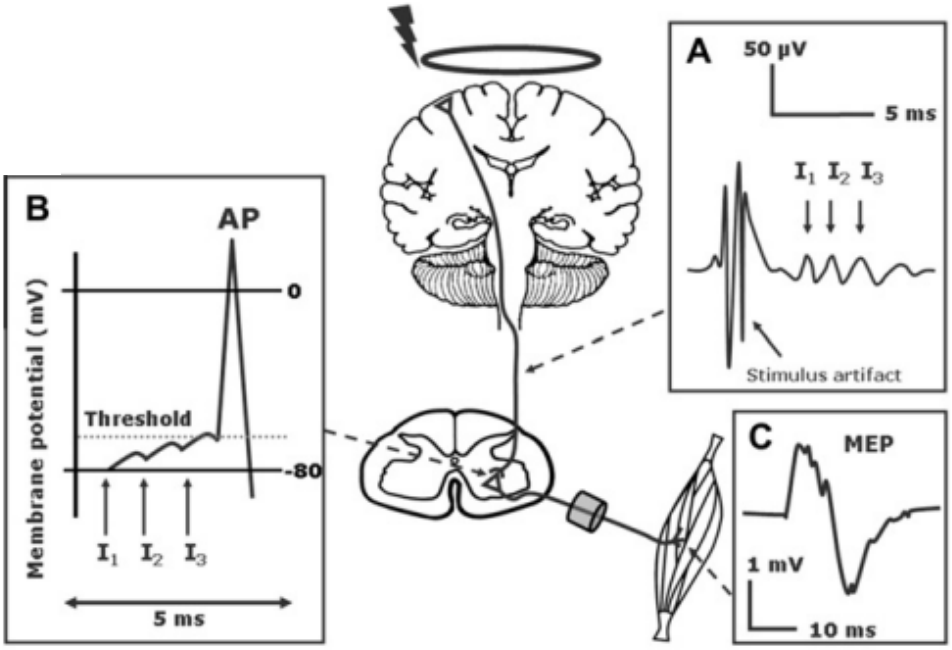


FIGURE 9. Generation of the motor evoked potential (MEP). A) Activation of the corticospinal neurons caused by TMS leading to the descending volleys ($I_1$–$I_3$). B) Temporal and spatial summation at the cortico-motoneuronal synapses caused by descending volleys leading to the action potential (AP). C) Motor evoked potential (MEP) caused by TMS induced signal propagation. (Groppa et al. 2012†)

Most of the studies concerning the descending volleys have been performed by stimulating the motor cortex. These studies show that TMS generates two types of the descending volleys: early and late volleys, direct D–waves and indirect I–waves, respectively. In the case of the shorter latency D–waves clearly larger stimulus than suprathreshold TMS pulse activates axons of the pyramidal cortical neurons directly and in the case of the longer latency I–waves stimulus

intensities slightly over suprathreshold level activate corticospinal neurons via indirect transsynaptic inputs from different sets of the intracortical neurons. I–waves have a high degree of synchronization, and they are the main type of volley generated by TMS, although this depends on the coil orientation. (Di Lazzaro et al. 2004; Groppa et al. 2012†; Laakso et al. 2014; Rossini et al. 2015) When motor cortex is stimulated by the single TMS pulse at the lowest intensity capable for evoking MEPs a single descending volley, $I_1$–wave, is generated. The size of this I-wave increases and is followed by later volleys, $I_2$– and $I_3$–waves, as the stimulus intensity is increased (Di Lazzaro et al. 1998) (Figure 9 and 10). Separate volleys generate excitatory synaptic potentials that summate at motoneurons leading to the larger MEP (Rossini et al. 2015). If the stimulus intensity is much higher than the lowest threshold for the MEP, the shorter latency D–wave appears (Figure 10). (Di Lazzaro et al. 1998)

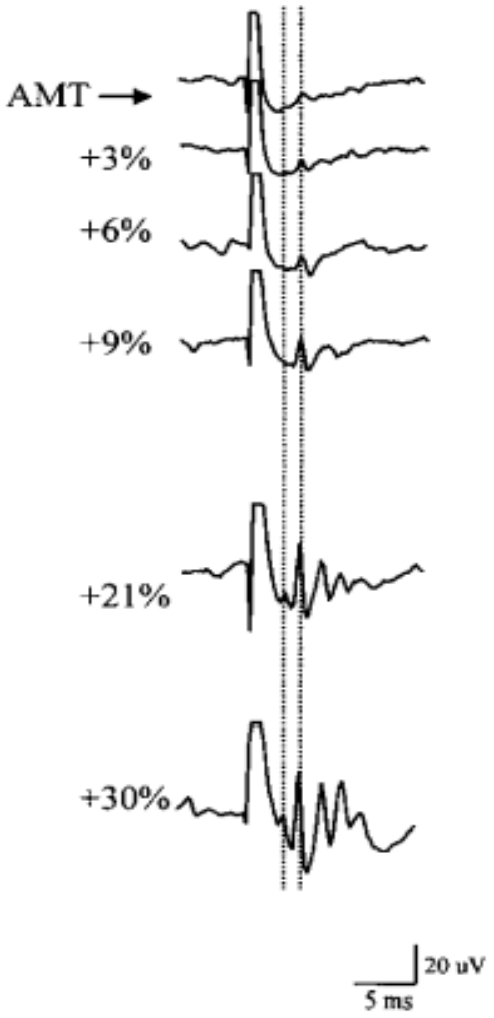


FIGURE 10. Descending volleys evoked by TMS using increasingly stronger stimulus intensities. AMT denotes active motor threshold. Left dotted line shows the peak latency of the D–wave which appears at the higher +21% intensity level. Right dotted line shows the peak latency of the first I–wave which appears at AMT stimulus level. (Di Lazzaro et al. 1998)

It should be also noted here that the intensity of the stimulus, the pulse configuration (mono–/diphasic) and the relative threshold of each volley to the direction of the induced current in the

cortex affect the descending volley pattern (Groppa et al. 2012†). I–waves with the shortest latency are elicited by orienting TMS–coil in antero-medial direction in the area of the central sulcus for monophasic current pulses and in the opposite direction for biphasic current waveforms (Laakso et al. 2014).

The strength of the cortico–motoneuronal excitation is determined by the strength of the descending corticospinal signals and spinal motoneurons' local excitability which are dependent on external as well as internal factors. External factor is for example the TMS pulse intensity, and internal factors are the maturation and connectivity of the corticospinal neurons. By manipulating these factors, the amplitude and latency of the MEP can be modified through a complex network of excitatory and inhibitory connections controlling the excitability of the motor neuron pool. Thus, increasing the strength of the cortico–motoneuronal excitation increases MEP's amplitude and shortens the latency. This can be achieved by increasing the TMS pulse intensity and by voluntary contraction of the muscle. These generate a stronger descending excitatory signal which in turn generates a faster temporo–spatial summation at the cortico–motoneuronal synapses. The stronger the facilitating stimulus is, the more motoneurons will be recruited and some of them may discharge more than once. (Groppa et al. 2012†; Rossini et al. 2015)

Because corticospinal excitatory signal elicited by TMS can be modified by more diverse temporal factors than CMAPs elicited by the peripheral nerve stimulation, MEPs are subject to larger phase cancellation, has a lower peak-to-peak amplitude, longer duration and the shape is more polyphasic than peripherally induced CMAPs'. This intrinsic fluctuation of excitability in the corticomotor system results in less consistent shape of MEPs than CMAPs. (Groppa et al. 2012†; Rossini et al. 2015) Temporal factors could include for example synaptic fluctuations due to short-term plasticity such as receptor saturation, receptor trafficking, changes in channel gating kinetics, synaptic vesicle pool depletion or control of the neurotransmitter release probability (Opitz et al. 2013). In addition, the coil orientation and TMS pulse configuration are related to the stimulus intensity threshold for inducing MEP. The coil orientations, as mentioned earlier, for the lowest stimulation intensity threshold producing MEP are in antero-medial direction in the area of the central sulcus for monophasic pulses and generates shortest latency I–waves (Davey et al. 1994; Laakso et al. 2014). For biphasic pulses the optimal orientation is opposite (Corthout et al. 2001; Laakso et al. 2014).

# 4 STUDYING FUNCTIONALITY OF MOTOR CORTEX

When mapping the motor cortex, the TMS pulse is applied at chosen cortical sites and corresponding MEPs are recorded as responses to the TMS pulse. By this way, a map of cortical sites, somatotopy, generating MEPs for certain muscle(s) can be obtained. TMS could be theoretically used for mapping any cortical region which generates measurable responses to stimuli. However, in practice it has been used mostly for mapping the motor cortex because the MEP is a reliable output measure and relatively easy to obtain. (Rossini et al. 2015) In this thesis, as already stated earlier, the possibility of classifying the stimulated hotspot locations according to corresponding TMS-induced MEP patterns is studied. From one point of view, this task is about studying the correlation between TMS locations and the corresponding MEP patterns. To the best of the author's knowledge, this type of classification has not been done before, thus no similar studies can be found. However, the mapping studies that studied the functionality of the motor cortex contain points worth noting, which are also useful when thinking about the classification task in this thesis. For this reason, this chapter presents, where applicable, the metrics used in the mapping as well as the influencing factors. Some of these are important when choosing parameters for TMS measurements. Part, on the other hand, can be used when analyzing the classification results. The same measures have also been used in the functional studies of the motor cortex, when the aim is to research the synergies between muscles and muscle groups. The information provided by these studies is also relevant when analyzing classification results. So, the last section of this chapter presents this information as applicable.

## 4.1 Outcome measures describing muscle representations of motor cortex

When mapping cortical representations of muscles there should be measures describing found areas and locations on the motor cortex. Typically used outcome measures are (1) hotspot, (2) center of gravity (CoG), (3) area and (4) volume. The hotspot is defined as the stimulus location on the scalp which gives repeatedly the largest MEP amplitudes for the TMS pulse, and it is used usually as a target location when determining a motor threshold (MT) for the muscle and as a starting location for the motor cortex mapping (Reijonen et al. 2020†, Weiss et al. 2013), see Chapter 4.2. CoG is defined as the location on the grid, formed by stimulus sites, to induce the largest MEP when the size and location of all MEPs are considered, for example Weiss et al. (2013). CoG provides information about the somatotopic orientation of the muscle

representation to another (Malcolm et al. 2006). Area represents the spatial extent of the obtained motor map, and it can be seen as the spatial extent of excitability of individual muscle or muscle groups (Malcolm et al. 2006, Plowman–Prine et al. 2008). Volume is defined to be the MEP amplitude weighted spatial extent of a motor map and it tells the excitability of different sites inside the map (Tardelli et al. 2022). These measures and studies based on them are useful also when analyzing classification results as they deal with the relationships between the representation areas of the motor cortex of several muscles.

## 4.2 Factors affecting measures

Measures described above are influenced by several factors by operator of the TMS device or by the subject. It is important to understand how these factors affect the results. In this section the most typical factors, which are also relevant in the classification task of this thesis, are discussed. These are the intensity of TMS, baseline muscle activation, used navigation method, TMS coil orientation and distance between stimulus locations.

### 4.2.1 Intensity of TMS

As already mentioned in Chapter 3.3, the intensity of the TMS pulse will affect the recorded MEP, as well as many internal corticospinal factors, causing MEP levels to be very individual and to fluctuate inconsistently. Because of this, if stimulation intensities are compared between and within the subject, they should be determined with respect to something.

Protocols typically determine MT for targeted muscle first, using the hotspot as a stimulus location, and then calculate all other stimulus intensities as some fractions of MT. MT is the minimum intensity of motor cortex stimulation which induce a reliable MEP of minimum acceptable amplitude in the target muscle. Thresholds for the hand and forearm muscles are the lowest and they are progressively getting higher for muscles in trunk, lower limb, and pelvic areas. Also, intrinsic fluctuations of cortical and spinal neuronal signaling affect MEP amplitude which causes uncertainty when estimating MT. (Groppa et al. 2012†, Rossini et al. 2015) Because these factors cannot be eliminated, it is even more important to keep other technical and physiological variables as constant as possible. These include coil position and orientation, background activity of the targeted muscle, individual arousal level and environmental noise. (Rossini et al. 2015)

There are two basic types of MTs: resting MT (rMT) and active MT (aMT). rMT is determined when the target muscle is at rest and can be controlled by the absence of the EMG. aMT is determined during a tonic contraction of the target muscle at a designated percentage of maximal voluntary contraction (MVC). For estimating both MT types there are two basic methods: relative frequency method and adaptive method. In the relative frequency method, stimulus intensity is gradually increased until induced MEP's peak–to–peak amplitude is > 50 μV for relaxed muscle and usually > 100–200 μV for contracted muscle. After this stimulus intensity is gradually decreased in small steps until there are five positive responses out of ten trials. This intensity plus one is used as rMT. (Groppa et al. 2012†; Rossini et al. 2015) However, despite of being commonly used protocol to estimate MT, it has been calculated that measurement accuracy for the relative frequency method would be better if 10 out of 20 trials are required for setting MT level (Awiszus 2012). In the adaptive method, an S–shaped function is used to model the probabilistic characteristics of MT, as well as the relationship between the TMS intensity and the probability of inducing a MEP. At each trial the new intensity level for the next TMS pulse is calculated by an adaptive staircase procedure. It has been shown that adaptive methods provide more accurate MT estimation that is usually also faster. (Awiszus 2011; Qi et al. 2011; Rossini et al. 2015; Silbert et al. 2013) However, there is no consensus as to which method should be used (Kallioniemi & Julkunen 2016).

As controlling the background EMG activity is the easiest when the subject is at rest, rMT is therefore maybe the most typical value, which is used to determine the intensity of TMS pulses. The most used intensities are from 105% to 120% of rMT. (Kallioniemi & Julkunen 2016) Increasing the stimulus intensity increases the MEP amplitude and the stimulated cortical area which causes motor maps to differ based on the mapping intensity (Tardelli et al. 2022). Kallioniemi & Julkunen (2016) studied the effect of different stimulus intensities on the mapped motor cortical representations. They used intensities 110% and 120% of rMT to conduct TMS mapping for first dorsal interosseus, abductor digiti minimi and abductor pollicis brevis. They also used so called upper threshold (UT) stimulus intensity, introduced by Mills & Nithi (1997), which is the lowest intensity producing at least 50 μV MEP amplitude at 100% of stimuli. In addition, they examined input–output responses at stimulus intensities from 90% to 150% of rMT for testing probability of inducing MEPs at target location. UT intensity was chosen because it maximizes the occurrence rate of the MEP responses with minimal stimulation intensity. Kallioniemi & Julkunen (2016) hypothesized that this might reduce problems in the selection of stimulus intensity because it considers the individual input–output response of the

motor cortex. They found out that confidence intervals for obtained cortical representation areas were the lowest when UT was used as the stimulus intensity, and the difference between areas obtained by stimulus intensity of 110% of rMT and UT was insignificant as well as difference between absolute stimulus intensities for 110% of rMt and UT. Differences between intensities of 120% of rMT and UT were significant. Furthermore, the curve for response probabilities of stimulus intensities for first dorsal interosseus muscle (Figure 11) reveals that both intensities, 110% of rMT and UT, are in the rising part of the curve, and intensity of 120% of rMT is almost in the saturated part. This means that intensities of 110% and UT are still sensitive to detect fluctuations in cortical excitability but intensity of 120% might have lost it. From these results Kallioniemi & Julkunen (2016) concluded that using UT as stimulus intensity could be better than using more commonly used intensity levels. It is also worth noting that earlier Kiers et al. (1993) found out that increasing the stimulus intensity increases MEP amplitude, but also decreases amplitude variability. Based on these results it could be suggested that stimulus intensity of 110% of rMT is better if sensitivity for fluctuations in cortical excitability is an essential factor in the study. On the other hand, if stability and probability of occurrence of the response are important, it may be more reasonable to choose a stimulus intensity of 120% of rMT or even a higher value.

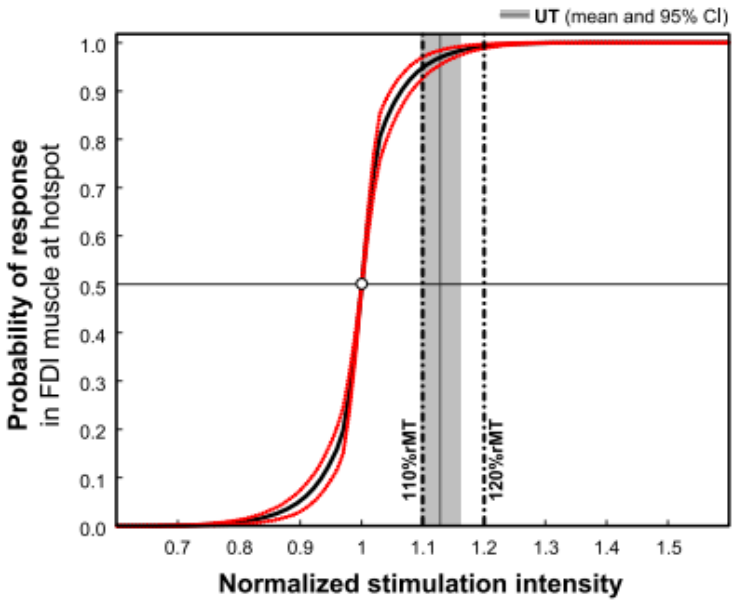


FIGURE 11. The cumulative distribution function (black line) and standard error of mean (red lines) plotted against the normalized stimulation intensity. The vertical dotted lines represent the stimulus intensities based on rMT. The grey area with the grey vertical line displays the 95% confidence interval and mean for the UT. (From Kallioniemi & Julkunen 2016)

### 4.2.2 Baseline activation of the targeted muscles

As mentioned in Chapter 3.3, voluntary activation of the muscle increases the strength of the cortico–motoneuronal excitation and thus MEP amplitude. For this reason, it is important to address the meaning of the background activation of targeted muscles when using TMS as stimulation method.

Ngomo et al. (2012) studied the difference between passive and active recordings when the first dorsal interosseus muscle was targeted. They had 12 subjects and they calculated MTs, MEP amplitudes, map areas, map volumes and CoG. Results were obtained during three separate sessions. Time interval between session one and two was four days (short-term), and between session two and three at least one month (long-term). Intensities of the stimuli were 110% of both rMT and aMT. They found out that rMT is significantly higher than aMT and MEP amplitudes were higher in active than in passive condition, although this difference was not statistically significant. Map areas and volumes as well as CoG did not differ significantly between conditions. (Ngomo et al. 2012) The results concerning MTs are consistent with the study performed by Wassermann (2002). Darling et al. (2006), in turn, found out that MEP amplitudes are significantly larger when muscle is activated. Ngomo et al. (2012) concluded that the reason for the difference between their and Darling et al. (2006) results could be lower stimulation intensities used in their study.

Overall, the level of the baseline activation of the targeted muscles influences the MEP amplitude due to changes in cortical and spinal excitability. When targeted muscle is in active state the stimulation threshold is lower and MEPs are larger compared to inactive state. However, if active state is used, the degree of activation must be determined to compare obtained results between or within subject for different recording sessions which makes it more complicated than passive state recordings.

### 4.2.3 Navigation method

When trying to link any cortical stimulus location with corresponding responses, accuracy of choosing the locations of TMS pulses is crucial for the reliability of the obtained mapping. Control of the TMS coil location is called navigation and can be based on surface landmarks (Figure 12) or magnetic resonance imaging (MRI) (Figure 13). When using landmark navigated

TMS (lmTMS) a flexible cab with grid on it is used to determine stimulus locations, for example Malcolm et al. (2006) and Plowman–Prine et al. (2008). When using MRI, or so called neuronavigated TMS (nTMS), an individual cortical structure is segmented from MRI data, registered with targeting system, and used to calculate the location of the TMS coil relative to the cortex. (Singh et al. 1997) The calculated location is shown on the screen. TMS operator uses this visual information to place the coil to the chosen location and orientation. (Tardelli et al. 2022)

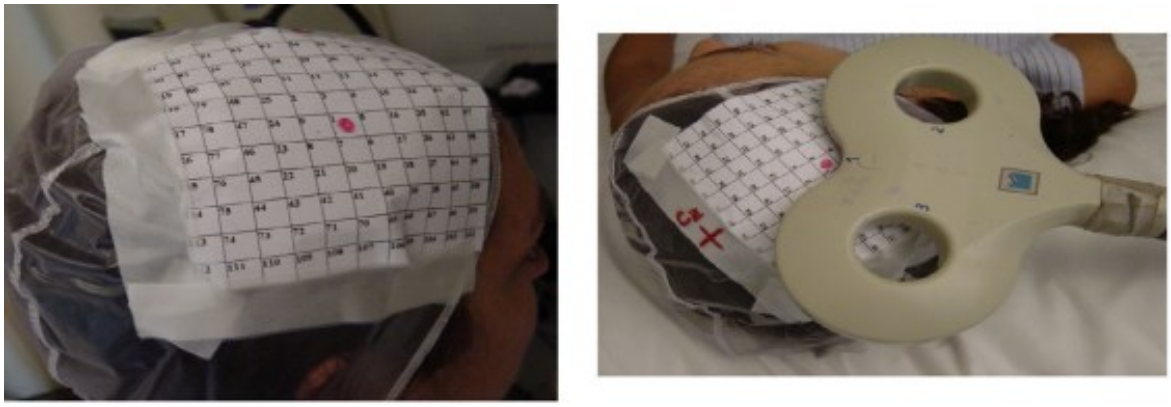

FIGURE 12. Landmark-based navigation with a flexible cab with grid (left) and a coil placement according to grid (right). (From Rossini et al. 2015)

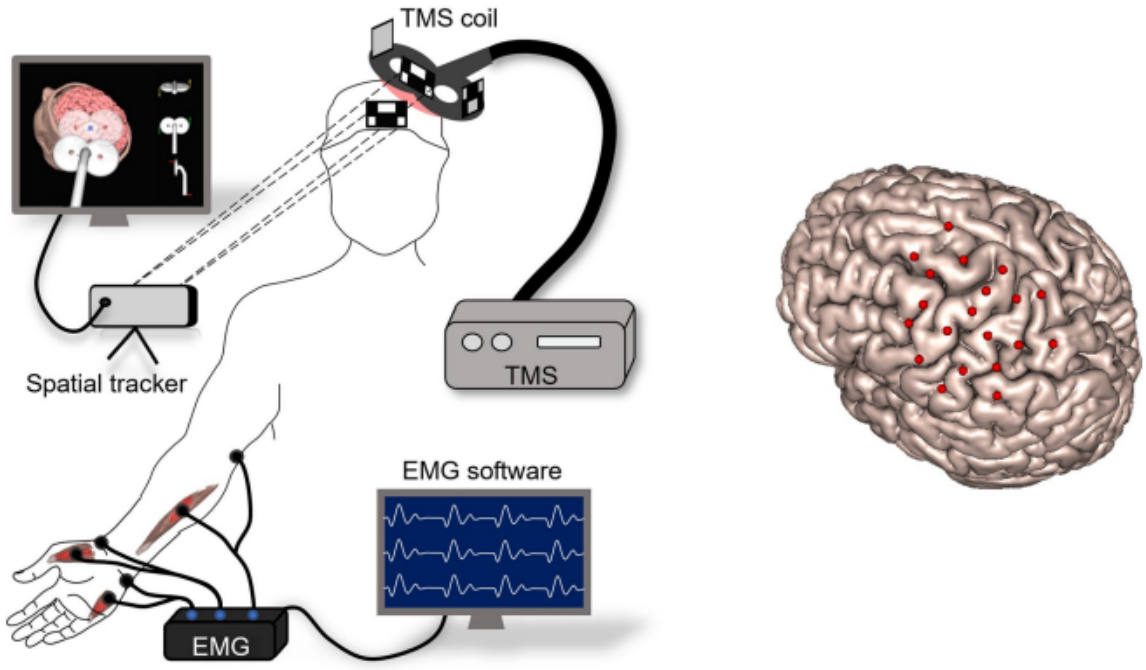


FIGURE 13. Neuronavigated TMS. (Left) Illustration of the TMS coil tracking system. (Right) TMS-coil locations shown on the cortex segmented from MRI data. (From Tardelli et al. 2022)

Malcolm et al. (2006), Plowman–Prine et al. (2008) and Nazarova et al. (2020) studied the test–retest reliability of TMS mapping of motor representations. Malcolm et al. (2006) investigated reliability for four hand muscles (first dorsal interosseus, abductor pollicis brevis, extensor digitorum communis and flexor carpi radialis). Plowman–Prine et al. (2008) investigated reliability for swallowing muscles (suprahyoid and pharynx). Both studies had 20 subjects and used the lmTMS and intraclass correlation coefficients (ICC)[1] for analysis. Subjects were assessed on two sessions with a time interval of two weeks between them. Nazarova et al. (2020), in turn, studied the test–retest reliability using nTMS. They stimulated three upper limb muscles (abductor pollicis brevis, abductor digiti minimi and extensor digitorum communis). They had 20 subjects, and two mapping sessions were performed with time intervals of 5–10 days between them. The results of these studies, summarized in Table 1, show that the reliability for the map area, volume, rMT and CoG is from moderate to high level for both navigation methods. However, the results for CoG show that nTMS might be more accurate. From these results it could also be suggested that the choice of the targeted muscles affect the results.

TABLE 1. Intraclass correlation coefficients (ICC) for TMS mapping parameters given in studies from Malcolm et al. (2006), Plotwman–Prine et al. (2008) and Nazarova et al. (2020).

| **Parameter** | **ICC for Malcolm et al 2006** | **ICC for Plowman–Prine et al 2008** | **ICC for Nazarova et al 2020** |
|---|---|---|---|
| **rMT** | 0.90–0.97 | 0.98 | 0.99 |
| **map area** | 0.63–0.86 | 0.91 & 0.76 | 0.70–0.85 |
| **map volume** | | 0.70 & 0.68 | 0.72–0.79 |
| **center of gravity** | 0.69–0.86 | | |
| **center of gravity ML** | | | 0.98–0.99 |
| **center of gravity AP** | | | 0.95–0.96 |

Values for Malcolm et al. (2006) and Nazarova et al. (2020) are given as range of ICC among stimulated muscles for each parameter. Values for Plowman–Prine et al (2008) are given for suprahyoids & pharynx, respectively. AP denotes antero-posterior direction and ML denotes medio-lateral direction.

[1] Relative reliability describes the degree of variation among subjects over repeated measurements and is often calculated as intraclass correlation coefficient (ICC) value, which is generally interpreted so that values ICC > 0,75 are considered high, 0,50 < ICC < 0,74 moderate and ICC < 0,50 is considered poor. (Nazarova et al. 2021, Plowman–Prine et al. 2008)

Furthermore, Gugino et al. (2001) investigated differences on spatial accuracy between nTMS and landmark-based navigation when activating first dorsal interossei. They found out that the nTMS was significantly more accurate than lmTMS. In their study distances between the actual stimulus location and optimal location on the cortex and scalp were about 12 mm and 13 mm for lmTMS against about 2 mm and 3 mm for nTMS. The optimal location was defined as the location of the cortical surface giving the greatest mean MEP amplitude for targeted muscle. In addition, differences between the coil angles for lmTMS were about 11 degrees against about 2 degrees for nTMS. Gugino et al. (2001) also found out that MEP amplitude, map area and probability for eliciting MEP response were significantly higher when using nTMS than using lmTMS. Similar results from Julkunen et al. (2009) confirm this.

### 4.2.4 Effect of coil orientation

Earlier in Chapter 3.2, TMS coil design and the current waveform and direction were discussed. In addition to these, the coil orientation affects the MEP response induced by the TMS pulse. This determines the direction of the electric field induced by the magnetic field targeted to specific location on the motor cortex influencing corticocortico and corticospinal projections. Recently, computational and imaging methods have allowed researchers to estimate how the coil orientation affects the distribution and the strength of the electric field on the underlying cortical structure. Modelling studies have shown that the distribution and strength of the induced electric field in the brain tissue depend on the individual geometry of cortex as well as different tissue's direction dependent anisotropic conductivity.

Opitz et al. (2013) used the finite element method (FEM) and the individual MRI – and diffusion tensor imaging data to construct the head model for simulation of the electric field parameters for different coil orientations and tilt angles. They discovered that the estimated strength of the electric field on the primary motor cortex for different coil orientations correlates significantly with MEP amplitudes on an individual basis. The highest electric fields were estimated for the locations where gyri were perpendicular to the induced current. Laakso et al. (2014), in turn, modelled TMS induced electric field using the FEM and individual models of the head and brain. Their results showed that the coil orientation affects the strength and depth of the electric field. At the gyral crowns their results are similar with Opitz et al. (2013). However, deeper in the sulcus, the electric field was the strongest if the current flow was parallel to the sulcus.

Furthermore, Reijonen et al. (2020††) studied the effect of coil placement and orientation on the assessment of the focal excitability. First, they located the hotspot for the first dorsal interosseus muscle and the optimal coil orientation for it. After this, they determined six targets along the central sulcus near the hotspot and estimated coil orientations producing the highest MEPs for these targets. Estimated orientations were used to determine rMTs for each target. They also recorded MEP amplitudes as a function of the coil orientation at the hotspot and targets. Finally, they performed motor mapping around the hotspot and calculated CoG based on MEP values. When modelling electric fields of the target locations MRI data was used for constructing head model and FEM was used to calculate the electric field strength inside this. Reijonen et al. (2020††) found out that the optimal coil orientations were approximately perpendicular to the central sulcus, but also deviated at many locations pointing to the hotspot or CoG of the motor map and showed high intra– and inter–individual variability (Figure 14). When the distance from the hotspot increased, the exitability of the cortex decreased which could be seen in increasing rMT levels as a function of the distance. Electric fields were the strongest at the gyral crowns at both the target location and the hotspot.

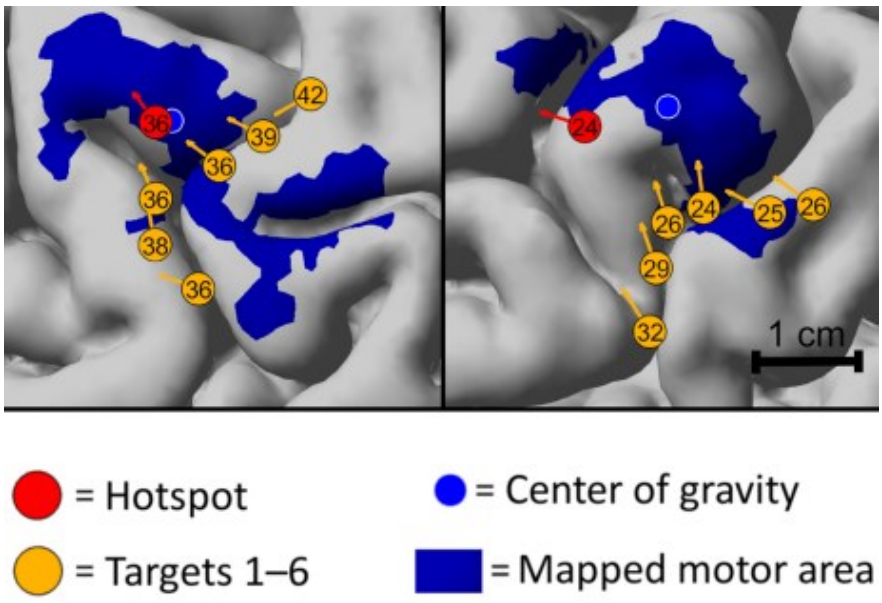


FIGURE 14. Illustration showing coil orientations indicated by arrows for the targets and the hotspot, center of gravity and mapped motor area for two subjects. (From Reijonen et al. 2020††)

More recently, Souza et al. (2022) developed an electronically controlled TMS transducer with which they were able to control the orientation of the TMS–induced electric field very precisely. In their study, they estimated the orientation of the electric field using a spherical head model

and measured MEP responses from the abductor pollicis brevis using different TMS coil orientations. Souza et al. (2022) found that maximal MEP amplitudes and the shortest latencies for these are achieved when the coil is oriented close to perpendicular to the central sulcus, see Figure 15. They also found that increasing the stimulus intensity reduced the orientation sensitivity to the TMS pulse. They concluded from their results that since neuron populations have different excitation thresholds, all components of the induced electric field affect the excitation of neurons and all cortical mechanisms are involved in the generation of MEPs. Furthermore, by changing the stimulus orientation, neuron populations can be excited at different points in the cortex. Souza et al. (2022) also pointed out that they used a spherical head model to estimate the orientation of the electric field and that MRI–based electric field modeling would help in estimating the orientation relative to the individual cortex surface.

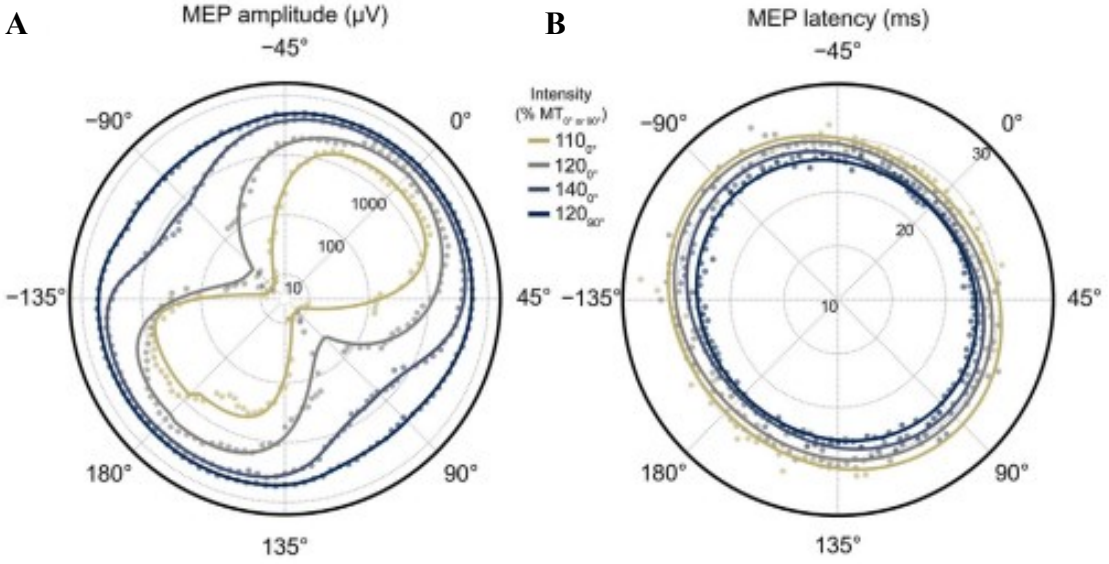


FIGURE 15. MEP amplitudes and latencies reported as functions of the stimulus intensity and orientation. A) Stimulus amplitudes. B) MEP latencies. 0° refers to the anteromedial orientation close to perpendicular to the central sulcus. (From Souza et al. 2022)

Studies described here show that the key factor for determining the electric field strength (and coil orientation) on the stimulation location is the direction of the current flow with respect to the orientation of the gyri and sulci. However, when measuring specific muscles, the optimal coil orientations for chosen stimulation locations away from the hotspot can vary significantly from being perpendicular in respect to the sulcus. These results also show that when using TMS, the optimal coil orientation should be sought by examining different options due to individual shape of the cortex.

### 4.2.5 Distance between stimulus locations

When mapping the motor cortex, usually fixed locations for TMS pulses are used. This fixed pattern of locations is called a grid and it may be coarser, distance between stimulation sites being larger, or finer, distance between stimulation sites being smaller. de Goede et al. (2018) used a robotic arm guided nTMS to maximize the accuracy of the coil positioning and stimulated four locations at 2 mm and four at 5 mm distance around the determined hotspot for the abductor digiti minimi. They had eight subjects. The stimulation intensity was 110% of rMT and the number of stimulations was 75 at each location. No significant differences were found for the calculated mean MEP amplitudes, nor for the amplitude variances, at the stimulation locations at group level. These results may be criticized by small number of subjects (de Goede et al. 2018), but they might also suggest that larger distance than 5 mm is needed between stimulation locations to induce detectable changes in MEP amplitudes. In addition, Weiss et al. (2013) used distance of 5 mm between the stimuli and Krause et al. (2006), in turn, used 10 mm distance between the stimuli. When comparing deviations these two groups calculated for CoG it might be suggested that using finer grid results in more accurate determination of CoG. This is logical as using more points for calculation of the average values influences accuracy. However, it should be noted here that there seem to be lack of studies comparing the effect of inter–stimulus distance. Moreover, different studies use different mapping procedures and calculations. Thus, comparing the results is not on a very solid base.

## 4.3 Functional analysis of motor cortex

TMS has made it possible to find representations of different muscles on the motor cortex in a noninvasive and painless way. The method can be used to map the motor cortex from a wide variety of perspectives, for example age-related development of the cortex (Säisänen et al. 2020) or reorganization and plasticity of the cortex as a result of immobilization, training or injury (Raffin & Siebner 2019; Röricht et al. 1999). However, a few studies are presented here from the point of view of multi muscle mapping and functional analysis as these aimed to research the synergies between muscles and muscle groups. This information can be used to analyze the classification results obtained in this thesis.

After the first steps in the mapping, research began to focus on the more functional direction as scientists became interested in how different muscle synergies might appear in the motor cortex.

Melgari et al. (2008) studied overlapping representations and covariation of MEPs from simultaneous recordings of 12 hand, forearm and arm muscles induced by stimulating the hotspot of the opponens pollicis muscle and obtained from 10 healthy right–handed subjects. They suggested that overlapping of representations is related to the co–activation of the target muscles and covariation is measure of intensity and direction of the co–activation. They found out that there is high level overlapping for hand–hand, hand–forearm and forearm–forearm muscle pairs. Low overlapping levels were found for forearm–arm and arm–arm muscle pairs. They also found the lack of covariation for forearm–arm and hand–arm muscle pairs. High covariation was found especially between wrist extensors and hand muscles. Moreover, hand position had significant effect to both overlapping degree and covariation. Prone hand position was indicated with larger overlapping between muscle pairs belonging to hand and forearm than supine position. No changes were observed for more proximal muscles. From their results Melgari et al. (2008) concluded that organization of the muscle representations in the motor cortex do not have only structural but also functional, task–devoted and synergistic, dimension.

Also, Tardelli et al. (2022) studied forearm and hand muscle coactivation and overlapping of cortical motor representations. They stimulated 20 locations around target muscle's hotspot and calculated areas and volumes of cortical representations for three muscles recorded simultaneously as well as overlapping of areas and volumes for each muscle pair and muscle triplet. Selected muscles were two intrinsic hand muscles: flexor pollicis brevis and abductor digiti minimi, and one forearm muscle: flexor carpi radialis. They found higher overlapping of cortical representations between the forearm and hand muscles than between the intrinsic themselves. This was partly conflicting result with previous study from Melgari et al. (2008) presented previously. Tardelli et al. (2022) suggested that this was because of neutral hand posture used in their study and thus proprioceptive feedback was different. They also noticed that using stronger stimulation intensities caused the map areas to overlap more but did not affect overlapping of map volumes or map topographies. They concluded that (1) different muscles share cortical areas with specific muscles, (2) high overlap degree of motor representations is connected to synergistic actions between muscles and (3) individual muscles are recruited by a complex network of neurons instead of specific set of neurons.

Moreover, Fricke et al. (2017) used an interesting setup for studying motor synergies. They did not map muscle representations on the motor cortex but movement representations. In their research 49 different locations around the hotspot of the abductor pollicis brevis were

stimulated and finger joint movements were recorded as a response to TMS using a custom–built data glove. Subjects also performed the hand function test containing grasps for real physical objects wearing the data glove. These movements were classified into precision and power grasps and then reconstructed from TMS-evoked movements as a linear combination of the components obtained by principal component analysis (PCA). From their results Fricke et al. (2017) concluded that it could be suggested that two types of grasps have differential organization on the motor cortex and movement representations are synergistically organized on the motor cortex.

Regarding muscle synergies, also so–called action maps have been found on the motor cortex in animal studies (Brecht et al. 2004; Graziano et al. 2002; Graziano 2016; Harrison et al. 2012). These maps include representation areas of different ethological movements. When the cortical location representing certain action has been stimulated, the corresponding spatiotemporal activation pattern of several muscles has been elicited. However, due to invasive methods used to find these action maps, studies have not been performed in humans. Thus, it is still unclear if such a functional structure exists in humans.

Furthermore, it could be possibly intuitively and logically concluded that the overlapping of representations realized between different muscles on the motor cortex in different hotspot (or other) locations indicates, in addition to synergies, which muscles' MEP patterns can be most effectively separated into classes according to the selected (hotspot) points. Thus, the overlap of the muscle representations on the cortex would also tell something about the categorization of different points, or the categorization (classification result) would tell something about the overlap of the representations.

# 5 SURFACE ELECTROMYOGRAPHY

The action potential triggered on the muscle fiber membrane travels from the synapse to the ends of the muscle fiber. Potential changes on the muscle fiber membrane associated to the action potential can be measured using electrodes placed into the muscle or on the skin over the muscle as explained in Section 2.5. These types of recordings are called intramuscular EMG and surface EMG (sEMG), respectively. (Enoka 2015, 195) In this chapter sEMG is described to the extent it is used in this study.

## 5.1 Measure of muscle activation

Recording the potential difference across the cell membrane would require placing one electrode inside the membrane and another outside the membrane. However, when using sEMG, both electrodes are placed on the skin outside of the muscle. Thus, sEMG recordings do not indicate changes in the membrane potential but are indicators of extracellular field potentials that are associated with potential changes in the muscle cell membrane. Moreover, because an action potential of the lower motor neuron usually induces an action potential in all muscle fibers belonging to the same motor unit (the lower motor neuron and all muscle fibers innervated by it), sEMG recording indicates muscle activation by the nervous system. When using sEMG, potential changes from multiple muscle fibers under electrodes are recorded, Figure 16. (Enoka 2015, 195, 197; Kamen & Gabriel 2010, 10–11)

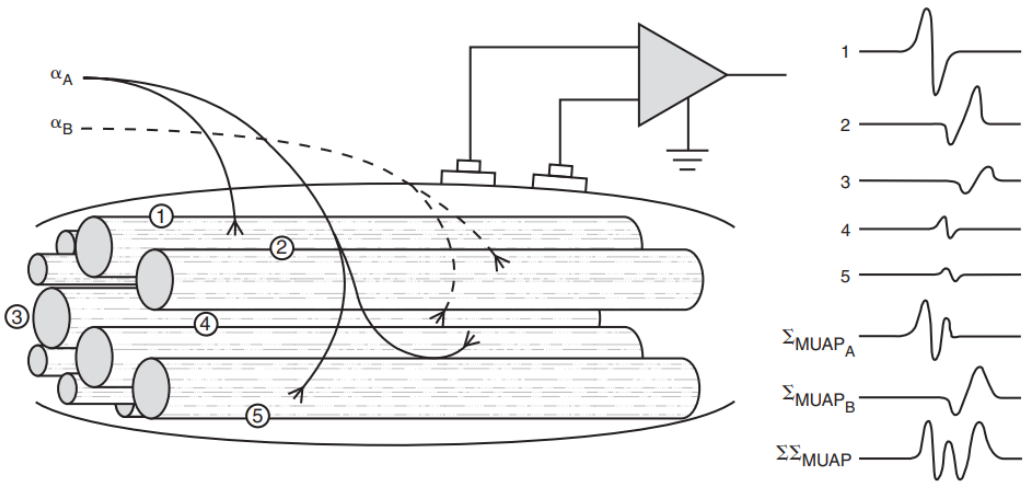


FIGURE 16. Surface electromyography signal is spatiotemporal sum of the potential changes from multiple muscle fibers (numbers 1–5) innervated by motor nerves ($\alpha_A$ and $\alpha_B$) and motor unit action potentials (MUAP A and B). (From Kamen & Gabriel 2010, 11)

The signal recorded by sEMG includes the action potentials of multiple motor units and the amplitude of sEMG represents the spatiotemporal sum of the potential changes from multiple muscle fibers. (Enoka 2015, 195; Kamen & Gabriel 2010, 10–11) sEMG signal provides information about the timing and intensity of muscle activation but is also influenced by other factors. (Enoka 2015, 197)

## 5.2 Contaminated recordings

Action potentials conducting along the muscle fiber create the field potential having negative and positive phases. In addition, action potentials from individual muscle fibers inside the motor units as well as action potentials from different motor units do not happen at the same time. This results in an effect known as amplitude cancellation in sEMG recordings. (Enoka 2015, 197) Furthermore, an electrode location can increase the level of amplitude cancellation if electrodes are located too close to the neuromuscular junction (Kamen & Gabriel 2010, 68). A common way to minimize this problem is to measure the peak value of the MVC and to use this for normalizing sEMG amplitude. (Enoka 2015, 197)

sEMG signal can also be contaminated by unwanted content like radio–frequency noise or movement of the electrodes relative to the muscle fibers. If these disturbances happen at known frequencies, it is possible to decrease their influence on the recorded sEMG signal by using different signal filtering techniques. Depending on the frequencies of the unwanted factors, low–pass–, high–pass–, band–pass– or band–stop–filtering can be used to modify and eliminate the wanted frequency content of the sEMG recording. (Enoka 2015, 198) Common frequency band used to extract useful content from the raw signal has been 10–500 Hz (Park & Lee 1998; Phinyomark et al. 2012; Simão et al. 2019).

The field potentials associated with action potentials can also be conducted beyond the muscle fibers. Because of this sEMG signals originating from the muscles nearby the recorded one are included in the recorded signal at least to some extent. This effect is known as crosstalk and its contribution to the recorded signal increases with fat thickness or if the electrodes are placed over the tendon. Quantifying and removing effects of the crosstalk is difficult task that cannot be done completely because the frequency content of the crosstalk overlaps with the frequencies of the target muscle fiber action potentials and components of the crosstalk have different effect to the sEMG recording at small and large distances. However, there are approaches for this like

calculating the cross–correlation coefficients for indicating the crosstalk or using a comparison between differential and double–differential recordings. (Enoka 2015, 199; Kamen & Gabriel 2010, 88, 119, 125–126)

### 5.3 Monopolar and bipolar electrodes

sEMG can be recorded using mono- or bipolar electrodes. Selection between these affects the sensitivity and specificity of recordings. Monopolar electrode configuration is more sensitive to changes in muscle activity. However, it is also more sensitive to common signal components from distant sources, or crosstalk, which decreases signal–to–noise ratio. This makes it more difficult to detect changes in electrical activity recorded from muscles. To avoid or minimize this it is important to conduct measurements in an electrically isolated room and place electrodes over the electrically identified motor point. (Gabriel 2011)

Another electrode arrangement, the bipolar configuration, being a differential recording process, decreases amplitudes and rate of change in the signal. However, bipolar electrode configuration also reduces crosstalk because it suppresses common signal components from distant sources. (Gabriel 2011) Thus, bipolar configuration is spatially more selective than monopolar configuration which provides a more global view of muscle activation. In this context, it should also be noted that a muscle fiber orientation is three dimensional and this may change as a function of joint position and muscle force. Because of this there is usually an alignment error as bipolar electrodes should be aligned with the muscle fiber direction. Due to alignment error amplitude and frequency content may be altered. Monopolar configuration, in turn, does not require this kind of alignment. (Mohr et al. 2018)

# 6 CLASSIFICATION OF EMG PATTERNS

To the author's knowledge, there are no studies concerning classification of MEP patterns based on locations of the cortical stimulation. EMG signals are usually classified into categories according to the movements or pathology (for example Hudgins et al. 1993; Kocer 2010; Phinyomark 2013). However, the way corticocortical and corticospinal processes are activated is different from TMS–induced activation of these same processes. Thus, the signals induced by these processes and measured with sEMG are not similar in nature between the two situations. Also, MEPs are transient signals when EMG induced by the natural movement is continuous signal. Because of these reasons, according to the studies found, it is difficult to draw conclusions about the performance of classification methods when classifying MEP patterns according to cortical locations used to give TMS stimuli. In any case, this chapter discusses the classification of sEMG signals and classification theory, as this knowledge is the starting point for building a classifier that classifies MEP patterns according to the corresponding cortical location of TMS stimuli. Among the classifiers, the focus is especially on a multilayer perceptron (MLP), because this was chosen as the classifier structure of this study.

## 6.1 Earlier studies on sEMG classification

From the viewpoint of classification, the raw EMG signal consists of unwanted and interference parts as well as useful information part. Classification using a raw signal is possible but usually different feature extraction methods are used to distinguish characteristics needed for good quality classification from recorded signals. In this section classification results with different classifiers and features extracted from voluntary movement induced EMG signals are presented.

Englehart et al. (1999) studied time–frequency domain features for the classification of the sEMG signal. They used features calculated by the short–time Fourier transform, the wavelet transform, and the wavelet packet transform as well as time domain features used by Hudgins et al. (1993). They also used a Euclidean distance class separability criterion and the PCA for reduction of the dimension of the feature vector. Linear discriminant analysis (LDA) and MLP were used as classifiers. sEMG recordings from the biceps brachii and the triceps brachii were classified into four separate classes corresponding to flexion and extension of the elbow, and pronation and supination of the forearm. In their study Englehart et al. (1999) achieved the best

classification accuracy of 93.75% when using the wavelet packet transform together with LDA and PCA.

Phinyomark et al. (2012), in turn, studied classification using LDA classifier, and 26 time and 11 frequency domain features calculated from EMG recorded from five muscles: extensor carpi radialis longus, extensor carpi ulnaris, extensor digitorum communis, flexor carpi radialis and biceps brachii. They classified sEMG signals according to six upper limb movements. It was discovered that time domain features showed good redundancy, especially those based on energy and complexity, and frequency information. When using only one feature, auto–regressive coefficients– and Cepstral coefficients–features achieved classification accuracies of 92.1% and 91.5%, respectively. For the three–element feature vector classification accuracy was 94.2%. Also, the subset feature combination (integrated EMG, slope sign change, zero crossing, Wilson amplitude) used by Du et al. (2010) was tested and the classification accuracy of ~ 96% was achieved. Features based on frequency domain were not efficient. Later Phinyomark et al. (2013) studied performance of 50 time and frequency domain features when classifying sEMG recordings from four electrode pair locations according to ten upper limb movements. In this research the LDA classifier was compared with random forest, decision tree, quadratic discriminant analysis, support vector machines, K–nearest neighbor and MLP. The LDA produced the best results, and the best single feature was a sample entropy with 94.49% accuracy. The best feature combination was the sample entropy, the Cepstral coefficients, the waveform length, and the root mean square with 98.87% classification accuracy. Also, many other classifiers have been studied. These include artificial neural networks, Bayesian classifier, fuzzy logic and deep neural netwoks (for example Ahsan et al. 2011; Chan et al. 2000; Coskun et al. 2021; Furui et al. 2021; Phunruangsakao et al. 2022).

## 6.2 Principles of classification

The classification can be supervised or unsupervised. Unsupervised methods generate associations between the training data when the class information is unknown, for example Rajan & Rayner (1995). Supervised classification methods, in turn, generate mapping from the input vectors to the known class information, for example Alonso et al. (2014). Only supervised classifying is discussed here, because classifying sEMG patterns according to the known cortical location of stimuli is a supervised process.

In the supervised classification there are $K$ classes $C_i$, $i = 1, ..., K$ and the classifier is built using a training data set $X$, which is in the form shown below (Alpaydin 2014, 32–33).

$$X = \{\boldsymbol{x}^t, \boldsymbol{r}^t\}_{t=1}^N$$

where $\boldsymbol{x}$ denotes input vector to be classified, $t$ denotes an index of the sample in the set $X$, $N$ is amount of the samples in the set $X$ and $\boldsymbol{r}$ denotes a class label vector, which has $K$ dimensions and can be written as follows (Alpaydin 2014, 33).

$$r_i^t = \begin{cases} 1, if\ \boldsymbol{x}^t \in C_i \\ 0, if\ \boldsymbol{x}^t \in C_j, j \neq i \end{cases}$$

The problem in the classification is to find boundaries in the input space that separate classes from each other's. All possible boundaries define hypothesis class $H$ from which $C$ comes. In other words, the goal is to define hypothesis $h \in H$, or set of boundaries, that can classify samples belonging to $C$ as correctly as possible. So, the hypothesis $h_i$ predicts if a sample $\boldsymbol{x}^t$ comes from $C_i$ and can be written in the next form. (Alpaydin 2014, 24, 33–34)

$$h_i(\boldsymbol{x}^t) = \begin{cases} 1, if\ \boldsymbol{x}^t \in C_i \\ 0, if\ \boldsymbol{x}^t \in C_j \end{cases}$$

Because the training set $X$ represents only subsets of classes $C$, it is unknown how well $h_i(\boldsymbol{x})$ matches $C_i$. For this reason, the empirical error tells how many samples from the given data set were classified incorrectly, or how many predictions $h_i$ give wrong values when compared to the values given in $X$. This error $E$ of hypothesis $h_i$ given the data set $X$ is written as follows.

$$E(\{h_i\}_{i=1}^K | X) = \sum_{t=1}^{N} \sum_{i=1}^{K} 1(h_i(\boldsymbol{x}^t) \neq r_i^t)$$

where $1(a \neq b)$ equals 1 if $a \neq b$, and 0 if $a = b$. (Alpaydin 2014, 24, 34)

$H$ includes all possible hypothesis $h \in H$, or all possible sets of boundaries, and the goal is to choose the best sets for the classifier. The best set is the one which also classifies samples never seen before correctly. The classifier, which works perfectly, not only for the given training data, but also for the data not seen in the building phase of the classifier, is said to have good generalization capabilities. (Alpaydin 2014, 24) Because the training data can represent only subset of all possible cases to be classified, it is crucial that the training data is as representative as possible.

Different classification methods can be seen as different tools for finding the best set among all possible sets of boundaries, or hypothesis $h \in H$. There are numerous different methods developed for supervised classification. These can be roughly divided into parametric and nonparametric methods; examples are given in Table 2. In parametric methods data samples are assumed to come from known distribution, which can be modeled precisely. This kind of model can usually be defined using a relatively small number of parameters affecting the complexity of the classifier, which is naturally an advantage. The disadvantage is that assumption about distribution and model validity does not necessarily hold being source of error. (Alpaydin 2014, 65, 185)

TABLE 2. Different parametric and nonparametric classification methods.

| **Parametric methods** | **Nonparametric methods** |
|---|---|
| Maximum likelihood | K-nearest neighbor |
| Bayes' estimator | Decision tree |
| Maximum a posteriori estimator | Linear discriminant |
| Nearest mean | Multilayer perceptron |

When using nonparametric methods, no assumptions about distributions are made being advantage of these methods. The only assumption is that similar inputs have similar outputs. In the case of classification this means that the classifier is built using the training data, and when an unseen, or testing, sample is shown to the classifier, it finds the most similar training samples and classifies the new sample to the class including those. Another advantage is that nonparametric models are more robust to the presence of outliers because parameters of parametric methods can be quite sensitive to outliers, for example mean and covariance of the Gaussian. However, in nonparametric methods the model complexity depends on the complexity of the problem introduced by the training data set. This increases the need for memory and computational power, which is naturally a disadvantage. (Alpaydin 2014, 185–186, 199–200)

### 6.3 Multilayer perceptron as classifier

Cognitive scientists' and neuroscientists' goal is to understand how the brain is functioning and what is the meaning of different brain structures. When trying to solve problems connected to

this goal scientists have developed mathematical models of the brain for simulation studies. Engineers have found these models useful when building different applications, for example classifiers. (Alpaydin 2014, 267) In this section the nonparametric classification method MLP is described as it was used in this thesis.

MLP classifier is constructed of basic units called perceptron, which is illustrated in Figure 17. Each unit $i$ has inputs which can be inputs given for the classifier or outputs from other perceptrons in the classifier. Each input $x_d$ connected to unit $i$ is multiplied by its own connection weight $w_{di}$ and each unit $i$ has its own output $y_i$, which is some function $f_i$ of weighted sum of the inputs and is called an activation function. Weighted sum can be written as a dot product between the input $\boldsymbol{x} = [1, x_1, \ldots, x_D]$ and weight $\boldsymbol{w} = [w_{0i}, w_{1i}, \ldots, w_{Di}]$ vectors, where $0^{\text{th}}$ elements represent a bias unit $x_0 = +1$ and the weight $w_{0i}$ connected to it, respectively, as shown in Figure 17. (Alpaydin 2014, 271–273)

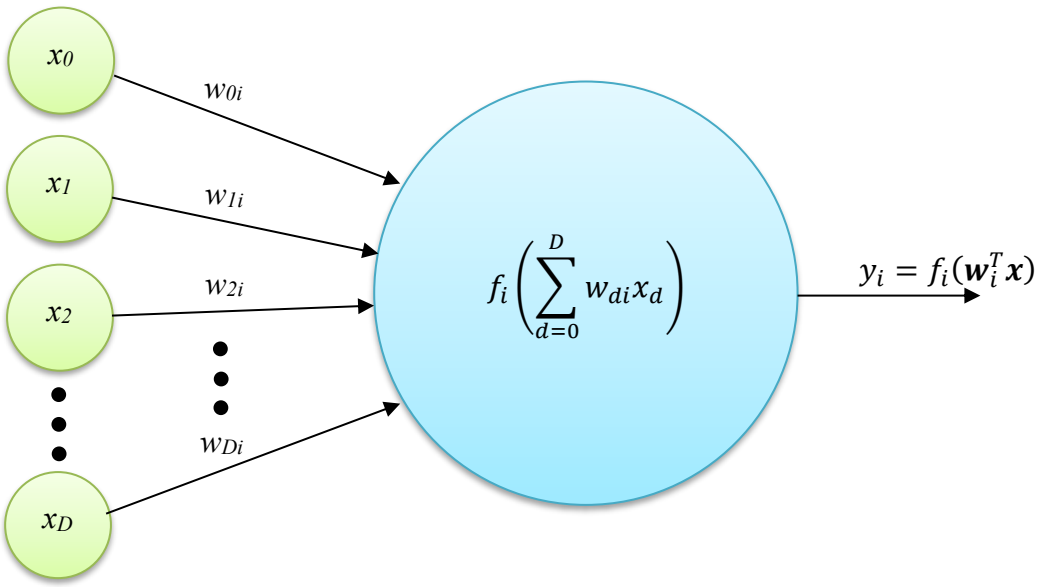


FIGURE 17. Basic unit of the multilayer perceptron, where $x_d$, $d = 0, \ldots, D$, are inputs to the unit $i$, $w_{di}$, are weights connecting input $d$ to unit $i$, $y_i$ is output of the unit being a function $f$ of weighted sum of inputs, $x_0 = +1$ is a bias unit. (According to Alpaydin 2014, 271)

MLP is a network of perceptron units where there are one or more layers of perceptrons, so called hidden units, between input and output layers of the network, see Figure 18. The advantage of this kind of structure is that it has a universal approximation capability meaning that it can implement any set of nonlinear boundaries or high-dimensional surfaces between different classes. Inputs “activate” hidden units, which activate hidden units of the next layer

or output units. (Alpaydin 2014, 279–280; Hornik et al. 1989) In other words, the MLP forms a function of weights which maps the input space to the output (or class) space.

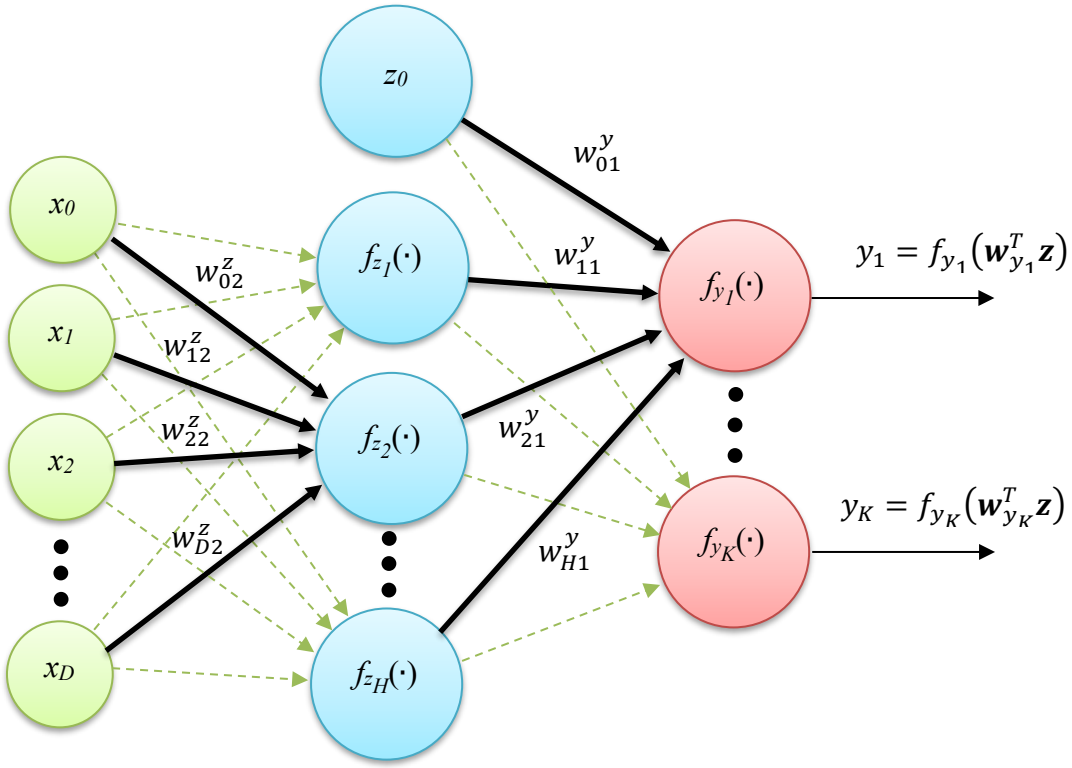


FIGURE 18. Illustration of the multilayer perceptron with one hidden layer, where $x_1, \ldots, x_D$ are inputs of the network. The hidden layer $z$ consists of $H$ units, whose activation functions are $f_{z_1}, \ldots, f_{z_H}$. Outputs from the hidden layer are $z_1, \ldots, z_H$. The output layer consists of $K$ units, whose activation functions are $f_{y_1}, \ldots, f_{y_K}$, and outputs are $y_1, \ldots, y_K$. Weights $w^z$ connect inputs to the hidden layer and weights $w^y$ connect outputs of the hidden layer to the output layer. Vector $\boldsymbol{w}_{y_K}$, denotes the vector of weights from the hidden layer to the unit $K$ in the output layer. Vector $\boldsymbol{z}$ contains outputs from the hidden layer. Other vectors for inputs and weights are formed similarly. The input layer as well as the hidden layer have bias units $x_0 = +1$ and $z_0 = +1$, respectively. (According to Alpaydin 2014, 281)

The network described here as an example has one hidden layer. However, the number of hidden layers does not need to be limited. There can be as many hidden layers as is practical for the problem to be solved. The network having one hidden layer is easier to analyze, but with more than one hidden layer it is possible to implement more complex relations between input and output. (Alpaydin 2014, 280–281)

The problem is to find values for the weights $w_{ij}$ minimizing an error $E$ between the predicted class and the correct class for given training sample. An idea of mathematical methods developed for this task is based on the gradients of the error function calculated with respect to the weights as written by the following equation.

$$\nabla_{w_{ij}} E = \frac{\partial E}{\partial w_{ij}}$$

where $i = 0, \ldots, D$ and $j = 1, \ldots, H$ for weights of the hidden layer, and $i = 0, \ldots, H$ and $j = 1, \ldots, K$ for weights of the output layer corresponding to the Figure 18.

Gradients determine the tangent of the error function in the point specified by the weight values or the direction in which the value of the error function is decreasing (or increasing). Thus, weights are updated in the direction of calculated gradients. When gradient equals zero, the minimum (or maximum) point has been found and the learning process can be terminated. (Alpaydin 2014, 249–250) Figure 19 shows the three-dimensional (two weights and error value) illustration of this procedure.

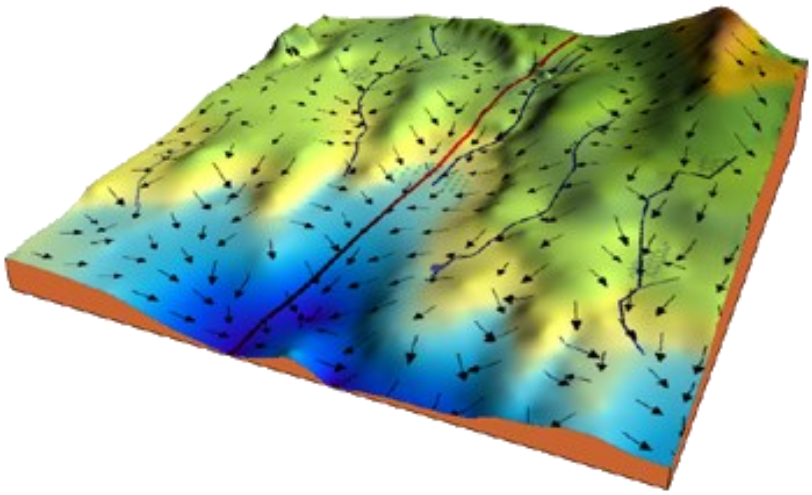

FIGURE 19. Graph illustrating weight optimization: the error function defines a surface where gradients (arrows) show the direction of decreasing error values, which is used to decide what is the direction where possible minimum point could be found. (From Read the Docs, 2017)

When MLP is used as a classifier, the number of the output units is usually the same as the number of classes. The class $i$ chosen to be a result of classification can be written as following.

$$Choose\ C_i\ if\ y_i = \max_k y_k$$

where $k = 1, \ldots, K$ is index for the $k^{\text{th}}$ output $y_k$. Furthermore, cross-entropy is used as an error function for classifiers and is written as follows.

$$E^t(\boldsymbol{w}_{z_h}, \boldsymbol{w}_{y_k} | \boldsymbol{x}^t, \boldsymbol{r}^t)\big|_{h=0,\ldots,H;k=0,\ldots K} = -\sum_t \sum_i r_i^t log y_i^t$$

where $i = 1, \ldots, K$ denotes number of the class, $\boldsymbol{w}_{y_k}$ denotes the weight vector connecting outputs of the hidden layer to $k^{\text{th}}$ unit in the output layer, $\boldsymbol{w}_{z_h}$ denotes the weight vector connecting inputs to $h^{\text{th}}$ unit in the hidden layer, $\boldsymbol{x}$ denotes input sample, $\boldsymbol{r}$ denotes the correct class labels and $t$ denotes $t^{\text{th}}$ training sample, see Figure 18. (Alpaydin 2014, 273, 288–289)

Because the prediction error $E$ depends on the correct and the predicted class labels, it depends on the activation functions inside the network. Thus, gradients of $E$ are calculated as derivatives with respect to the weights. Whichever functions are chosen as the activation function, they should be differentiable and nonlinear because mapping from the input space to the output space should be nonlinear as true nature of the data is unknown. The activation function for the hidden layer unit is usually Gaussian, sigmoid, or hyperbolic tangent. For the output layer unit, it is usually, in the case of classifier, a so called softmax function. Functions shown below are the hyperbolic tangent on the left and the softmax on the right as they were used in this thesis.

$$z_i = \tanh(\boldsymbol{w}_i^T \boldsymbol{x}) = \frac{e^{2\boldsymbol{w}_i^T \boldsymbol{x}} - 1}{e^{2\boldsymbol{w}_i^T \boldsymbol{x}} + 1} \qquad y_j = \frac{e^{\boldsymbol{w}_{y_j}^T \boldsymbol{z}}}{\sum_k e^{\boldsymbol{w}_{y_k}^T \boldsymbol{z}}}$$

where abbreviations are written according to Figure 18 and $\boldsymbol{w}_i$ denotes the weight vector connecting input $\boldsymbol{x}$ to the unit $i$ in the hidden layer, $\boldsymbol{w}_{y_j}$ denotes the weight vector connecting output vector $\boldsymbol{z}$ of the hidden layer to the output layer's unit $j = 1, \ldots, K$; $e$ denotes an exponential function and $k = 1, \ldots, K$ is index for the $k^{\text{th}}$ output. (Alpaydin 2014, 273, 280)

Weight values are updated every time after one pair of training samples and corresponding class label is introduced to the network or changes are accumulated and values are updated after a complete pass of the whole training set. Calculated gradients are multiplied by some coefficient called learning factor, which determines how big is a step taken in the direction of the gradient. There are multiple different methods and variants developed for more stable convergence of the optimization algorithm and finding the minimum point of the error function. These methods are based on, for example, conjugate gradients, second order gradients or controlling the step size taken when updating weights. (Alpaydin 2014, 275, 285, 290–291; Battiti 1992)

# 7 PURPOSE OF THE STUDY

The main goal of this study was to investigate whether it is possible to separate cortical TMS locations on the basis of the corresponding MEP patterns measured from multiple muscles of the upper limb. As already stated earlier, to the author's best knowledge there are no previous studies in which a similar type of classification would have been studied. In previous classification studies EMG signals have been usually classified into categories according to voluntary movements or pathologies (for example Hudgins et al. 1993; Kocer 210; Phinyomark 2013). Therefore, the perspective in this study is new.

In previous motor cortex mapping studies of multiple muscles, it has been found that muscle representations on the motor cortex overlap (for example Melgari et al. 2008; Tardelli et al. 2022) and different movements would also have different representations on the cortex (Fricke et al. 2017). Researchers have concluded from these results that the muscles are synergistically organized on the motor cortex. From another point of view, one could ask whether there is a muscle or group of muscles producing MEP patterns which accurately distinguish the corresponding cortical stimulus locations from each other. Or in other words, is there a single muscle or single group of muscles from which, based on the recorded MEP patterns, it can be calculated, which has been the corresponding stimulus location on the motor cortex. When performed from this point of view, the classification result does not tell about muscle synergies. It tells about the separability of cortical stimulus points when the measure is classification accuracy produced by MEP patterns recorded from certain muscle combination. This information can be used in the future, when the aim is to separate the cortical areas corresponding to different gestures from each other. In the future, a practical application could be, for example, a surgeon's tool, which is used to plan operations in such a way that the desired functions are saved.

Because other studies concerning the same problem could not be found, the problem was set to a very basic level for starting to paint the big picture. Cortical locations forming classes were chosen from different upper limb segments and specific stimulus locations were determined as hotspots of chosen muscles. Research questions and hypothesis are listed below.

*Primary research question.* Is it possible to classify cortical TMS locations according to corresponding MEP patterns from multiple upper limb muscles?

*Hypothesis of primary research question.* The classification of MEP patterns as described presumably produces good results. Earlier in Section 3.3 it was pointed out that by increasing the stimulus intensity, the amplitude of MEPs also increases (Groppa et al. 2012†; Rossini et al. 2015). In addition, in Section 4.2.1, it was stated that the MT value is at its lowest in the hand and forearm area and increases to the proximal direction (Groppa et al. 2012†; Rossini et al. 2015). In this work, three hotspots from three segments of the hand and arm (hand, forearm and upper arm) are used as stimulation points and the stimulus intensities are calculated as a percentage of rMT. Based on this, the amplitude alone will act as a factor differentiating MEP patterns induced by stimulating different hotspots. In addition, there are a total of 16 muscles recorded. One could assume that there is always a combination of these that produces MEP patterns being separable according to determined hotspot locations. It should also be noted here that according to the results of Melgari et al. (2008) and Tardelli et al. (2022) discussed in Section 4.3, the overlap of the cortical representations differs between different muscles of the hand and arm. This means that the probability for different muscles of producing MEPs simultaneously when certain cortical area is stimulated differs between muscles. Based on this, the probabilities for different muscles to produce simultaneous MEPs and amplitudes of those simultaneous MEPs determine typical MEP patterns for each stimulated hotspot. Obviously, the more those patterns differ from each other, the better the classification accuracy will be and vice versa.

*Secondary research question 1.* What is the minimum muscle combination size producing the highest classification accuracy?

*Hypothesis of secondary research question 1.* As discussed in Section 3.3, individual corticocortico and corticospinal connections as well as local excitability of the spinal motoneurons influence TMS responses. Because of this, the minimum muscle combination size producing the highest classification accuracy is presumably individual. However, it should be noted here that a large enough sample size is required to show individuality.

*Secondary research question 2.* Is there a muscle combination with that size (secondary research question 1) being the most optimal?

*Hypothesis of secondary research question 2.* Melgari et al. (2008) and Tardelli et al. (2022) found overlapping representations of muscles as explained previously. Some muscles are

overlapping more and some less. One might assume that depending on individual corticocortical and corticospinal connections, different hotspot locations would have different sets of overlapping and non-overlapping muscles, and for overlapping muscles, the degree of overlap would differ between hotspot locations. Therefore, it would be logical that there exist a muscle combination(s) producing MEP patterns that are more separable from each other for different hotspots than other combinations do, in which case the classification accuracy would be higher than for other combinations.

*Secondary research question 3.* How often is each measured muscle included in the most optimal combinations, i.e., which are the most informative muscles?

*Hypothesis of secondary research question 3.* As with hypothesis of secondary research question 1, this is probably very individual because corticocortical connections are individual, so the prevalence of individual muscles in the combinations producing the highest classification accuracy presumably varies between individuals at least to some extent. Furthermore, one could also assume that there is some systematicity. The human body has anyway systematic structure and between individuals' way of use of that structure resembles each other from which one could suggest that there exist some systematicity in prevalence of separate muscles in the most optimal combinations. Intuitively thinking, at least hotspot muscles could be thought to be included in the most optimal combinations. However, this may not be the case. It should be kept in mind that the only reason for muscle to be included in the combination is its MEPs' capability to separate selected hotspots from each other. This depends on what extent cortical representation areas of the recorded muscles are overlapping and how these overlappings are with respect to each other in stimulated hotspot locations. Anyway, again a large enough sample size is needed to show this.

# 8 METHODS

10 healthy 20–45 years old subjects participated in this study. Six of them were women and four were men. The recruitment was carried out by announcement on the University of Jyväskylä's website and social media channels and through word of mouth. Subjects did not have any neurological or musculoskeletal disease. Contraindications to TMS were checked according to Wassermann (1998). All of them were right–handed which was verified by Edinburgh handedness score (Oldfield 1971). Subjects participated in one measurement session and before the data collection they provided a written consent. Due to the too high rMT values (see later in Section 8.3), sequences of 120% of rMT could be run for seven, and three participants had to be rejected completely. All the experimental procedures conducted in this study were approved by the University of Jyväskylä ethics committee. In this chapter these procedures are explained.

## 8.1 Experimental setup and protocol

The setup, illustrated in Figure 20, consisted of four parts: preparation, hotspot hunting, rMT measurement and running TMS-sequences. In the preparation part sEMG electrodes were attached to 16 right side upper limb muscles. After this subject sat on the measurement chair upper limbs placed to the pillow palms facing downwards forearms in pronated position. This position was kept similar during all stimulations to keep proprioceptive feedback from the upper limb as constant as possible, see Figure 21. Next, sEMG electrodes were wired and signal quality was checked for all channels. Finally, the subject’s head and the TMS coil were registered for the use of Localite nTMS system. After this in the hotspot hunting and rMT measurement phases hotspots for three muscles, abductor pollicis brevis (APB), flexor carpi radialis (FCR) and biceps brachii long head (BBl), were located and rMT values were measured, see Section 8.3 for more information. In the sequence running phase TMS sequences were run at 120% of rMT stimulus intensity so that 50 stimuli were applied to each hotspot. Stimuli were pseudorandomized into sequences of 25 stimuli, where the intensity was kept the same. Thus, there were a total of 6 separate sequences. For each stimulus, sEMG responses from all 16 muscles were measured and recorded. Duration of the entire measurement session was 3.5–4 hours.

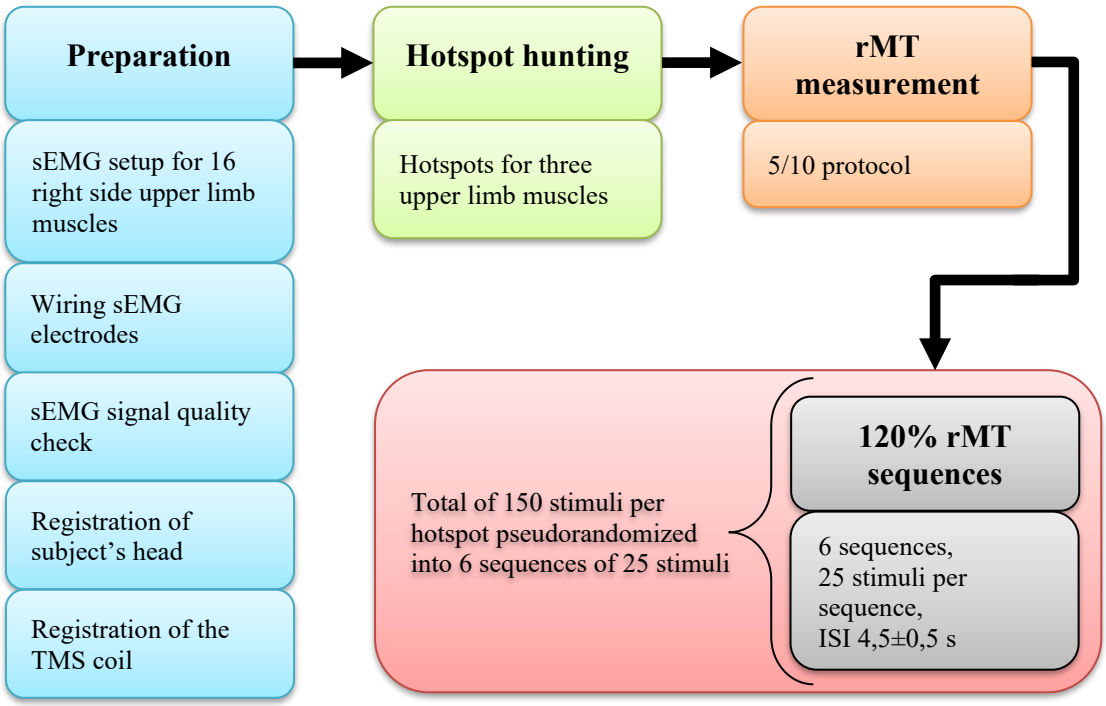


FIGURE 20. Illustration of the experimental protocol (sEMG refers to surface electromyography, rMT to resting motor threshold and ISI to interstimulus interval).

FIGURE 21. Subject on a TMS chair with sEMG electrodes attached and wired - a pillow was used to stabilize the hand and arm.

## 8.2 Electromyography

sEMG was recorded from 16 right side upper limb muscles. These are given in Table 3. Bipolar Ambu BlueSensor N-00-S/25 diameter 6 mm surface electrodes were used. The locations of sEMG electrodes were based on the innervation zones according to Barbero et al (2012, 81–82, 105–120) and study from Piccoli et al (2014). The ground electrode was placed on the styloid process of the ulna. Before placing the electrodes, skin was shaved, scrubed with fine sandpaper, and cleaned with alcohol on electrode locations. After attaching and wiring the electrodes, the background noise in the sEMG signal was visually controlled to be under ±10 µV. Bittium Biosignals Ltd NeurOne system black model main unit, Tesla amplifiers, JackBox and software version 1.5.2–mr1 were used to collect sEMG signals. A/D resolution of this system is 24 bits and system gain is 50. Sampling frequency was set to 2000 Hz, for which device filter was 500 Hz low–pass filter.

TABLE 3. Recorded muscles. (Muscles whose hotspots were used for classification are shown in red.)

| | | |
|---|---|---|
| **Upper arm** | deltoid posterior | (PD) |
| | deltoid anterior | (AD) |
| | deltoid lateral | (LD) |
| | triceps brachii lateral head | (TBlat) |
| | triceps brachii medial head | (TBmed) |
| | biceps brachii short head | (BBs) |
| | biceps brachii long head | (BBl) |
| **Forearm** | brachioradialis | (B) |
| | flexor carpi ulnaris | (FCU) |
| | flexor carpi radialis | (FCR) |
| | flexor digitorum superficialis | (FDS) |
| | extensor digitorum communis | (EDC) |
| | extensor carpi ulnaris | (ECU) |
| **Hand** | 1st dorsal interosseus | (FDI) |
| | abductor pollicis brevis | (APB) |
| | abductor digiti minimi | (ADM) |

## 8.3 Transcranial magnetic stimulation

MagVenture MagPro R30 stimulator and MagVenture C–B60 figure–of–eight coil were used for the motor cortex stimulation, see Figure 22. Localite TMS navigator version 3.3.32 and the standard MNI ICBM152 non–linear symmetric T1 average brain data were used for navigating the coil locations (Localite 2014). TMS pulse waveform was biphasic. First, the hotspots for BBl, FRC and APB were located by checking which points give the strongest MEPs for those muscles (hotspot hunting). At this point, the orientation of the coil was varied to find the most optimal hotspot for each selected muscle. Hotspot locations were saved for the neuronavigation, which was used to show to operator the coil location with respect to the saved hotspot. Tolerances for the coil position and orientation for all stimuli were two millimeters and two degrees measured from the saved hotspot. Next, rMT values for each hotspot muscles were measured and recorded using the 5/10 relative frequency method described in Section 4.2.1.

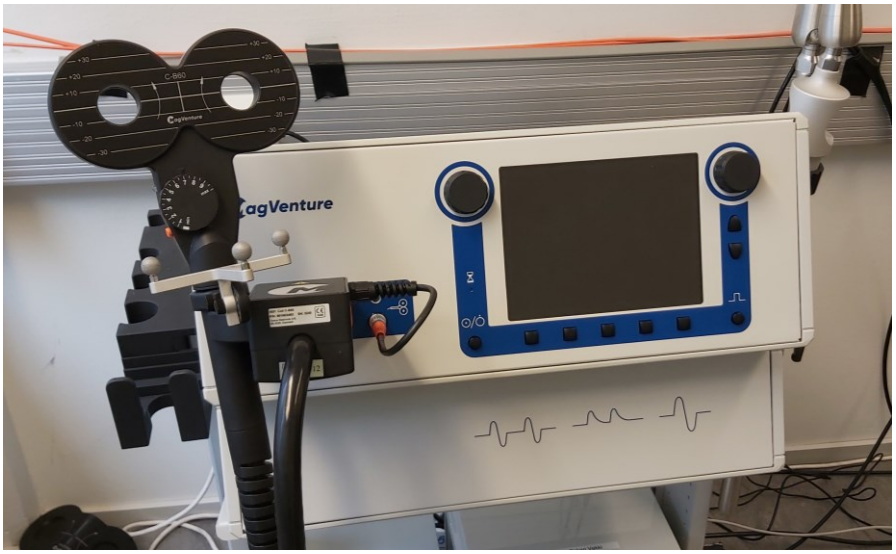


FIGURE 22. MagVenture MagPro R30 stimulator and C-B60 figure–of–eight coil.

After locating hotspots and measuring rMTs, the TMS sequences at 120% of rMT stimulus intensity, generated using the MagVenture Paired–Pulse composer version 1.0.0, were run. The interstimulus interval (ISI) between stimuli was randomized to 4,5±0,5 seconds. Sequences contained 50 stimuli per hotspot. These were pseudorandomized into subsequences of 25 stimuli, where the stimulus intensity was held constant. Thus, there were a total of 6 subsequences in randomized order. Neuronavigation was used when running these sequences as previously explained. Since the intensity used in the sequences was 120% of rMT, it could

exceed the maximum intensity of the used stimulator. If the rMT exceeded 83% of this, sequences could not been run. Because of this, sequences could be run for seven subjects, as was already explained earlier.

## 8.4 Data preprocessing

All data processing (preprocessing, classification and analyzing) was done with Python 3.9 and the Scientific Python Development Environment (Spyder) 5.1.5. Data was loaded using Neurone loader package (Heilmeyer & Ball 2019). Preprocessing was carried out with the algorithms included in the Scipy 1.9.1 and the Numpy 1.21.5 packets written for Python. Whole preprocessing is illustrated in Figure 23.

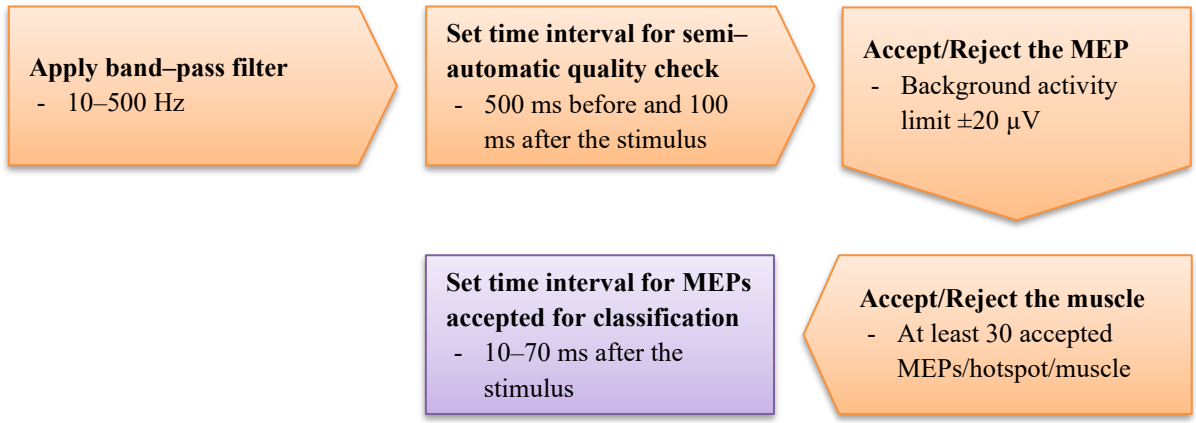


FIGURE 23. Schematic illustration of the data preprocessing.

In the pre-processing phase, the data of each muscle and each sequence was initially filtered with a band-pass filter implemented with a butterworth filter, the band of which was set to 10–500 Hz. The filter itself was a first order filter and it was applied once forward and once backward to the signal resulting in a second order filter. This was done because otherwise the filtering would produce a phase shift with respect to the original signal (Gustafsson 1996). After this, a time interval was extracted around each stimulus from 500 ms before the stimulus to 100 ms after the stimulus for review, see Figure 24. If signal values greater than ±15 µV occurred during the 500 ms before the stimulus, the response was checked manually. Otherwise, it was accepted automatically. In manual review, the response was rejected if it had values above/under ±20 µV during 500 ms before the stimulus or the signal was otherwise too disturbed during the chosen time interval. A minimum of 30 accepted MEPs per hotspot was required for each measured muscle to be accepted for classification. Finally, MEPs were

extracted from the sEMG signal between the time interval 10–70 ms after the stimulus. Since the sampling frequency was 2000 Hz, the length of one MEP was 120 samples.

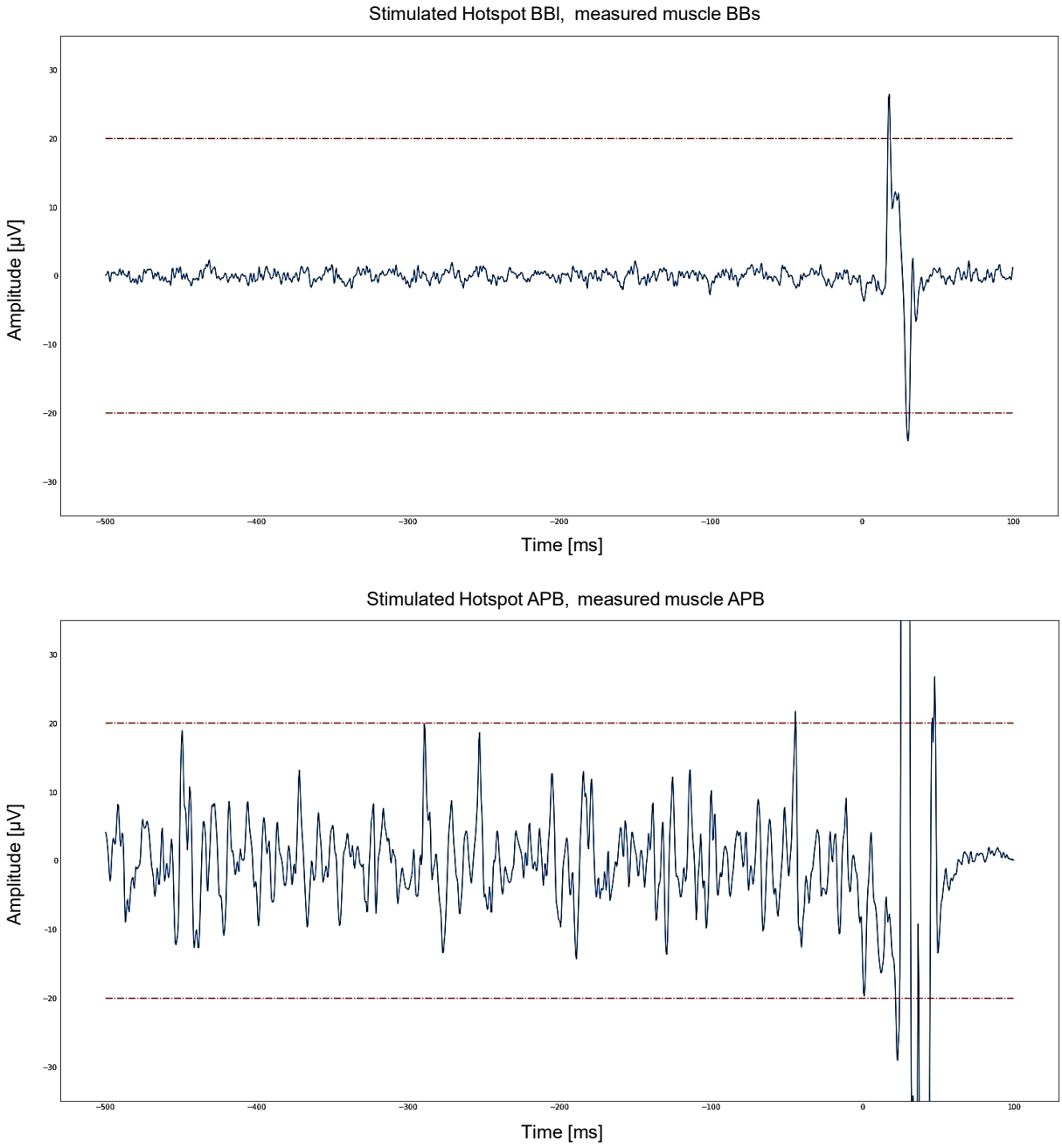


FIGURE 24. Examples of accepted (top) and rejected (bottom) MEP in a same representative participant. Dashed lines show ±20 μV rejection limit.

## 8.5 Classification

The main research question in this thesis was whether the MEP responses measured in the 16 muscles of the hand and arm could be classified according to the hotspots of three hand and arm muscles (APB, FCR and BBl) used to apply stimulation. The raw data vector after preprocessing was used for building and testing the classifiers. The amount of collected data was relatively small and it was not known how non-linear the data is in nature. As discussed earlier in Section 6.3, MLP has been shown to have the property of being a universal approximator (Hornik et al. 1989). So, it was chosen as a starting point for this kind of study. The input for the MLP was formed by concatenating the MEPs evoked by a single stimulus into a vector, see Figure 25. Each element of the vector formed one input unit to the MLP. The elements contained in the vector were scaled by subtracting the mean value of each element in the training data set and dividing the result by the element–specific standard deviation. Test data was also scaled using the same mean and standard deviation values. This scaling is applied for the MLP to converge better (Alpaydin 2014, 285).

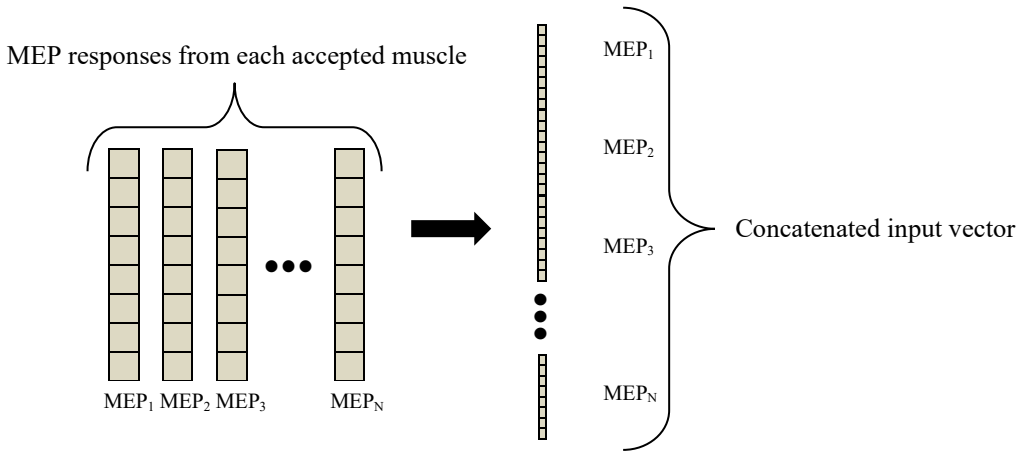


FIGURE 25. Multilayer perceptron's input vector. Each element in the concatenated vector forms one input unit. $MEP_1$, …, $MEP_N$ denote motor evoked potential signals for muscles 1, …, N, where N is number of the accepted muscles.

The full data set was divided into training and test data in a ratio of 70/30%, respectively, see Figure 26. The division into training and testing data was randomized and performed separately for each individual MLP trained. Next, the size of the network was set to be two hidden layers, both layers with three units. The activation function and the weight optimization algorithm were chosen as a hyperbolic tangent (see Section 6.3) and a limited memory Broyden–Fletcher–Goldfarb–Shanno (LBFGS) algorithm (Liu & Nocedal 1989), respectively. The regularization

parameter controlling the step taken toward the minimum point of the error function was set to 0.1. These parameters were searched and chosen by using the data of one subject, and the GridSearchCV and MLPClassifier algorithms included in the Scikit 1.0.2 machine learning and data mining packet for Python. Accuracy was chosen to be the measure of MLP's performance, meaning the amount of correctly classified test samples.

When searching for suitable parameters, 8-fold cross-validation (Alpaydin 2014, 559) was used in the training phase, i.e., the training data was divided into eight parts, each of which served in turn as a validation set measuring the network's performance, while the other 7/8 parts of the training data were used as a training set to optimize the network's weight values. The accuracy was estimated by averaging the results for the validation sets and the combination of parameters producing the highest average was selected. The final test accuracy was calculated for this parameter set using the test set, see Figure 26.

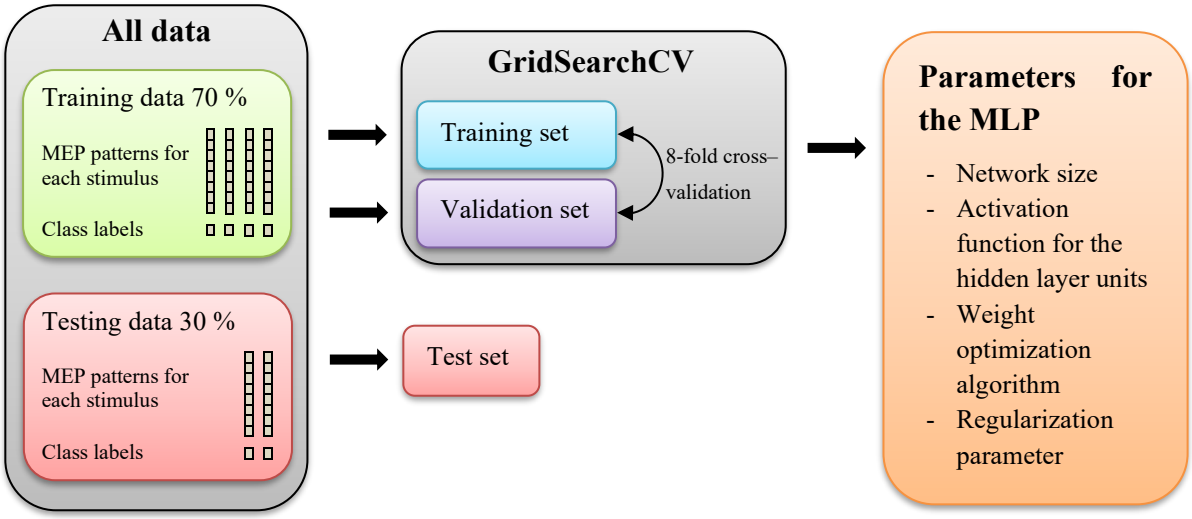


FIGURE 26. Splitting the data into training and test data, and the training and validation set.

With the selected network construction, one MLP was initially built for each possible muscle combination. The number of possible muscle combinations depended on the number of muscles accepted for classification, being a maximum of 65535, if at least 30 accepted MEPs per hotspot were obtained from all 16 recorded muscles (Section 8.4). Simplified model for the final MLP construction is shown in Figure 27. Construction of the input layer and hidden layers was explained in this section and formation of the output layer was explained in Section 6.3.

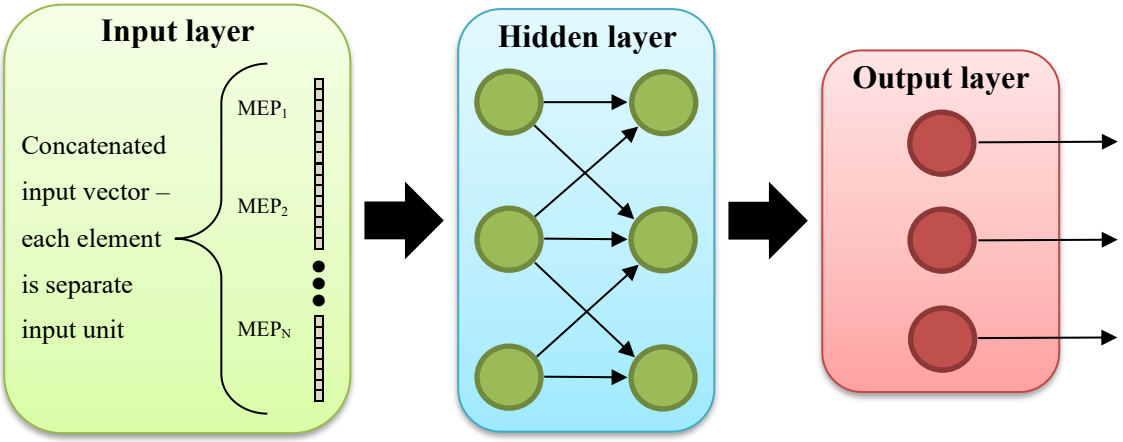


FIGURE 27. Simplified presentation of the final MLP classifier. $MEP_1$, $MEP_2$, …, $MEP_N$ denote MEPs for muscles 1, 2, …, N, where N is amount of the accepted muscles.

## 8.6 Evaluation of the classifier's performance

The performance of the MLP classifiers was evaluated by the classification accuracy and confusion matrices. The classification accuracy is defined as the number of correctly classified samples of the test set. In this work, all classes contained an equal number of samples. Thus, the data was well balanced, and the classification accuracy could be chosen as the performance measure (Ballabio et al. 2018). The confusion matrix, on the other hand, tells the amount of the classes predicted, when it is known what the correct class would have been, see Figure 28. In other words, one can read from the confusion matrix which classes were classified correctly and which classes were confused with each other and to what extent (Alpaydin 2014, 564).

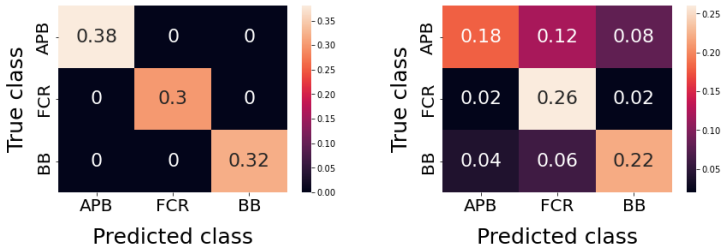


FIGURE 28. Examples of confusion matrices for two selected muscle combinations.

In the confusion matrix, the row indicates the correct class, and the column indicates the class predicted by the classifier. The sum of all cells equals one, and the values on the diagonal of the matrix from the upper left to the lower right corner describe the portion of correctly classified samples, which, when summed, gives the classification accuracy. The values of other

cells tell how classes mixed with each other in the case of misclassification. From one point of view, the values of the confusion matrix represent a measure of how separable the MEP patterns obtained by stimulating different hotspots are. The less values are on other than the diagonal, the more separated the MEP patterns belonging to different classes are, and the more reliable the classification is.

## 8.7 Identification of the best classifier and corresponding muscle combination

Several combinations containing different muscles may produce the best classification accuracy. If classification result is as good with a smaller set of muscles as with a larger one, it can be assumed that the muscles of the smaller set have a better descriptive power in terms of the classification problem. On this basis, among the combinations with the same classification accuracy, the combinations containing less muscles were considered better or more descriptive.

Due to the large number of combinations (as stated in Section 8.5), initially only one classifier was trained for each combination. Since there were a maximum of only 50 samples (or MEP–patterns) per class (or hotspot), 70% of which were used for building the classifier and 30% for testing, the contribution of chance to the classification accuracy for a given combination could be high. It should also be noted that the weight coefficients of the trained MLP classifier represent the minimum of the multidimensional error function used in network optimization. The minimum point can be local or global, and it is found by changing the weight coefficients using the optimization algorithm. Weights are initialized randomly when optimization starts, which might lead to finding different minimum points, thus being also a source of randomness in the final classification accuracy. The method presented here for finding the best classifier was therefore aimed at reducing the uncertainty in the results caused by small training and test sets as well as MLP's optimization method, and at the same time to shorten the calculation time caused by the large number of combinations.

As already stated, initially only one classifier was trained for each combination. It was assumed that in this way the minimum size of the muscle combination with the maximum classification accuracy would be found out. From that combination size, 20 muscle combinations with the highest classification accuracies were taken, and 100 MLP classifiers were built for each. The data was randomized to the training and test sets independently for each classifier. Based on the classification results for these 100 classifiers, the classification accuracy distribution could

be formed for each of the 20 selected combinations. A mean value was defined for each distribution, which was set to describe the performance of separate classifiers. Next, the six muscle combinations with the highest mean values were taken into final investigation. Since the obtained distributions for accuracies were not normally distributed, the Monte Carlo bootstrap method (Carpenter & Bithell 2000) was used to estimate the mean of the distribution with its confidence intervals and standard deviations with significance level α set to 0.05. Finally, classification accuracies and confusion matrices for these six best classifiers were stored for comparison. The whole process is summarized in Figure 29.

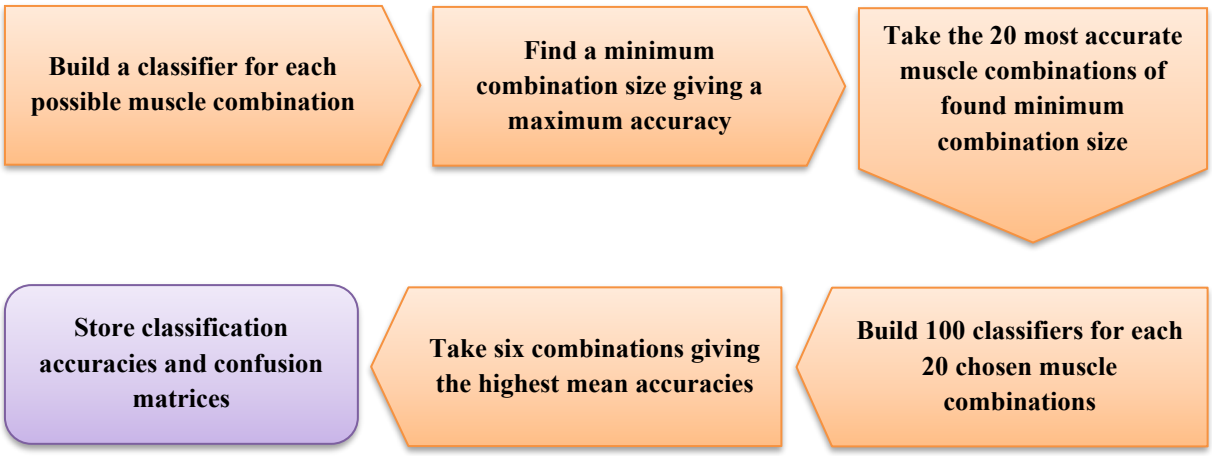


FIGURE 29. Schematic illustration of the selection process of the best classifiers.

The selected six muscle combinations giving the highest estimated mean accuracies were also statistically compared based on the distributions of the test accuracies. Python packages Statsmodels 0.13.2, Pingouin 0.5.3 and Scikit–posthocs 0.7.0 were used for these calculations. Significance level α was set to 0.05. The Shapiro-Wilk test (Shapiro & Wilk 1965) and Brown-Forsythe variation of the Levene test (Brown & Forsythe 1974) were used to test normality and homogeneity of variances, respectively. The statistical significance of the difference in distributions was tested with the Kruskal–Wallis test (Kruskal & Wallis 1952) and pairwise comparisons were calculated using Dunn's post–hoc test (Dunn 1964) with a Bonferroni adjustment. These calculations with estimated mean accuracy values were used to find out the most descriptive combination(s).

It is good to note that these results contain classification accuracies from three different perspectives: subject–specific, combination size–specific, and combination–specific accuracies. Subject–specific classification accuracy represents the classification accuracy of

individual subject. There can be several muscle combinations and combination sizes with a certain classification accuracy. The combination size–specific accuracy, on the other hand, refers to the classification accuracy achieved for one separate combination size. Thus, there can be many separate muscle combinations reaching the same accuracy in this context as well, but now their size is the same. The combination–specific accuracy refers to the accuracy achieved by one separate muscle combination. Naturally there can be only one of these accuracies per combination per built classifier.

## 8.8 The importance of the distances between hotspots and the combination size for the classification accuracy

In addition to the above, the correlation between the distance between the hotspot locations on the motor cortex and the maximum estimated mean classification accuracy among six chosen muscle combinations was calculated for all hotspot pairs in order to see if the distance between the points stimulated on the cerebral cortex can partially explain the classification result. Since the distributions of the estimated mean classification accuracy and the distances between hotspots were not normally distributed (tested with the Shapiro-Wilk normality test), Spearman's correlation coefficient (Spearman 1904) was used. Calculations were performed using the pairwise_corr function included in the Pingouin 0.5.3 package written in Python.

Correlations were also calculated between the maximum estimated mean classification accuracy and the corresponding minimum combination size. In the calculation, the data obtained from all accepted measured subjects were used and the correlation was calculated using Spearman's correlation coefficient, since the combination size is an ordinal scale variable.

# 9 RESULTS

The results first show the muscles accepted for building the classifiers for each subject. This is followed by a presentation of the results including the muscle combinations giving the highest classification accuracies, the prevalence of muscles in these, the minimum size combinations giving the maximum estimated mean classification accuracy, the performance analysis of the classifiers built with those combinations, and the statistical analysis of the most accurate combinations. Finally, the results are presented for the correlations calculated between the distances between hotspots and the maximum estimated mean classification accuracies, as well as between the smallest combination sizes that give the highest estimated mean classification accuracies and corresponding accuracies. Due to the large amount of data, the complete statistical results are given for readability in Appendix 1 and are referred to in the text when necessary. In addition, as previously stated, due to rMT values being too high for some subjects, the results are shown for seven subjects, which makes analysis unreliable and should be noted.

## 9.1 Accepted muscles for the classification

Muscles accepted for the classification (see Section 8.4) are presented in Table 4 for all subjects. As can be seen from the table, there is quite a lot of variation in the muscles accepted for classification between subjects. This means that different muscle sets for individual subjects were used when choosing the optimal muscle combination for classification. This should be remembered when analyzing the results, because the data used for different test subjects was not consistent with each other.

In this context, it should be noted that for some subjects, the rMTs became so high that the measurement at 120% of rMT intensity was unsuccessful, leading to the rejection of that subject. This was the case for three test subjects, which is why the table contains information about the accepted muscles for only seven subjects. Rejection in all these cases was due to too high rMT for the hotspot of BBl. In addition, some muscles were rejected due to bad quality sEMG signal. Because of this data measured from all 16 muscles could be used only in the case of one subject.

TABLE 4. Accepted muscles for each subject.

| | | S1 | S2 | S3 | S4 | S5 | S6 | S7 |
|---|---|---|---|---|---|---|---|---|
| **Number of accepted muscles** | | 12 | 10 | 16 | 13 | 15 | 15 | 13 |
| **Muscles** | PD | | | | | | | |
| | AD | | | | | | | |
| | LD | | | | | | | |
| | TBlat | | | | | | | |
| | TBmed | | | | | | | |
| | BBs | | | | | | | |
| | BBl | | | | | | | |
| | B | | | | | | | |
| | FCU | | | | | | | |
| | FCR | | | | | | | |
| | FDS | | | | | | | |
| | EDC | | | | | | | |
| | ECU | | | | | | | |
| | FDI | | | | | | | |
| | APB | | | | | | | |
| | ADM | | | | | | | |

Cells filled with the black color refers to 'not used' – status and S1 – S7 denotes subject 1 – subject 7.

### 9.2 Muscle combinations with the highest classification accuracies

At first, an MLP network was trained for each possible muscle combination. The classification accuracy, i.e., the number of correctly classified samples, was calculated for these combinations. Figure 30 shows an example of the best combinations for each combination size for subject 1. The same figure also includes the maximum combination size–specific and the subject–specific classification accuracies. At this stage, only one classifier was built for each muscle combination. For some combination sizes, several separate muscle combinations produce the maximum combination size–specific accuracy. For some subjects, there were hundreds or even thousands of these combinations.

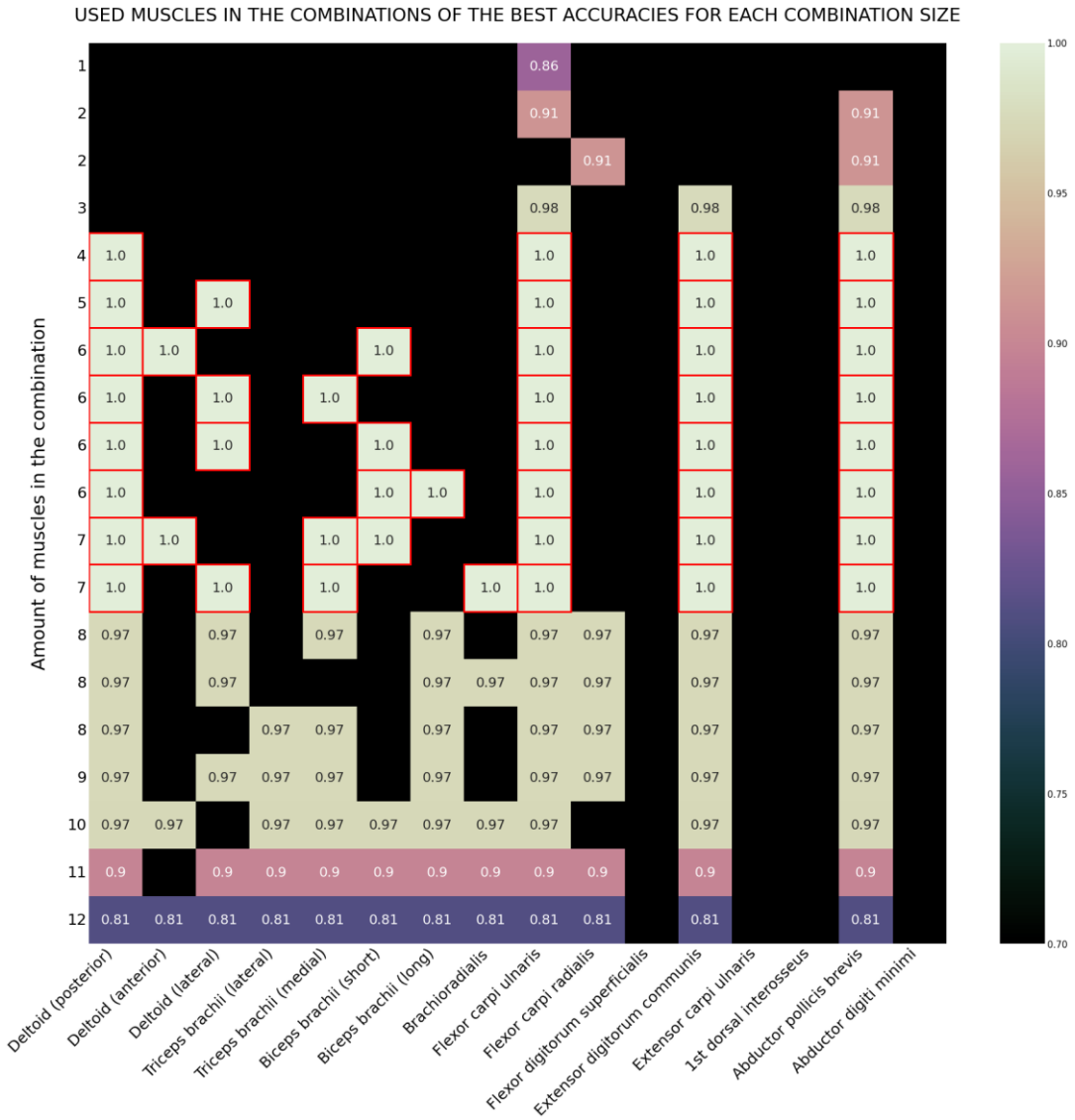


FIGURE 30. Used muscles (columns) giving the best combination size–specific accuracies for each combination size (rows) for subject 1. The best subject–specific accuracy for the subject in question is circled.

Next, the prevalence of each muscle in all combinations that achieved the maximum subject–specific classification accuracy was calculated. An example for two subjects is given in Figure 31. For some subjects, not a single muscle was found that appeared in all the combinations achieving the highest classification accuracy. On the other hand, for some subjects, there was only one combination that achieved the maximum subject–specific classification accuracy, in which case the prevalence of the muscles belonging to that combination was naturally 100%.

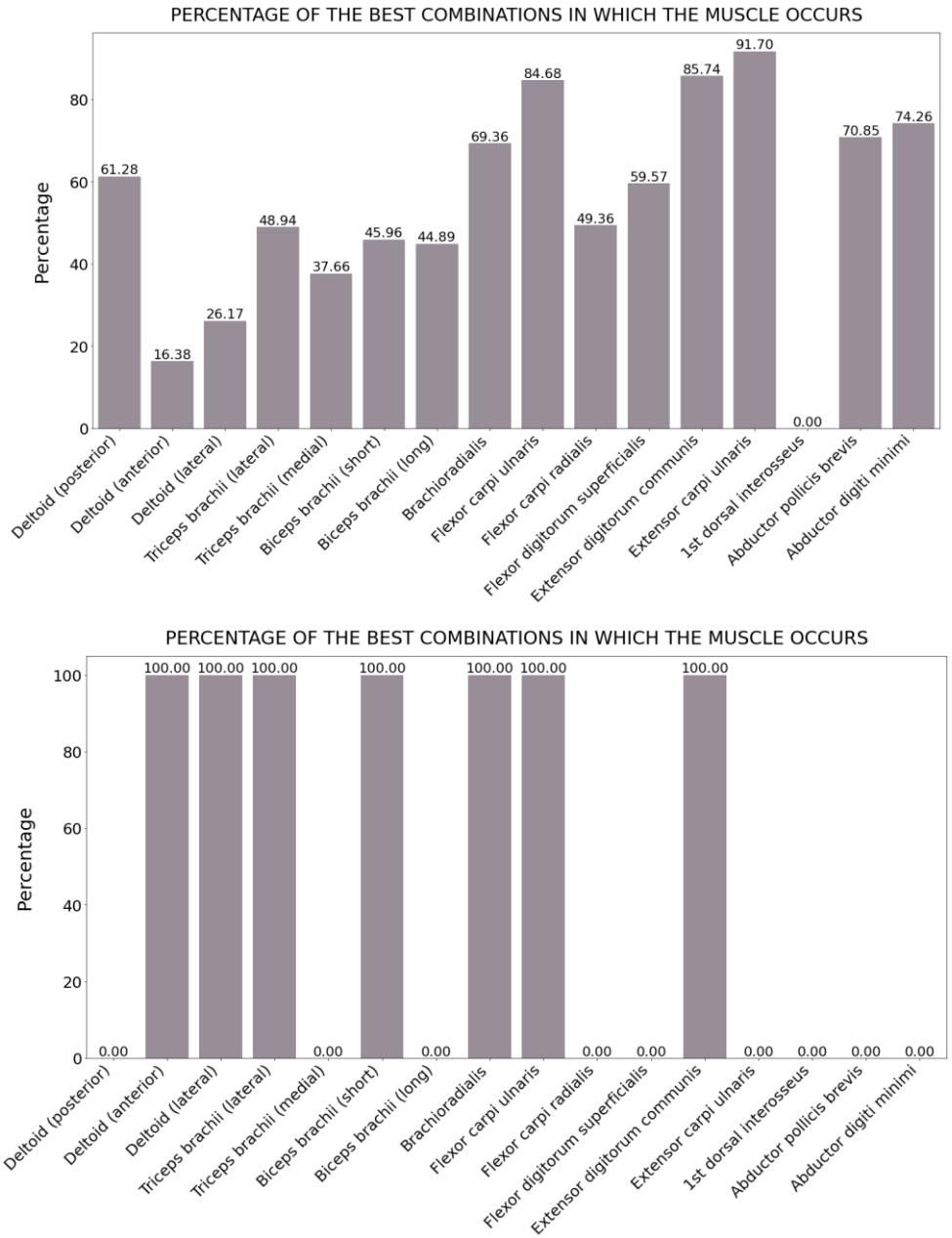


FIGURE 31. Prevalence of each muscle in the best combinations that achieve the maximum subject-specific classification accuracy among all combination sizes for two subjects (top: subject 5, below: subject 7).

In any case, the distribution of different muscles among the combinations giving the maximum subject–specific classification accuracy was highly individual and variable. This can also be seen in Figure 32, where the prevalence of muscles in the combinations that reached the maximum subject–specific classification accuracy calculated among all subjects is shown. It should be noted here that there were quite many unaccepted muscles which differed from

subject to subject. This could naturally affect the results, especially when the number of subjects was small.

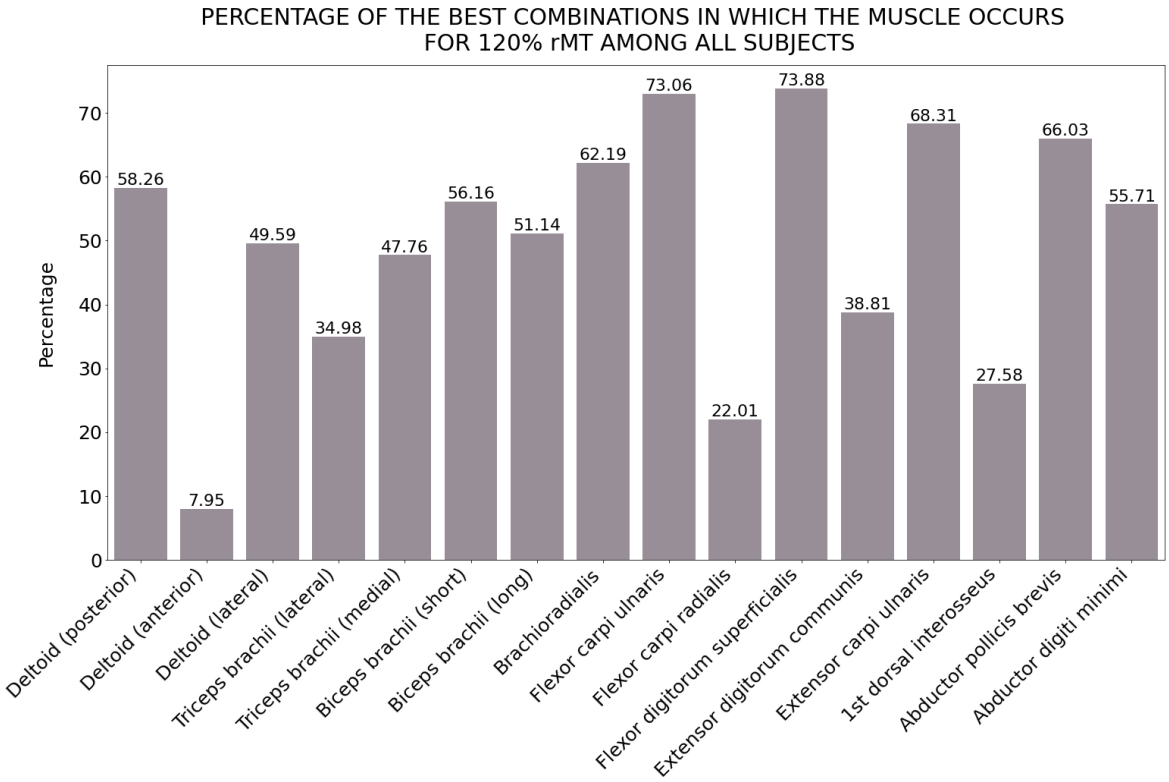


FIGURE 32. Prevalence of each muscle in the combinations achieving the maximum subject-specific classification accuracy among all subjects.

### 9.3 The best minimum size combinations

Based on the information summarized in Figure 30, it was possible to determine the smallest combination size that gives the maximum subject–specific classification accuracy. From this combination size, 20 combinations giving the highest classification accuracies were selected. Next, 100 MLP classifiers were built for each of those 20 combinations to form classification accuracy distributions. Then the six combinations with the highest estimated mean combination–specific classification accuracies were selected for deeper investigation as these were expected to be the most descriptive ones in terms of the classification task, as presented in Section 8.7. These combinations are shown in Figure 33 for selected subjects. In addition, the minimum sizes of the subject–specific muscle combinations that gave the highest estimated mean classification accuracies are reported together with the number of all available muscles per subject in Table 5.

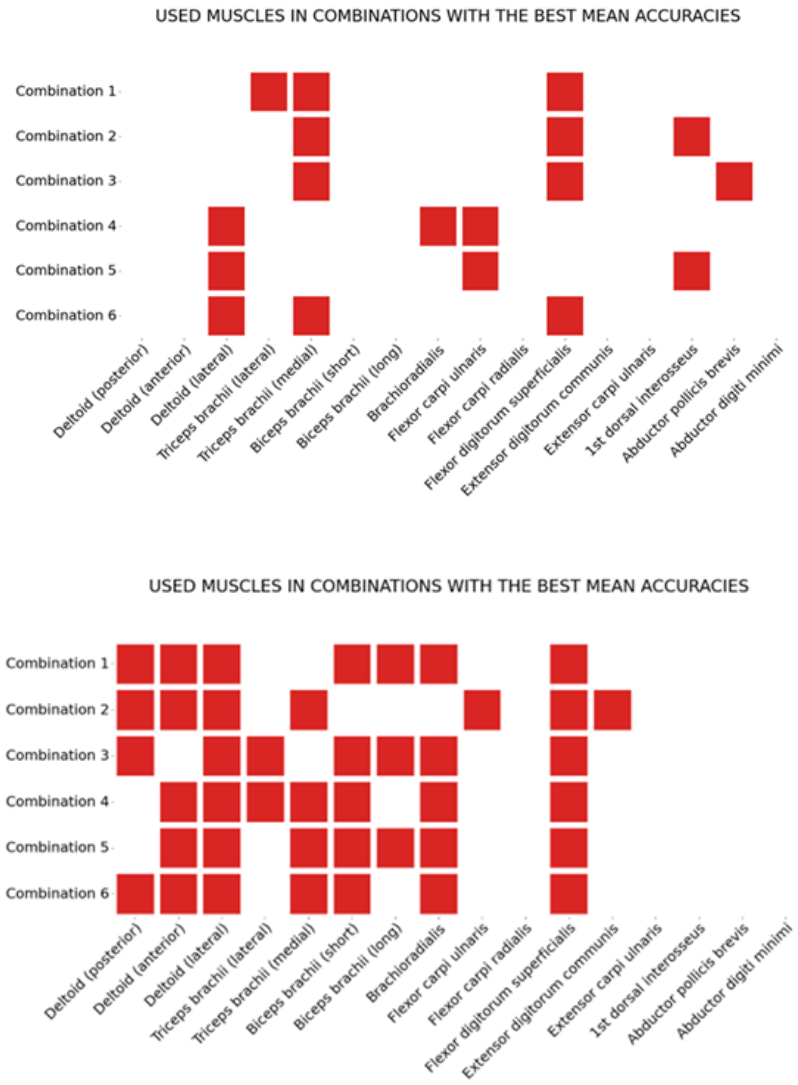


FIGURE 33. The six smallest muscle combinations giving the highest combination–specific estimated mean classification accuracies for the selected two subjects (top: subject 4, below: subject 7).

TABLE 5. The minimum sizes of the subject–specific muscle combinations that gave the highest estimated mean classification accuracies together with the number of all available muscles per subject.

| | **S1** | **S2** | **S3** | **S4** | **S5** | **S6** | **S7** |
|---|---|---|---|---|---|---|---|
| **All muscles** | 12 | 10 | 16 | 13 | 15 | 15 | 13 |
| **Used muscles** | 4 | 7 | 8 | 3 | 4 | 8 | 7 |

S1 – S7 denotes subject 1 – subject 7

From Figure 33 above it can be seen that muscle combinations producing the best estimated mean classification accuracies vary both between and within subjects. Again, it should be

recalled that muscles accepted for classification vary from subject to subject, which could affect these results. This variation can also be seen in Table 5. Statistical analysis of the accuracy distributions is given in Section 9.5.

## 9.4 Separability of the MEP patterns between different classes

The confusion matrices for the six muscle combinations giving the highest estimated mean classification accuracies for all subjects are shown in Figure 34. From these figures one can notice that the largest values are on the diagonal representing correctly classified cases. This is true for all subjects. When class APB is the correct class, it mixes quite often with class FCR and sometimes with class BB. When the correct class is FCR, it mixes sometimes with APB and rarely with BB. When the correct class is BB, it mixes rarely with both APB and FCR. Based on these results, it seems that the classes APB and FCR are most often confused with each other. However, the small sample size makes analysis difficult.

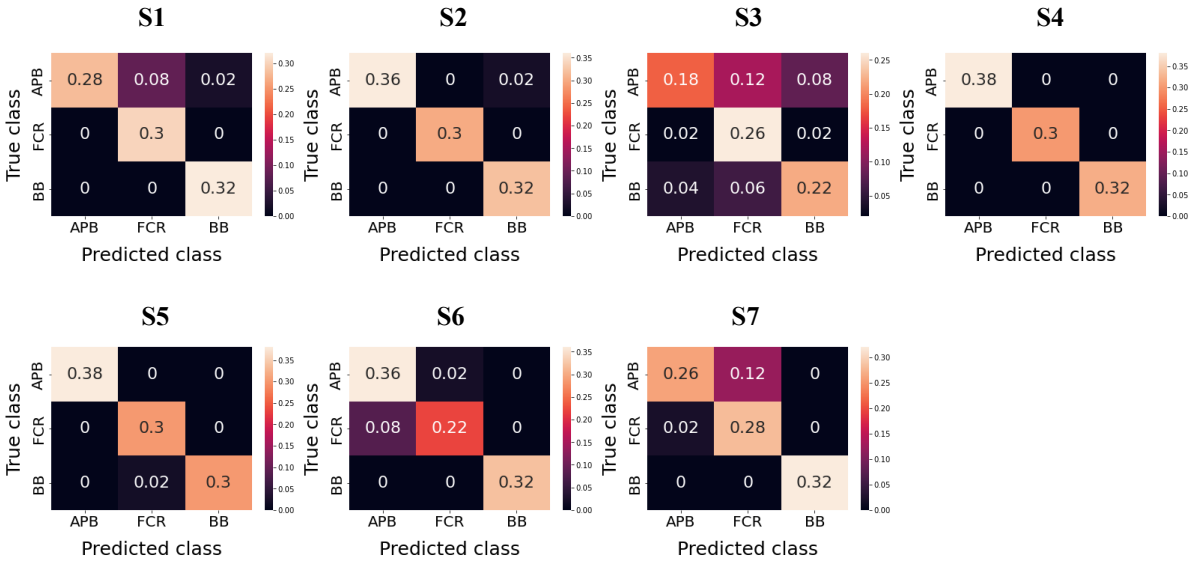


FIGURE 34. Confusion matrices for combinations that gave the highest estimated mean accuracy for each subject (S1 – S7 denotes subject 1 – subject 7).

In this context, it is also good to note that the sum of the diagonal of the confusion matrix is not necessarily the same as the highest estimated mean classification accuracy. This is because the estimation was calculated based on the accuracies provided by 100 classifiers, as described in Section 8.7, and confusion matrices were constructed using the classifier whose accuracy most closely matched the estimated value, in which case the two may not be exactly the same.

## 9.5 Statistical analysis of distributions of classification accuracies

A statistical analysis of the accuracy distributions produced by the six muscle combinations that gave the highest estimated mean classification accuracy was calculated. All distributions were non-normally distributed (Shapiro-Wilk $p < 0.05$), and their variances were not homogenous (Brown-Forsythe variation of Levene's homogeneity test $p < 0.05$). Furthermore, statistically significant differences were found in the accuracy distributions of the selected muscle combinations for all subjects (Kruskal-Wallis $p < 0.05$), and Dunn's post-hoc test was used to evaluate which combinations differed from each other significantly. Complete statistical analysis with short conclusions separately for each subject can be found in Appendix 1. Due to the large amount of data, here only the summary of these results is given for readability.

Based on the statistical analyses, the classification accuracy distributions of certain muscle combinations differ significantly from others. Table 6 gives the combinations that gave the highest estimated mean classification accuracies, whose accuracy distributions differ significantly from the distributions not reported in the table but not from each other.

TABLE 6. Combinations for each subject giving the highest estimated mean classification accuracies that differ from other statistically significantly.

| S1 | S2 | S3 | S4 | S5 | S6 | S7 |
|---|---|---|---|---|---|---|
| 1 | 1, 2, 3 | 1 | 1 | 1 | 1, 2, 3 | 1 |

Numbers are in order from the higher accuracy to lower so that smaller number represents higher estimated mean classification accuracy, and S1 – S7 denotes subject 1 – subject 7.

It can be seen from the table above that the accuracy distribution of combination one stands out from all others in five out of seven subjects. In other subjects, combinations one, two and three cannot be distinguished from each other significantly. If the goal were to choose only one combination as the optimal, it would be quite clearly combination number one. Further, the median of these subject–specific highest estimated mean accuracies was 0.910. The corresponding median of combination sizes giving subject–specific highest estimated mean accuracies was 7.

### 9.6 Correlation between the mean accuracies and the distance between hotspots

To evaluate the factors explaining the classification accuracy, the correlation values between the maximum estimated mean classification accuracy and the distance between the hotspot locations were also calculated. In the calculation maximum estimated mean classification accuracies from all subjects were used. The results are shown in Table 7 and calculated distances between hotspots and measured rMTs are given in Table 8.

TABLE 7. Correlations between the maximum estimated mean accuracy and distance between hotspots as well as corresponding confidence intervals and p-values.

| Hotspots | ρ | Confidence interval 95% | p |
|---|---|---|---|
| **APB and FCR** | 0.143 | [-0.68; 0.81] | 0.760 |
| **APB and BBl** | 0.750 | [-0.01; 0.96] | 0.052 |
| **FCR and BBl** | 0.714 | [-0.08; 0.95] | 0.071 |

ρ denotes Spearman's correlation coefficient[2], p denotes p-value for statistical significance

TABLE 8. Distances (mm) between hotspot locations (upper part) and measured rMTs for each subject (lower part).

| Hotspot pair | S1 | S2 | S3 | S4 | S5 | S6 | S7 |
|---|---|---|---|---|---|---|---|
| **APB – FCR** | 17.61 | 12.41 | 5.66 | 8.19 | 10.89 | 18.22 | 8.58 |
| **APB – BBl** | 18.14 | 24.01 | 13.70 | 18.21 | 23.87 | 18.85 | 13.72 |
| **FCR – BBl** | 9.92 | 11.74 | 8.45 | 11.41 | 13.68 | 12.71 | 6.11 |
| **Hotspot** | rMT as percentage of stimulator's maximum intensity | | | | | | |
| **APB** | 40% | 35% | 64% | 55% | 38% | 52% | 39% |
| **FCR** | 42% | 38% | 65% | 48% | 43% | 63% | 44% |
| **BBl** | 57% | 63% | 73% | 65% | 73% | 79% | 55% |

S1 – S7 denotes subject 1 – subject 7

The distance between APB's and BBl's hotspots as well as the distance between FCR's and BBl's hotspots was strongly correlated with the maximum estimated mean classification

[2] Correlation coefficient ρ is a measure of the strength of the relationship between studied variables, which is interpreted so that values $0.00 \leq |\rho| \leq 0.10$ are considered negligible, $0.10 < |\rho| < 0.40$ weak, $0.40 \leq |\rho| < 0.70$ moderate, $0.70 \leq |\rho| < 0.90$ strong and $0.90 \leq |\rho| \leq 1$ very strong correlation; positive and negative values indicate positive and negative correlation, respectively (Schober & Schwarte 2018).

accuracy. For the distance between APB's and FCR's hotspots, the correlation was weak. However, none of these results are statistically significant, although the results for the distances between APB and BBl and between FCR and BBl are close to statistical significance.

### 9.7 Correlation between the mean accuracies and the combination size

Correlation was also calculated between the maximum estimated mean classification accuracy and the corresponding minimum combination size. The result can be found in Table 8 and the correlation line is given in Figure 35. According to this result, the correlation between the maximum estimated mean classification accuracy and the corresponding minimum combination size is positive and weak. However, these results are not statistically significant, as can be seen from the p-value in Table 9.

TABLE 9. Correlation between the maximum estimated mean classification accuracy and the corresponding minimum combination size.

| ρ | Confidence interval 95% | p |
|---|---|---|
| 0.202 | [-0.65; 0.83] | 0.664 |

ρ denotes Spearman's correlation coefficient, p denotes p-value for statistical significance

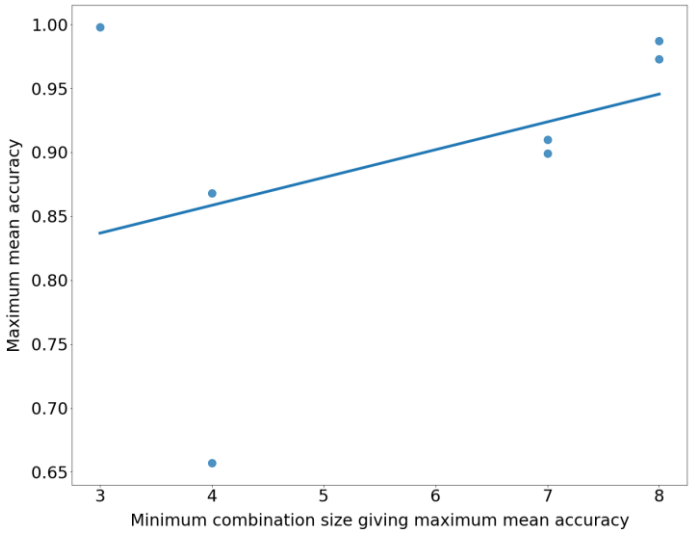


FIGURE 35. Correlation line between maximum estimated mean accuracy and corresponding minimum combination size producing that.

# 10 DISCUSSION

The main objective of this study was to investigate whether it is possible to classify TMS induced MEP patterns from multiple upper limb muscles according to corresponding cortical TMS locations. Since, to the author's best knowledge, no similar studies can be found, the research layout was planned at a rather rough level. The TMS method was used for giving stimuli to three hotspot locations selected for muscles from different segments of the upper limb. MEP responses corresponding to these stimuli were measured in 16 muscles of the hand and arm. The goal was to classify these responses into the corresponding classes indicated by the hotspot locations. The most optimal classifier was the one that could produce the highest classification accuracy with the smallest muscle combination among the recorded 16 muscles. The highest classification accuracy was defined as the highest mean classification accuracy estimated from the accuracy distribution of 100 classifiers built for a certain muscle combination. Due to the large number of muscle combinations, it would have been computationally too time consuming to build 100 classifiers for every possible combination. For this reason and due to randomness of classifiers' optimization process and relatively small number of training samples, the method described in Chapter 8.7 was used to search for six muscle combinations with minimum number of muscles and that achieved the highest estimated mean classification accuracies. The most optimal classifier among those six was chosen by calculating statistical analysis. In this chapter discussions about achieved results are given.

## 10.1 Feasibility to define cortical stimulation location by using classification of MEP patterns from multiple muscles

Complete classifier performance and statistical analyzes were performed on found muscle combinations as described in Chapter 8.7. These analyzes are presented in Appendix 1. The median of the highest estimated mean classification accuracy was 0.91 at 120% of rMT stimulus intensity as presented in Chapter 9.5. Based on these results, it can be concluded that the classification works well. This is not surprising, because the rMT values differ from each other quite clearly for most of the subjects, and at the same time the distances between the hotspot locations are mostly more than 10 mm (see Table 8, Chapter 9.6). Previously, Groppa et al. (2012†) and Rossini et al. (2015) have stated that MT values are at their lowest in the hand and forearm area and increase proximally. The same researchers have also pointed out that as the stimulus intensity increases, the amplitudes of MEPs increase. In addition, from de Goede et al.

(2018), it could be suggested that the distance between the stimulus points should be more than 5 mm, so that the amplitudes of the MEP responses stimulated from these locations would differ from each other significantly. Based on these studies and information in Table 8, it could be assumed that at least the amplitudes of MEP responses are one of the key factors the classifier is using when searching for decision boundaries (see Chapter 6.2). Of course, MLP classifier may also find other factors from MEP patterns that could be used for classification. Further, Melgari et al. (2008) and Tardelli et al. (2022) have shown that the representations of different muscles of the arm on the cortex overlap each other in different proportions for different muscles. Based on these considerations, it is not surprising that a combination(s) among the 16 muscles of the upper limb can be found, from which the recorded MEP responses can be successfully classified according to the corresponding hotspot locations especially in those situations where hotspots are clearly further from each other's than 5 mm. It should also be assumed that variation of the coil orientation on different hotspot locations could have affected the classification results as this affects MEP amplitudes (Souza et al. 2022). However, this study used the MNI average brain data to determine hotspot locations and coil orientations (see Chapter 8.3). Because of this, the coil orientations cannot be related to the individual shape of the subjects' motor cortex sulcus/gyrus, which makes it difficult to evaluate the effect of the orientation in this thesis either.

These conclusions are possibly strengthened by the results of subject 3 (see Appendix 1), which are clearly the least optimal among all subjects in terms of classification accuracy. This happens even though subject 3 was the only one for whom acceptable sEMG data was obtained from all 16 muscles (Table 4). Looking at Table 8, it can be noted that for subject 3 the distance between the APB's and FCR's hotspots is only 5.66 mm. Also, the distance between FCR's and BBl's hotspots is quite small, 8.45 mm. The distance between the hotspots of APB and BBl is 13.7 mm. Although this is already a bit longer, it is also short compared to the corresponding value of the other subjects. So, it would seem that short distances between stimulus locations could have an effect. At the same time, the rMT values measured for APB and FCR are very close to each other and quite high, being 64% and 65%, respectively. The rMT for BBl is also high at 75%. From the confusion matrix of subject 3 (Figure 34, Chapter 9.4) it can be seen that the different classes are clearly more confused than in the other subjects. This is logical, because as the stimulus intensities increase, the electric field induced on the cortex spreads more widely (Deng et al. 2014), selectivity of the TMS stimuli decreases (Souza et al. 2022) and the representation areas of the muscles on the cortex overlap more (Tardelli et al. 2022). If this is

the case, one could assume that the closer the stimulation points are to each other, the more the recorded MEP patterns start to resemble each other. This would make the classification task more difficult.

Different classes seem to be challenging for the MLP classifier in slightly different ways. From the confusion matrices in Figure 34, it is quite clear that of the selected hotspot locations, the hotspots of APB and FCR mixed with each other the most, i.e., the MEP patterns stimulated from these hotspots resembled each other the most. MEP patterns stimulated from the BBl hotspot seem to be generally better separated from the other two classes. These findings are reflected in the classification results. This may be because the rMT of BBl is higher and relatively farther from the rMT of APB and FRC, whose rMTs are closer to each other. In this case, the MEPs stimulated from the hotspot of BBl are generally higher in amplitude than those measured from the other two hotspots, whereby the MEP patterns stimulated from BBl differ more clearly from the MEP clusters stimulated from APB and FCR than the two differ from each other.

## 10.2 Minimum combination size producing the best separability of cortical TMS locations and muscle content of combination

The minimum muscle combination sizes that produced the highest estimated mean classification accuracy are given in Table 5 for each subject. As already pointed out earlier, the highest estimated mean classification accuracy was achieved for each subject with a clearly smaller number of muscles than the number of muscles accepted for the building of the classifier. Table 5 also shows that the minimum combination size of the most optimal classifier was very individual. The prevalence of different muscles in these combinations was also very individual, as can be seen from the graphs in Figures 31 and 32. No single muscle is clearly more included in the most optimal combinations than others, not even hotspot muscles. Interestingly there are muscles (AD, FCR and FDI) which are included more rarely than others in the most optimal combinations, FCR being one of the selected hotspot muscles, see Figure 32.

In Chapter 3.3 it was stated that when applying TMS, induced currents are distorted in the brain tissue due to regional differences in tissue conductivity (Groppa et al. 2012†) and furthermore, it seems that TMS pulse activates cortical interneurons and these, in turn, project to the

corticospinal tract (Opitz et al. 2013; Laakso et al. 2014). In addition, sub-cortical white matter may play some role as it includes axons of corticocortical loop fibers having possible effect to the corticospinal output neurons (Laakso et al. 2014). Triggered action potentials in cortical axons are conducted to other neurons transsynaptically creating signal propagation via cortical, subcortical, and spinal paths. (Groppa et al. 2012††) Due to these neurophysiological factors, TMS pulses targeted at hotspot locations of the same muscles activate different muscles with different MEP amplitudes in different people. Because of this, the MEP patterns differ between subjects, even if the stimulated location was the hotspot point of the recorded muscle.

As already pointed out earlier, Melgari et al. (2008) and Tardelli et al. (2022) noticed that muscle representation areas in the motor cortex overlap. Researchers have hypothesized that this reflects synergistic relationships between muscles. However, the classification accuracy like the one described in this work and the minimum size muscle combination corresponding to specific accuracy do not at least directly tell about the synergy between the selected muscles. In this work, the MLP classifier was used to select a group of muscles which produces MEP patterns that most optimally separate the stimulated hotspot locations from each other. The classification result therefore tells how separable the stimulated cortical locations are according to the MEP patterns recorded from the selected muscles. In other words, based on the MEP patterns of the selected muscle combination, it is possible to form the boundaries $h \in H$ that most optimally separate the different classes as explained in Chapter 6.2. In this case, the combination of muscles does not tell about synergy, but about the separability of cortical stimulus locations based on the recorded muscle activity. Each muscle included in the combination increases the probability of separating the defined cortical locations from each other. Thus, in other words, if some muscle is strongly connected (its representation area is strongly overlapping) with all hotspot muscles, it could be assumed that MEPs recorded from that muscle do not have very strong descriptive power with respect to the classification task in this study. Or vice versa, if representation(s) of certain muscle are overlapping very different ways within selected hotspot locations with other representations of recorded muscles, one could assume that this muscle has high descriptive power with respect to the classification task. The individual combination size and its muscle content could be assumed to tell something about how versatile the control of body areas corresponding to stimulus locations is. The more versatile the neuromuscular control is for a certain person, the more versatile the MEP patterns presumably are, and the more the classifier has opportunities to choose muscles for the combination that produces the most optimal classification result. Through this, there would be

a connection with muscle synergies, but not as straightforward as studies like Melgari et al. (2008) and Tardelli et al. (2022) explain.

In relation to muscle synergies, it has also been suggested that the motor cortex has representation areas for different actions, which have been found in animal studies as explained in Chapter 4.3 (Brecht et al. 2004; Graziano et al. 2002; Graziano 2016; Harrison et al. 2012). When stimulating such representation areas, spatiotemporal activation patterns of several muscles corresponding to different ethological movements have been elicited. Naturally, in different actions, some muscles may be more strongly represented than others. Thus, the classification results obtained now might also have some connection with these so–called action maps. Nevertheless, these animal findings have been based on the use of invasive methods. Because of this, it is still unclear whether similar functional maps can be found in humans as already stated.

It is also good to note that TMS pulse configuration affects the stimulus intensity threshold for inducing MEP (Davey et al. 1994; Laakso et al. 2014). In addition, the orientation of the coil affects the direction of the electric field induced by the TMS pulse on the cortex and the amplitude of the recorded MEP responses (Laakso et al. 2014; Opitz et al. 2013; Reijonen et al. 2020††; Souza et al. 2022) as explained in Chapter 4.2.4. It can be assumed that if these factors can affect the amplitudes of the recorded MEPs, they can presumably also affect the size of the selected muscle combination and the muscles included in the combination. Thus, the size of the combination and the muscles included in the combination not only tell about the individual neurophysiological characteristics, but also about the method of TMS stimulation.

Furthermore, the muscles from which an acceptable amount of data was obtained varied from subject to subject, which can be seen in Table 4. Naturally, this can affect the size of the chosen muscle combination and the muscles included in the combination as well.

## 10.3 Effect of muscle combination size and distance between cortical TMS locations to the separability of TMS locations

The relationship between the highest estimated mean classification accuracy and the size of the muscle combination giving that classification result was also examined. The correlation between these was positive, see Table 9 and Figure 35. This means that when measured at a

120% of rMT stimulus intensity, if the muscle combination size that produces the best classification result for the subject is larger, the classification result is likely to be better than for a subject with a smaller muscle combination size. This would seem logical, because a larger muscle combination size could be thought to be more descriptive. However, this creates a new problem. Why does the maximum possible number of muscles not produce the best classification result for any subject, as can be seen in Table 5? This may be due to individual corticocortical and corticospinal connections that determine which muscle combination produces MEP patterns separating the selected hotspot locations better than other combinations. If muscles are added to this combination and thus the amount of data to be given to the classifier is increased, this is unnecessary and can even disturb the separation of classes. It should also be noted that the size of the MLP classifier was fixed in this study. So, when adding muscles to the data, a point may be reached where the ability of the classifier to separate classes with more complex data decreases. In this case, a higher classification accuracy could possibly have been achieved if an MLP network that adapts to the complexity of the data had been used (Alpaydin 2014, 297–300).

Furthermore, according to Table 7, there is a positive correlation between the distances of each three hotspot pairs and the highest estimated mean classification accuracy. In other words, as the distance between hotspot locations increases, the classification result also improves. This is again logical because according to previous de Goede et al. (2018) results, one could assume that when the stimulus locations are further apart, the MEP responses obtained by stimulating them differ more clearly in amplitude. In any case, it is good to remember that none of the correlation results calculated and presented here were statistically significant, although the results for the distances between APB and BBl and between FCR and BBl are close to statistical significance.

### 10.4 Limitations of this study

The major limitations of this study were the small number of subjects (N = 7) and stimuli (30–50) given to the hotspot locations. The data used to build the MLP classifier is divided, as presented in Section 8.5, into training and test sets. In this work, the size of these sets was determined by the number of stimuli targeted at the hotspot locations. If the size of the training set remains too small, it cannot be trusted that the found minimum point of the error function would represent an optimal solution to the problem being addressed. Each sample of the training

set and the values of the weight coefficients used in the certain optimization iteration determine the point of the error function. If the training set is too small, the optimization algorithm sees too patchy part of the entire multidimensional surface of the error function used for optimization. On the other hand, if the test set is too small, the trained classifier cannot be tested with a sufficiently comprehensive number of samples that the classifier has not seen during the training phase. These problems can be compensated to some extent, e.g., with the cross-validation used in this work, but they cannot be completely eliminated if the amount of data is too small. However, it is difficult to estimate the sufficient size of the dataset because the shape of the error function to be optimized is not known in advance. One measure for a sufficient amount of data could be the variability of the classification accuracy of the built classifiers. When the classification accuracy no longer fluctuates when increasing the size of the dataset, it can be assumed that the result is more reliable. Of course, one should remember that uncertainty is also affected by the used optimization algorithm and its parameters. It must also be understood that when conducting research with real subjects, the time available for measurements becomes a limiting factor. Therefore, it was difficult to exceed the 50 stimuli per hotspot location used in this work.

Not only that the number of subjects or stimuli could be too small for training the MLP classifier from the point of view of the size of the training and test sets, but these were too small when accepting individual muscles for training the classifier. Some number had to be set as the minimum number of approved MEPs, with which the MLP classifier could still be built, see Sections 8.4 and 8.5. If the number of stimuli had been larger, a larger number of muscles could have been accepted for each subject. Actually, if the number of stimuli had been large enough all recorded muscles would have been accepted. Now it happened that different muscle groups were used for different test subjects, from which the minimum size muscle combination that produces the optimal classification result was searched for. Because of this, results are not perfectly comparable between subjects, and it is difficult to say if certain muscles are more important than others. In this context it should be noted that factors affecting the acceptance of the individual muscles were the limits set to the sEMG background activity (±20 μV) and to the number of acceptable MEPs (30). So, the number of the accepted muscles would have also been larger if former of these factors had been larger or later had been smaller. However, if the limit to the number of acceptable MEPs had been smaller, there would have been even less data for building the classifiers, thus affecting classification accuracies very probably negatively. In the former case, if the limit to the sEMG background activity had been larger, accepted MEP

signals would have been more complex and probably more difficult to classify, thus affecting classification accuracy again negatively. It is also good to note that the attachment of sEMG electrodes could have possibly affected the accepted number of muscles.

While the number of stimuli limits the reliability of the classification result, the small number of subjects limits the reliability of the conclusions in group level. It is clear that larger sample size studies are needed to find potential consistencies of optimal muscle patterns in group level. Now the results for prevalence of muscles belonging to the optimal muscle combinations is on unreliable basis because of small number of subjects. In addition, a similar study for the effect of bigger stimulus intensity to classification performance could possibly have been conducted if the sample size was bigger. Same measurement protocol was tried by using 140% of rMT stimulus intensity. Unfortunately, due to too high rMT values for BBl acceptable data was obtained only from four subjects. This amount was too small for conducting reliable analysis thus this part was omitted from the study. However, the sample size used in this study would not have been significantly increased without a significant extension of the time spent on the study, because in addition to measurement sessions the recruitment process takes time.

A limitation directly related to the structure of the MLP classifier is the size and other parameters of the classifier. In this work, these were set based on tests performed on data from one subject, see Chapter 8.5. Thus, there is assumption that data from one subject is enough to determine parameters for all subjects. However, this may have caused in some cases that the optimal classification result was not achieved. If the size of the MLP classifier is too small compared to the complexity of the training data used, the situation is somewhat the same as if a second-order function is used to model a fifth-order function. Of course, some kind of adjustment can be made, but the optimal result is not achieved. If, on the other hand, the size of the network is too large in relation to the complexity of the training data used, the network begins to adapt to the noise that always accompanies the actual useful data, in which case the network is said to overfit. In other words, the classifier learns the data as it is, not the solution to the problem contained in the data. Also in this case, it is difficult to say what would be the right size for the MLP classifier. One way is to monitor the error produced by the training and validation sets when teaching the network. If the error for the training set decreases and at the same time error for the validation set increases, it can be assumed that the network is too large or that too many iterations have been used in the training (Alpaydin 2014, 292).

Also, using the MNI average brain data (see Chapter 8.3) causes limitation. As already mentioned, the coil orientation with respect to the sulcus of the cortex affects recorded MEP amplitudes (Souza at al. 2022). It could be interesting and necessary to analyze this. However, due to the use of the MNI data these calculations could not have been done. Information from the real structure of the subject's cortex is needed, which could be obtained from MRI images.

In addition to the limitations already mentioned, it might have been good to conduct a familiarization session for each subject (Cuypers et al. 2014), where they would have been introduced to the TMS method for minimizing the effect of subjects' lack of habituation to TMS. This could have included e.g., running the two TMS sequences used in this study to two locations on the motor cortex. Now, this was not organized due to time constraints. This could affect, e.g., during the sequences, the EMG baseline variation and thus affect the number of acceptable MEPs.

Finally, the author's inexperience as a TMS operator almost certainly contributed to the results. The importance of different solutions became clearer as the work progressed. Such were, for example, the reliability of the hotspot hunting, the selection of the number of stimuli, attachment of sEMG electrodes, etc.

## 10.5 Future

As previously presented in Chapter 4.3, the motor cortex has begun to be mapped with the idea that different cortical locations do not represent only individual muscles, but synergistic functions, or spatiotemporal movement patterns, between different muscles, or gestures. However, methods are needed to connect the factors measured from voluntary movement to areas of the cortex. Such methods could be used not only for a more in-depth understanding of brain function, but also, for example, in surgery, when one wants to save certain functional areas in operations, or when building prosthesis controlled by the nervous system.

With the method presented in this work, the MEP patterns measured from the desired body part could possibly be connected to the locations of the motor cortex that induced them. If, in addition, it was possible to find a suitable similarity measure between the EMG signals measured from voluntary movement and the MEPs induced by TMS, the method used in this work could be used when one wants to predict areas of the motor cortex related to voluntary

movement. However, before this, the results obtained now should be verified by conducting a similar study with sufficient number of subjects and stimuli. This research represents the first experiment in which the aim is to calculate backwards the cortical location that induced the muscular activity based on the factors measured from the musculature. The cortical locations used now were clearly separated and thus the MEP patterns induced from them were presumably quite easily classified into the classes according to the selected cortical locations. In the future, one question to be solved will therefore be whether MEP patterns stimulated from locations of the motor cortex that are clearly closer to each other can be classified in a similar way. In this context, it would be also interesting to solve what is the minimum distance between the locations at which this can still be done, and what is the minimum muscle combination size giving the best classification result. It should be noted that the coil orientation affects MEP amplitudes (Chapter 4.2.4) thus being a possible factor influencing the classification accuracy and necessary issue to be studied in the future.

One interesting question to be solved could also be whether it is possible to find a certain stimulus intensity, possibly individual, with which the classification, like the one performed now, works the best. In other words, stimulus intensity at which MEP patterns are the most separable to the classes defined by cortical locations that produced them. That stimulus intensity could be assumed to be the intensity that produces location–specific MEP patterns that are as stable as possible while still maintaining location–specific specificity without induced electric field "leaking over" on the motor cortex.

# 11 CONCLUSION

In this thesis the feasibility of classifying TMS induced MEP patterns from multiple upper limb muscles according to cortical TMS locations was the main research question. In this context, the effect the recorded muscle combination's size on the classification accuracy was also investigated. This study also investigated whether it is possible to find a certain muscle combination that gives the highest classification accuracy, or which are the most informative muscles.

The MLP classifier and the achieved classification accuracy by it were used as a tool. The achieved classification accuracies were mostly good, which was to be expected due to the relatively easy classification problem since classes were chosen to be hotspot locations representing muscles from different segments of the upper limb. Thus, distances between these locations on the motor cortex were mainly quite large and rMT values varied enough to produce MEPs that presumably varied class wise at least in amplitude.

The muscle combinations that gave the highest classification accuracies for different subjects were very individual both in terms of their size and the muscles contained in them. On individual level, from one to three muscle combinations were found, with which the achieved classification accuracies were statistically significantly higher than the results given by other combinations. These results point out which are the individual muscle combinations producing the most separable MEP patterns for selected cortical TMS locations. Thus, the classification result when obtained by presented method is not a measure of similarity but difference. This was hypothesized to possibly indicate the individual versatility of neuromuscular control, although classification results cannot be connected to synergies between muscles same way as previous studies, e.g., Melgari et al. (2008) or Tardelli et al. (2022), have connected multi–muscle mapping results to the synergies. When evaluating the results, however, it is good to remember that the present study had limitations that make the analysis difficult and somewhat unreliable. The most significant limitations were related to the small number of test subjects and the number of stimuli given in the TMS sequences.

In the future, these results can be used as an aid in planning experimental setups when studying how different neuromuscular functions are possibly organized in the motor cortex. This kind of functional mapping of the cortex is currently one of the major directions in research.

## REFERENCES


Ahsan, R., Ibrahimy, M. I., Khalifa, O. O. (2011). Neural Network Classifier for Hand Motion Detection from EMG Signal. 5th Kuala Lumpur International Conference on Biomedical Engineering. IFMBE Proceedings 35. doi:10.1007/978-3-642-21729-6_135.

Alonso, A. M., Casado, D., López–Pintado, S., Romo, J. (2014). Robust Functional Supervised Classification for Time Series. Journal of Classification 31 (3), 325–350. doi:10.1007/s00357-014-9163-x.

Alpaydin, E. (2014). Introduction to Machine Learning (3rd ed.). MIT Press.

Awiszus, F. (2011). Fast estimation of transcranial magnetic stimulation motor threshold: is it safe?. Brain Stimulation 4 (1), 58–59. doi:10.1016/j.brs.2010.09.004.

Awiszus, F. (2012). On relative frequency estimation of transcranial magnetic stimulation motor threshold. Clinical Neurophysiology 123 (11), 2319–2320. doi:10.1016/j.clinph.2012.04.014.

Ballabio, D., Grisoni, F., Todeschini, R. (2018). Multivariate comparison of classification performance measures. Chemometrics and Intelligent Laboratory Systems 174, 33–44. doi:10.1016/j.chemolab.2017.12.004.

Barbero, M., Merletti, R., Rainoldi, A. (2012). Atlas of Muscle Innervation Zones: Understanding Surface Electromyography and Its applications. Springer Verlag.

Barker, A. T., Jalinous, R., Freeston, I. L. (1985). Non-invasive magnetic stimulation of human motor cortex. The Lancet 325 (8437), 1106–1107. doi:10.1016/S0140-6736(85)92413-4.

Battiti, R. (1992). First- and Second-Order Methods for Learning: Between Steepest Descent and Newton's Method. Neural Computation 4 (2), 141–166. doi:10.1162/neco.1992.4.2.141.

Benagiano, V., Rizzi, A., Lorusso, L., Flace, P., Saccia, M., Cagiano, R., Ribatti, D., Roncalli, L., Ambrosi, G. (2017). The functional anatomy of the cerebrocerebellar circuit: A review and new concepts. The Journal of Comparative Neurology 526 (5), 769–789. doi:10.1002/cne.24361.

Bonassi, G., Pelosin, E., Lagravinese, G., Bisio, A., Grasselli, G., Bove, M., Avanzino, L. (2021). Somatosensory inputs modulate the excitability of cerebellar-cortical interaction. Clinical Neurophysiology 132 (12), 3095–3103. doi:10.1016/j.clinph.2021.08.026.

Borich, M. R., Brodie, S. M., Gray, W. A., Ionta, S., Boyd, L. A. (2015). Understanding the role of the primary somatosensory cortex: Opportunities for rehabilitation. Neuropsychologia 79, 246–255. doi:10.1016/j.neuropsychologia.2015.07.007.

Brecht, M., Schneider, M., Sakmann, B., Margrie, T.W. (2004). Whisker movements evoked by stimulation of single pyramidal cells in rat motor cortex. Nature 427, 704–710. doi:10.1038/nature02266.

Brooks, J. X., Cullen, K. E. (2013). The Primate Cerebellum Selectively Encodes Unexpected Self-Motion. Current Biology 23 (11), 947–955. doi:10.1016/j.cub.2013.04.029.

Brown, M. B. & Forsythe, A. B. (1974). Robust tests for equality of variances. Journal of the American Statistical Association 69, 364–367. doi:10.1080/01621459.1974.10482955.

Burke, D., Hicks, R., Gandevia, S. C., Stephen, J., Woodforth, I., Crawford, M. (1993). Direct comparison of corticospinal volleys in human subjects to transcranial magnetic and electrical stimulation. Journal of Physiology 470, 383–393. doi:10.1113/jphysiol.1993.sp019864.

Carpenter, J. & Bithell, J. (2000). Bootstrap confidence intervals: when, which, what? A Practical guide for medical statisticians. Statistics in Medicine 19 (9), 1141–1164. doi:10.1002/(sici)1097-0258(20000515)19:9<1141::aid-sim479>3.0.co;2-f

Chao, C.–C., Karabanow, A. N., Paine, R., de Campos, A. C., Kukke, S. N., Wu, T., Wang, H., Hallett, M. (2015). Induction of Motor Associative Plasticity in the Posterior Parietal Cortex–Primary Motor Network. Cerebral Cortex 25 (2), 365–373. doi:10.1093/cercor/bht230.

Chan, F. H. Y., Yang, Y.–S., Lam, F. K., Zhang, Y.–T., Parker, P. A. (2000). Fuzzy EMG Classification for Prosthesis Control. IEEE Transactions on Rehabilitation Engineering 8 (3), 305–311. doi:10.1109/86.867872.

Cohen, L. G., Bandinelli, S., Topka, H. R., Fuhr, P., Roth, B., Hallett, M. (1991). Topographic Maps of Human Motor Cortex in Normal and Pathological Conditions: Mirror Movements, Amputations and Spinal Cord Injuries. Electroencephalography and Clinical Neurophysiology 43, 36–50.

Cohen, L. G., Bradley, J. R., Nilsson, J., Dang, N., Panizza, M., Bandinelli, S., Friauf, W., Hallett, M. (1990). Effects of coil design of local magnetic stimulation. Technical considerations. Electroencephalography and Clinical Neurophysiology 75 (4), 350–357. doi:10.1016/0013-4694(90)90113-X.

Corthout, E., Barker, A. T., Cowey, A. (2001). Transcranial magnetic stimulation – Which part of the current waveform causes the stimulation. Experimental Brain Research 141 (1), 128–132. doi:10.1007/s002210100860.

Coskun, M., Yildirim, O., Demir, Y., Acharya, U. R. (2021). Efficient deep neural network model for classification of grasp types using sEMG signals. Journal of Ambient Intelligence and Humanized Computing. doi:10.1007/s12652-021-03284-9.

Crandall, S. R., Cruikshank, S. J., Connors, B. W. (2015). A Corticothalamic Switch: Controlling the Thalamus with Dynamic Synapses. Neuron 86 (3), 768–782. doi:10.1016/j.neuron.2015.03.040.

Cuypers, K., Thijs, H., Meesen, R. L. J. (2014). Optimization of the Transcranial Magnetic Stimulation Protocol by Defining a Reliable Estimate for Corticospinal Excitability. Plos One 9 (1). doi:10.1371/journal.pone.0086380.

Darling, W. G., Wolf, S. L., Butler, A. J. (2006). Variability of motor potentials evoked by transcranial magnetic stimulation depends on muscle activation. Experimental Brain Research 174 (2), 376–385. doi:10.1007/s00221-006-0468-9.

Davey, N. J., Romaiguére, P., Maskill, D. W., Ellaway, P. H. (1994). Suppression of voluntary motor activity revealed using transcranial magnetic stimulation of the motor cortex in man. Journal of Physiology 477 (2), 223–235. doi:10.1113/jphysiol.1994.sp020186.

de Goede, A. A., ter Braack, E. M., van Putten, M. J. A. M. (2018). Accurate Coil Positioning is Important for Single and Paired Pulse TMS on the Subject Level. Brain Topography 31 (6), 917–930. doi:10.1007/s10548-018-0655-6.

Deng, Z.–D., Lisanby, S., Peterchev, A. V. (2014). Coil design considerations for deep transcranial magnetic stimulation. Clinical Neurophysiology 125 (6), 1202–1212. doi:10.1016/j.clinph.2013.11.038.

Dietrichs, E. (2008). Clinical manifestation of focal cerebellar disease as related to the organization of neural pathways. Acta Neurologica Scandinavica 188, 6–11. doi:10.1111/j.1600-0404.2008.01025.x.

Di Lazzaro, V., Oliviero, A., Pilato, F., Saturno, E., Dileone, M., Meglio, M., Cioni, B., Colosimo, C., Tonali, P. A., Roithwell, J. C. (2004). Direct recording of the output of the motor cortex produced by transcranial magnetic stimulation in a patient with cerebral cortex atrophy. Clinical Neurophysiology 115 (1), 112–115. doi:10.1016/S1388-2457(03)00320-1.

Di Lazzaro, V., Oliviero, A., Profice, P., Saturno, E., Pilato, F., Insola, A., Mazzone, P., Tonalli, P., Rothwell, J. C. (1998). Comparison of descending volleys evoked by transcranial

magnetic and electric stimulation in conscious humans. Electroencephalography and Clinical Neurophysiology 109, 397–401. doi:10.1016/S0924-980X(98)00038-1.

Du, Y.–C., Lin, C.–H., Shyu, L.–Y., Chen, T. (2010). Portable hand motion classifier for multi-channel surface electromyography recognition using grey relational analysis. Expert Systems with Applications 37 (6), 4283–4291. doi:10.1016/j.eswa.2009.11.072.

Dunn, O. J. (1964). Multiple Comparisons Using Rank Sums. Technometrics 6 (3), 241–252. doi:10.1080/00401706.1964.10490181.

Englehart, K., Hudgins, B., Parker, P. A., Stevenson, M. (1999). Classification of the myoelectric signal using time-frequency based representations. Medical Engineering & Physics 21 (6–7), 431–438. doi:10.1016/S1350-4533(99)00066-1.

Enoka, R. M. (2015). Neuromechanics of Human Movement (5th ed.). Human Kinetics.

Fregosi, M., Contestabile, A., Hamadjida, A., Rouiller, E. M. (2017). Corticobulbar projections from distinct motor cortical areas to the reticular formation in macaque monkeys. The European Journal of Neuroscience 45 (11), 1379–1395. doi:10.1111/ejn.13576.

Fricke, C., Gentner, R., Rumpf, J.–J., Weise, D., Saur, D., Classen, J. (2017). Differential spatial representation of precision and power grasps in the human motor system. NeuroImage 158, 58–69. doi:10.1016/J.NEUROIMAGE.2017.06.080.

Furui, A., Igaue, T., Tsuji, T. (2021). EMG pattern recognition via Bayesian inference with scale mixture-based stochastic generative models. Expert Systems with Applications 185. doi:10.48550/arXiv.2107.09853.

Gabriel, D. A. (2011). Effects of monopolar and bipolar electrode configurations on surface EMG spike analysis. Medical Engineering & Physics 33 (9), 1079–1085. doi:10.1016/j.medengphy.2011.04.016.

Graziano, M.S., Taylor, C.S., Moore, T. (2002). Complex movements evoked by microstimulation of precentral cortex. Neuron 34 (5), 841–851. doi:10.1016/s0896-6273(02)00698-0.

Graziano, M. S. A. (2016). Ethological Action Maps: A Paradigm Shift for the Motor Cortex. Trends in Cognitive Sciences 20 (2), 121–132. doi:10.1016/j.tics.2015.10.008.

Groppa, S., Oliviero, A., Eisen, A., Quartarone, A., Cohen, L. G., Mall, V., Kaelin–Lang, A., Mima, T., Rossi, S., Thickbroom, G. W., Rossini, P. M., Ziemann, U., Valls–Solé, J., Siebner, H. R. (2012†). A Practical guide to diagnostic transcranial magnetic stimulation: Report of an IFCN committee. Clinical Neurophysiology 123 (5), 858–882. doi:10.1016/j.clinph.2012.01.010.

Groppa, S., Schlaak, B. H., Münchau, A., Werner–Petroll, N., Dünnweber, J., Bäumer, T., van Nuenen, B. F. L., Siebner, H. R. (2012††). The Human Dorsal Premotor Cortex Facilitates the Excitability of Ipsilateral Primary Motor Cortex Via a Short Latency Cortico-Cortical Route. Human Brain Mapping 33 (2), 419–430. doi:10.1002/hbm.21221.

Gugino, L. D., Romero, J. R., Aglio, L., Titone, D., Ramirez, M., Pascual–Leone, A., Grimson, E., Weisenfeld, N., Kikinis, R., Shenton, M.–E. (2001). Transcranial magnetic stimulation coregistered with MRI: a comparison of a guided versus blind stimulation technique and its effect on evoked compound muscle action potentials. Clinical Neurophysiology 112 (10), 1781–1792. doi:10.1016/S1388-2457(01)00633-2.

Gustafsson, F. (1996). Determining the initial states in forward-backward filtering. IEEE Transactions on Signal Processing 44 (4), 988–992. doi:10.1109/78.492552.

Hallett, M. (2000). Transcranial magnetic stimulation and the human brain. Nature 406 (13), 147–150. doi:10.1038/35018000.

Hallett, M. (2007). Transcranial Magnetic Stimulation: A Primer. Neuron 55 (2), 187–199. doi:10.1016/j.neuron.2007.06.026.

Harrison, T.C., Ayling, O.G.S., Murphy, T.H. (2012). Distinct cortical circuit mechanisms for complex forelimb movement and motor map topography. Neuron 74 (2), 397–409. doi:10.1016/j.neuron.2012.02.028.

Heilmeyer, F. A. & Ball, T. (2019). neurone_loader: A Python module for loading EEG data recorded with Bittium NeurOne. The Journal of Open Source Software 4 (42), 1626. doi:10.21105/joss.01626.

Hornik, K., Stinchcombe, M. & H. White. 1989. Multilayer Feedforward Networks Are Universal Approximators. Neural Networks 2 (5), 359–366. doi:10.1016/0893-6080(89)90020-8.

Hudgins, B., Parker, P., Scott, R. N. (1993). A New Strategy for Multifunction Myoelectric Control. IEEE Transactions on Biomedical Engineering 40 (1), 82–94. doi:10.1109/10.204774.

Humphries, M. D., Stewart, R. D., Gurney, K. N. (2006). A Physiologically Plausible Model of Action Selection and Oscillatory Activity in the Basal Ganglia. The Journal of Neuroscience 26 (50), 12921–12942. doi:10.1523/jneurosci.3486-06.2006.

Julkunen, P., Säisänen, L., Danner, N., Niskanen, E., Hukkanen, T., Mervaala, E., Könönen, M. (2009). Comparison of navigated and non-navigated transcranial magnetic

stimulation for motor cortex mapping, motor threshold and motor evoked potentials. NeuroImage 44 (3), 790–795. doi:10.1016/j.neuroimage.2008.09.040.

Kallioniemi, E. & Julkunen, P. (2016). Alternative Stimulation Intensities for Mapping Cortical Motor Area with Navigated TMS. Brain Topography 29 (3), 395–404. doi:10.1007/s10548-016-0470-x.

Kam, K., Worrell, J. W., Janczewski, W. A., Cui, Y., Feldman, J. L. (2013). Distinct Inspiratory Rhythm and Pattern Generating Mechanisms in the preBötzinger Complex. The Journal of Neuroscience 33 (22), 9235–9245. doi:10.1523/JNEUROSCI.4143-12.2013.

Kamen, G. & Gabriel, D. A. (2010). Essentials of Electromyography. Human Kinetics.

Kammer, T., Beck, S., Thielscher, A., Laubis-Herrmann, U., Topka, H. (2001). Motor thresholds in humans: a transcranial magnetic stimulation study comparing different pulse waveforms, current directions and stimulator types. Clinical Neurophysiology 112 (2), 250–258. doi:10.1016/S1388-2457(00)00513-7.

Kandel, E. R., Koester, J. D., Mack, S. H., Siegelbaum, S. A. (2021). Principles of neural science (6th ed.). McGraw-Hill Companies.

Kertzman, C., Schwarz, U., Zeffiro, T. A., Hallett, M. (1997). The role of posterior parietal cortex in visually guided reaching movements in humans. Experimental Brain Research 114 (1), 170–183. doi:10.1007/pl00005617.

Kiers, L., Cros, D., Chiappa, K. H., Fang, J. (1993). Variability of motor potentials evoked by transcranial magnetic stimulation. Electroencephalography and clinical Neurophysiology 89 (6), 415–423. doi:10.1016/0168-5597(93)90115-6.

Kihara, M., Nishikawa, S., Nakasaka, Y., Tanaka, H., Takahashi, M. (2001). Autonomic consequences of brainstem infarction. Autonomic Neuroscience 86 (3), 202–207. doi:10.1016/S1566-0702(00)00238-1.

Kim, J., Kim, Y., Nakajima, R., Shin, A., Jeong, M., Park, A .H., Jeong, Y., Jo, S., Yang, S., Park, H., Cho, S.–H., Cho, K.–H., Shim, I., Chung, J. H., Paik, S.–B., Augustine, G. J., Kim, D. (2017). Inhibitory Basal Ganglia Inputs Induce Excitatory Motor Signals in the Thalamus. Neuron 95 (5), 1181–1196. doi:10.1016/j.neuron.2017.08.028.

Kocer, S. (2010). Classification of Emg Signals Using Neuro-Fuzzy System and Diagnosis of Neuromuscular Diseases. Journal of Medical Systems 34 (3), 321–329. doi:10.1007/s10916-008-9244-7.

Kolkman, K. E., McElvain, L. E., du Lac, S. (2011). Diverse Precerebellar Neurons Share Similar Intrinsic Excitability. The Journal of Neuroscience 31 (46), 16665–16674. doi:10.1523/JNEUROSCI.3314-11.2011.

Krause, P., Förderreuther, S., Straube, A. (2006). TMS motor cortical brain mapping in patients with complex regional pain syndrome type I. Clinical Neurophysiology 117 (1), 169–176. doi:10.1016/j.clinph.2005.09.012.

Kruskal, W. H. & Wallis, W. A. (1952). Use of ranks in one-criterion variance analysis. Journal of the American Statistical Association 47, 583–621. doi:10.1080/01621459.1952.10483441.

Laakso, I., Hirata, A., Ugawa, Y. (2014). Effects of coil orientation on the electric field induced by TMS over the hand motor area. Physics in Medicine and Biology 59 (1), 203–218. doi:10.1088/0031-9155/59/1/203.

Latchoumane, C.–F. V., Ngo, H.–V. V., Born, J., Shin, H.–S. (2017). Thalamic Spindles Promote Memory Formation during Sleep through Triple Phase-Locking of Cortical, Thalamic, and Hippocampal Rhythms. Neuron 95 (2), 424–435. doi:10.1016/j.neuron.2017.06.025.

Liu, D. C., & Nocedal, J. (1989). On the limited memory BFGS method for large scale optimization. Mathematical Programming 45 (1–3), 503–528. doi:10.1007/BF01589116.

Localite. (2014). Instruction Manual – TMS Navigator. SW-Version 3.0. Localite.

Lorey, B., Naumann, T., Pilgramm, S., Petermann, C., Bischoff, M., Zentgraf, K., Stark, R., Vaitl, D., Munzert, J. (2014). Neural Simulation of Actions: Effector– Versus Action–Specific Motor Maps Within the Human Premotor and Posterior Parietal Area?. Human Brain Mapping 35 (4), 1212–1225. doi:10.1002/hbm.22246.

Maccabee, P. J., Amassian, V. E., Eberle, L. P, Cracco, R. Q. (1993). Magnetic coil stimulation of straight and bent amphibian and mammalian peripheral nerve in vitro: locus of excitation. Journal of Physiology 460, 201–219. doi:10.1113/jphysiol.1993.sp019467.

Maccabee, P. J., Nagarajan, S. S., Amassian, V. E., Durand, D. M., Szabo, A. Z., Ahab, A. B., Cracco, R. Q., Lai, K. S., Eberle, L. P. (1998). Influence of pulse sequence, polarity and amplitude on magnetic stimulation of human and porcine peripheral nerve. Journal of Physiology 513 (2), 571–585. doi:10.1111%2Fj.1469-7793.1998.571bb.x.

Malcolm, M. P, Triggs, W. J., Light, K. E., Shechtman, O., Khandekar, G., Gonzales Rothi, L. J. (2006). Reliability of motor cortex transcranial magnetic stimulation in four muscle representations. Clinical Neurophysiology 117 (5), 1037–1046. doi:10.1016/j.clinph.2006.02.005.

Melgari, J.–M., Pasqualetti, P., Pauri, F., Rossini, P. M. (2008). Muscles in ‘‘Concert’’: Study of Primary Motor Cortex Upper Limb Functional Topography. PlosOne 3 (8). doi:10.1371/journal.pone.0003069.

Merton, P. A. & Morton, H. B. (1980). Stimulation of the cerebral cortex in the intact human subject. Nature 285 (22), 227. doi:10.1038/285227a0.

Mills, K. R. & Nithi, K. A. (1997). Corticomotor threshold to magnetic stimulation: normal values and repeatability. Muscle & Nerve 20 (5), 570–576. doi:10.1002/(SICI)1097-4598(199705)20:5<570::AID-MUS5>3.0.CO;2-6.

Mohr, M., Schön, T., von Tscharner, V., Nigg, B. M. (2018). Intermuscular Coherence Between Surface EMG Signals Is Higher for Monopolar Compared to Bipolar Electrode Configurations. Frontiers in Physiology 17. doi:10.3389/fphys.2018.00566.

Moreno–López, Y., Olivares–Moreno, R., Cordero–Erausquin, M., Rojas–Piloni, G. (2016). Sensorimotor Integration by Corticospinal System. Frontiers in Neuroanatomy 10. doi:10.3389/fnana.2016.00024.

Nakamura, H., Kitagawa, H., Kawaguchi, Y., Tsuji, H. (1997). Intracortical facilitation and inhibition after transcranial magnetic stimulation in conscious humans. Journal of Physiology 498 (3), 817–823. doi:10.1113/jphysiol.1997.sp021905.

Nazarova, M., Novikov, P., Ivanina, E., Kozlova, K., Dobrynina, L., Nikulin, V. V. (2021) Mapping of multiple muscles with transcranial magnetic stimulation: absolute and relative test-retest reliability. Human Brain Mapping 42 (8), 2508–2528. doi:10.1002/hbm.25383.

Ngomo, S., Leonard, G., Moffet. H., Mercier, C. (2012). Comparison of transcranial magnetic stimulation measures obtained at rest and under active conditions and their reliability. Journal of Neuroscience Methods 205 (1), 65–71. doi:10.1016/j.jneumeth.2011.12.012.

Oldfield, R. C. (1971). The assessment and analysis of handedness: The Edinburgh inventory. Neuropsychologia 9 (1), 97–113. doi:10.1016/0028-3932(71)90067-4.

Opitz, A., Legon, W., Rowlands, A., Bickel, W. K., Paulus, W., Tyler, W. J. (2013). Physiological observations validate finite element models for estimating subject–specific electric field distributions induced by transcranial magnetic stimulation of the human motor cortex. NeuroImage 81, 253–264. doi:10.1016/j.neuroimage.2013.04.067.

Park, S.–H., Lee, S.–P. (1998). EMG Pattern Recognition Based on Artificial Intelligence Techniques. IEEE Transactions on Rehabilitation Engineering 6 (4), 400–405. doi:10.1109/86.736154.

Petrov, P. I., Mandija, S., Sommer, I. E. C., van der Berg, C. A. T., Neggers, S. F. W. (2017). How much detail is needed in modeling a transcranial magnetic stimulation figure–8 coil: Measurements and brain simulations. PlosOne 12 (6). doi:10.1371/journal.pone.0178952.

Phinyomark, A., Phukpattaranont, P., Limsakul, C. (2012). Feature reduction and selection for EMG signal classification. Expert Systems with Applications 39 (8), 7420–7431. doi:10.1016/j.eswa.2012.01.102.

Phinyomark, A., Quaine, F., Charbonnier, S., Serviere, C., Tarpin–Bernard, F., Laurillau, Y. (2013). EMG feature evaluation for improving myoelectric pattern recognition robustness. Expert Systems with Applications 40 (12), 4832–4840. doi:10.1016/j.eswa.2013.02.023.

Phunruangsakao, C., Achanccaray, D., Izumi, S.–I. & Hayashibe M. (2022). Multibranch convolutional neural network with contrastive representation learning for decoding same limb motor imagery tasks. Frontiers in Human Neuroscience 16. doi:10.3389/fnhum.1032724.

Piccoli, M. B., Rainoldi, A., Heitz, C., Wüthrich, M., Boccia, G., Tomasoni, E., Spirolazzi, C., Egloff, M., Barbero, M. (2014). Innervation zone locations in 43 superficial muscles: Toward a standardization of electrode positioning. Muscle & Nerve 49 (3), 413–421. doi:10.1002/mus.23934.

Plowman–Prine, E. K., Triggs, W. J., Malcolm, M. P., Rosenbek, J. C. (2008). Reliability of transcranial magnetic stimulation for mapping swallowing musculature in the human motor cortex. Clinical Neurophysiology 119 (10), 2298–2303. doi:10.1016/j.clinph.2008.06.006.

Popa, L. S., Hewitt, A. L., Ebner, T. J. (2012). Predictive and Feedback Performance Errors Are Signaled in the Simple Spike Discharge of Individual Purkinje Cells. The Journal of Neuroscience 32 (44), 15345–15358. doi:10.1523/jneurosci.2151-12.2012.

Poppele, R. E., Rankin, A., Eian, J. (2003). Dorsal spinocerebellar tract neurons respond to contralateral limb stepping. Experimental Brain Research 149 (3), 361–370. doi:10.1007/s00221-003-1378-8.

Purves, D., Augustine, G. J., Fitzpatrick, D., Hall, W. C., LaMantia, A.–L., Platt, M. L., White, L. E. (2018). Neuroscience (6th ed.). Sinauer Associates.

Qi, F., Wu, A. D., Schweighofer, N. (2011). Fast estimation of transcranial magnetic stimulation motor threshold. Brain Stimulation 4 (1), 50–57. doi:10.1016/j.brs.2010.06.002.

Quallo, M. M., Kraskov, A., Lemon, R. N. (2012). The Activity of Primary Motor Cortex Corticospinal Neurons during Tool Use by Macaque Monkeys. The Journal of Neuroscience 32 (48), 17351–17364. doi:10.1523/JNEUROSCI.1009-12.2012.

Raffin, E. & Siebner, H. R. (2019). Use-Dependent Plasticity in Human Primary Motor Hand Area: Synergistic Interplay Between Training and Immobilization. Cerebral Cortex 29 (1), 356–371. doi:10.1093/cercor/bhy226.

Rajan, J. J. & Rayner, P. J. W. (1995). Unsupervised time series classification. Signal Processing 46 (1), 57–74. doi:10.1016/0165-1684(95)00072-L.

Rastogi, P., Lee, E. G., Hadimani, R. L., Jiles, D. C. (2019). Trasncranial Magnetic Stimulation: Development of a Novel Deep-Brain Triple-Halo Coil. IEEE Magnetic Letters 10. doi:10.1109/LMAG.2019.2903993.

Read the Docs. (2017). Gradient Descent – ML Glossary documentation. Referred 11.4.2023. https://ml-cheatsheet.readthedocs.io/en/latest/gradient_descent.html.

Redgrave, P., Prescott, T. J., Gurney, K. (1999). The basal ganglia: a vertebrate solution to the selection problem? Neuroscience 89 (4), 1009–1023. doi:10.1016/S0306-4522(98)00319-4.

Reijonen, J., Pitkänen, M., Kallioniemi, E., Mohammadi, A., Ilmoniemi, R., Julkunen, P. (2020†). Spatial extent of cortical motor hotspot in navigated transcranial magnetic stimulation. Journal of Neuroscience 346. doi:10.1016/j.jneumeth.2020.108893.

Reijonen, J., Säisänen, L., Könönen, M., Mohammadi, A., Julkunen, P. (2020††). The effect of coil placement and orientation on the assessment of focal excitability in motor mapping with navigated transcranial magnetic stimulation. Journal of Neuroscience Methods 331. doi:10.1016/j.jneumeth.2019.108521.

Ren, S., Wang, Y., Yue, F., Cheng, X., Dang, R., Qiao, Q., Sun, X., Li, X., Jiang, Q., Yao, J., Qin, H., Wang, G., Liao, X., Gao, D., Xia, J., Zhang, J., Hu, B., Yan, J., Wang, Y., Xu, M., Han, Y., Tang, X., Chen, X., He, C., Hu, Z. (2018). The paraventricular thalamus is a critical thalamic area for wakefulness. Science 362 (6413), 429–434. doi:10.1126/science.aat2512.

Rossi, S., Hallett, M., Rossini, P. M., Pascual–Leone, A., The Safety of TMS Consensus Group[3]. (2009). Safety, ethical considerations, and application guidelines for the use of

[3] Avanzini, G., Bestmann, S., Berardelli, A., Brewer, C., Canli, T., Cantello, R., Chen, R., Classen, J., Demitrack, M., Di Lazarro, V., Epstein, C. M, George, M. S., Fregni, F., Ilmoniemi, R., Jalinous, R., Karp, B., Lefaucheur, J.–P., Lisanby, S., Meunier, S., Miniussi, C., Miranda, P., Padberg, F., Paulus, W., Peterchev, A., Porteri, C., Provost, M., Quartarone, A., Rotenberg, A., Rothwell, J., Ruohonen, J., Siebner, H., Thut, G., Valls–Solé, J., Ugawa, Y., Zangen, A., Ziemann, U.

transcranial magnetic stimulation in clinical practice and research. Clinical Neurophysiology 120 (12), 2008–2039. doi:10.1016/j.clinph.2009.08.016.

Rossini, P. M., Burke, D., Chen, R., Cohen, L. G., Daskalakis, Z., Di Lorio, R., Di Lazzaro, V., Ferreri, F., Fitzgerald, P. B., George M. S., Hallett, M., Lefaucheur, J. P., Langguth, B., Matsumoto, H., Miniussi, C., Nitsche, M. A., Pascual-Leone, A., Paulus, W., Rossi, S., Rothwell, J. C., Siebner, H. R., Ugawa, Y., Walsh, V., Ziemann, U. (2015). Non–invasive electrical and magnetic stimulation of the brain, spinal cord, roots and peripheral nerves: Basic principles and procedures for routine clinical and research application. An updated report from an I.F.C.N. Committee. Clinical Neurophysiology 126 (6), 1071–1107. doi:10.1016/j.clinph.2015.02.001.

Roth, Y., Zangen, A., Hallett, M. (2002). A Coil Design for Transcranial Magnetic Stimulation of Deep Brain Regions. Journal of Clinical Neurophysiology 19 (4), 361–370. doi:10.1097/00004691-200208000-00008.

Rovó, Z., Ulbert, I., Acsády, L. (2012). Drivers of the Primate Thalamus. The Journal of Neuroscience 32 (49), 17894–17908. doi:10.1523/JNEUROSCI.2815-12.2012.

Rybak, I. A., Shetsova, N. A., Lafreniere–Roula, M., McCrea, A. (2006), Modelling spinal circuitry involved in locomotor pattern generation: insights from deletions during fictive locomotion. The Journal of Physiology 577 (1), 617–639. doi:10.1113/jphysiol.2006.118703.

Röricht, S., Meyer, B.–U., Niehaus, L., Brandt, S. A. (1999). Long–term reorganization of motor cortex outputs after arm amputation. Neurology 53 (1), 106–111. doi:10.1212/wnl.53.1.106.

Schmitt, L. I., Wimmer, R. D., Nakajima, M., Happ, M., Mofakham, S., Halassa, M. M. (2017). Thalamic amplification of cortical connectivity sustains attentional control. Nature 545 (7653), 219–242. doi:10.1038/nature22073.

Schober, P., Boer, C., Schwarte, L. A. (2018). Correlation Coefficients: Appropriate Use and Interpretation. Anesthesia & Analgesia 126 (5), 1763–1768. doi:10.1213/ane.0000000000002864.

Scott, S. H. (2016). A Functional Taxonomy of Bottom-Up Sensory Feedback Processing for Motor Actions. Trends in Neurosciences 39 (8), 512–526. doi:10.1016/j.tins.2016.06.001.

Sergio, L. E., Hamel–Pâquet, C., Kalaska, J. F. (2005). Motor Cortex Neural Correlates of Output Kinematics and Kinetics During Isometric-Force and Arm-Reaching Tasks. Journal of Neurophysiology 94 (4), 2353–2378. doi:10.1152/jn.00989.2004.

Shapiro, S. S., & Wilk, M. B. (1965). An analysis of variance test for normality (complete samples). Biometrika 52, 591–611. doi:10.1093/biomet/52.3-4.59.

Silbert, B. I., Patterson, H. I., Pevcic, D. D., Windnagel, K. A., Thickbroom, G. W. (2013). A comparison of relative-frequency and threshold–hunting methods to determine stimulus intensity in transcranial magnetic stimulation. Clinical Neurophysiology 124 (4), 708–712. doi:10.1016/j.clinph.2012.09.018.

Simão, M., Mendes, N., Gibaru, O., Neto, P. (2019). A Review on Electromyography Decoding and Pattern Recognition for Human–Machine Interaction. IEEE Access 7, 39564–39582. doi:10.1109/ACCESS.2019.2906584.

Singh, K. D., Hamdy, S., Aziz, Q., Thompson, D. G. (1997). Topographic mapping of trans-cranial magnetic stimulation data on surface rendered MR images of the brain. Electroencephalography and Clinical Neurophysiology 105 (5), 345–351. doi:10.1016/s0924-980x(97)96699-6.

Sommer, M., Ciocca, M., Chieffo, R., Hammond, P., Neef, A., Paulus, W., Rothwell, J. C., Hannah, R. (2018). TMS of primary motor cortex with a biphasic pulse activates two independent sets of excitable neurons. Brain Stimulation 11 (3), 558–565. doi:10.1016/j.brs.2018.01.001.

Souza, V. H., Nieminen, J. O., Tugin, S., Koponen, L. M., Baffa, O., Ilmoniemi, R. J. (2022). TMS with fast and accurate electronic control: Measuring the orientation sensitivity of corticomotor pathways. Brain Stimulation 15 (2), 306–315. doi:10.1016/j.brs.2022.01.009.

Spearman, C. (1904). The proof and measurement of association between two things. American Journal of Psychology 15 (1), 72–101. doi:10.2307/1412159.

Säisänen, L., Könönen, M., Niskanen, E., Lakka, T., Lintu, N., Vanninen, R., Julkunen, P., Määttä, S. (2021). Primary hand motor representation areas in healthy children, preadolescents, adolescents, and adults. NeuroImage 228. doi:10.1016/j.neuroimage.2020.117702.

Tardelli, G. P., Souza, V. H., Matsuda, R. H., Garcia, M. A. C., Novikor, P. A., Nazarova, M. A., Baffa, O. (2022). Forearm and Hand Muscles Exhibit Hight Coactivation and Overlapping of Cortical Motor Representations. Brain Topography. Online publication. doi:10.1007/s10548-022-00893-1.

Thut, G., Claude–Alain, H., Viviani, P., Morand, S., Spinelli, L., Blanke, O., Landis, T., Michel, C. (2000). Internally driven vs. externally cued movement selection: a study on the

timing of brain activity. Cognitive Brain Research 9 (3), 261–269. doi:10.1016/S0926-6410(00)00004-5.

Ueno, S. & Matsuda, T. (1992). Magnetic Stimulation of the Human Brain. Annals of the New York Academy of Sciences–Series 649, 366–368. doi: 10.1111/j.1749-6632.1992.tb49632.x.

Varela, C., Kumar, S., Yang, J. Y., Wilson, M. A. (2014). Anatomical substrates for direct interactions between hippocampus, medial prefrontal cortex, and the thalamic nucleus reuniens. Brain Structure & Function 219 (3), 911–929. doi: 10.1007/s00429-013-0543-5.

Wassermann, E. M. (1998). Risk and safety of repetitive transcranial magnetic stimulation: report and suggested guidelines from the International Workshop on the Safety of Repetitive Transcranial Magnetic Stimulation, June 5–7, 1996. Electroencephalography and clinical Neurophysiology 108, 1–16. doi:10.1016/s0168-5597(97)00096-8.

Wassermann, E. M. (2002) Variation in the response to transcranial magnetic brain stimulation in the general population. Clinical Neurophysiology 113 (7). 1165–1171. doi:10.1016/S1388-2457(02)00144-X.

Wassermann, E. M., McShane, L. M., Hallett, M., Cohen, L. G. (1992). Noninvasive mapping of muscle representations in human motor cortex. Electroencephalography and Clinical Neurophysiology 85 (1), 1–8. doi:10.1016/0168-5597(92)90094-R.

Weiss, C., Nettekoven, C., Rehme, A. K., Neuschmelting, V., Eisenbeis, A., Goldbrunner, R., Grefkes, C. (2013). Mapping the hand, foot and face representations in the primary motor cortex – Retest reliability of neuronavigated TMS versus functional MRI. NeuroImage 66, 531–542. doi:10.1016/j.neuroimage.2012.10.046.

Whitmire, C. J., Waiblinger, C., Schwarz, C., Stanley, G. B. (2016). Information Coding through Adaptive Gating of Synchronized Thalamic Bursting. Cell Reports 14 (4), 795–807. doi:10.1016/j.celrep.2015.12.068.

Xue, A., Kong, R., Yang, Q., Eldaief, M. C., Angeli, P. A., DiNicola, L. M., Braga, R. M., Buckner, R. L., Yeo, B. T. T. (2021). The detailed organization of the human cerebellum estimated by intrinsic functional connectivity within the individual. Journal of Neurophysiology 125 (2), 358–384. doi:10.1152/jn.00561.2020.

Zhao, D., Liu, C., Cui, M., Liu, J., Meng, F., Lian, H., Wang, D., Hu, F., Liu, D., Li, C. (2021). The paraventricular thalamus input to central amygdala controls depression-related behaviors. Experimental Neurology 342. doi:10.1016/j.expneurol.2021.113744.

Ziemann, U., Muellbacher, W., Hallett, M., Cohen, L. G. (2001). Modulation of practice-dependent plasticity in human motor cortex. Brain 124, 1171–1181. doi:10.1093/brain/124.6.1171.

APPENDIX 1: Results for 120% of rMT stimulus intensity **SUBJECT 1**

Results for statistical analysis were calculated using significance level $\alpha = 0.05$. Statistically significant results are indicated by **.

**Shapiro–Wilk normality test**

| | W | p-value |
|---|---|---|
| **C1** | 0.740 | < 0.001** |
| **C2** | 0.690 | < 0.001** |
| **C3** | 0.721 | < 0.001** |
| **C4** | 0.859 | < 0.001** |
| **C5** | 0.774 | < 0.001** |
| **C6** | 0.875 | < 0.001** |

C1–C6 denotes Combination 1 – Combination 6, respectively.

| **Levene (Brown–Forsythe variation) homogeneity** | **W** | **p-value** |
|---|---|---|
| | 8.860 | < 0.001** |

| **Kruskal-Wallis** | **Degrees of freedom** | **H** | **p-value** |
|---|---|---|---|
| | 5 | 82.404 | < 0.001** |

**Dunn's post–hoc test**

| | C1 | C2 | C3 | C4 | C5 | C6 |
|---|---|---|---|---|---|---|
| **C1** | 1 | 0.005** | < 0.001** | < 0.001** | < 0.001** | 0.592 |
| **C2** | | 1 | 0.272 | 0.272 | < 0.001** | < 0.001** |
| **C3** | | | 1 | 1 | 0.121 | 0.121 |
| **C4** | | | | 1 | 0.120 | 0.121 |
| **C5** | | | | | 1 | 1 |
| **C6** | | | | | | 1 |

C1–C6 denotes Combination 1 – Combination 6, respectively.

Pairwise comparisons using Dunn's test indicated for subject 1 that combination 1 accuracies were significantly different from those of combinations 2 ($p = 0.005$), 3 ($p < 0.001$), 4 ($p < 0.001$) and 5 ($p < 0.001$). Combination 2 accuracies were different from those of combinations 1 ($p = 0.005$), 5 ($p < 0.001$) and 6 ($p < 0.001$). Combination 3 and 4 accuracies were different only from those of combination 1 ($p < 0.001$). Combination 5 accuracies were different from those of combinations 1 ($p < 0.001$) and 2 ($p < 0.001$). Finally, combination 6 accuracies were different only from those of combination 2 ($p < 0.001$). No other differences were statistically significant.

**Estimated mean test accuracies, their confidence intervals (lower -, upper +) and standard deviations for each selected combination**

| | Mean test accuracy | Standard deviation | Confidence interval - | Confidence interval + |
|---|---|---|---|---|
| **C1** | 0.899 | $3.740 \times 10^{-5}$ | 0.899 | 0.899 |
| **C2** | 0.891 | $4.695 \times 10^{-5}$ | 0.891 | 0.891 |
| **C3** | 0.888 | $3.756 \times 10^{-5}$ | 0.888 | 0.888 |
| **C4** | 0.888 | $4.894 \times 10^{-5}$ | 0.888 | 0.888 |
| **C5** | 0.883 | $4.514 \times 10^{-5}$ | 0.883 | 0.883 |
| **C6** | 0.881 | $6.481 \times 10^{-5}$ | 0.881 | 0.881 |

C1–C6 denotes Combination 1 – Combination 6, respectively.

**Conclusions of statistical analysis for subject 1 and stimulus intensity 120% of rMT**

When the results of Dunn's post–hoc test and estimated means are combined, it can be noticed that even though the estimated mean values of the classification accuracy for combinations 1 and 6 clearly differ from each other, distributions for the combinations in question do not differ statistically significantly from each other. Distributions of all other combinations differ significantly from the distribution of the combination 1. Combination 2 differs statistically significantly from combinations 1, 5 and 6, but not from 3 and 4.

Results for statistical analysis were calculated using significance level $\alpha = 0.05$. Statistically significant results are indicated by **.

**Shapiro–Wilk normality test**

| | W | p-value |
|---|---|---|
| **C1** | 0.631 | < 0.001** |
| **C2** | 0.669 | < 0.001** |
| **C3** | 0.673 | < 0.001** |
| **C4** | 0.629 | < 0.001** |
| **C5** | 0.860 | < 0.001** |
| **C6** | 0.691 | < 0.001** |

C1–C6 denotes Combination 1 – Combination 6, respectively.

| **Levene (Brown–Forsythe variation) homogeneity** | **W** | **p-value** |
|---|---|---|
| | 8.433 | < 0.001** |

| **Kruskal-Wallis** | **Degrees of freedom** | **H** | **p-value** |
|---|---|---|---|
| | 5 | 181.262 | < 0.001** |

**Dunn's post–hoc test**

| | C1 | C2 | C3 | C4 | C5 | C6 |
|---|---|---|---|---|---|---|
| **C1** | 1 | 1 | 0.116 | < 0.001** | < 0.001** | < 0.001** |
| **C2** | | 1 | 0.268 | < 0.001** | < 0.001** | < 0.001** |
| **C3** | | | 1 | < 0.001** | < 0.001** | < 0.001** |
| **C4** | | | | 1 | 1 | < 0.001** |
| **C5** | | | | | 1 | 0.002** |
| **C6** | | | | | | 1 |

C1–C6 denotes Combination 1 – Combination 6, respectively.

Pairwise comparisons using Dunn's test indicated for subject 2 that combination 1, 2 and 3 accuracies were significantly different from those of combinations 4 ($p < 0.001$), 5 ($p < 0.001$) and 6 ($p < 0.001$). Combination 4 accuracies were different from those of combinations 1 ($p < 0.001$), 2 ($p < 0.001$), 3 ($p < 0.001$) and 6 ($p < 0.001$). Combination 5 accuracies were different from those of combinations 1 ($p < 0.001$), 2 ($p < 0.001$), 3 ($p < 0.001$) and 6 ($p = 0.002$). Finally, combination 6 accuracies were different from those of combination 1 ($p < 0.001$), 2 ($p < 0.001$), 3 ($p < 0.001$), 4 ($p < 0.001$) and 5 ($p = 0.002$). No other differences were statistically significant.

**Estimated mean test accuracies, their confidence intervals (lower -, upper +) and standard deviations for each selected combination**

| | Mean test accuracy | Standard deviation | Confidence interval - | Confidence interval + |
|---|---|---|---|---|
| **C1** | 0.973 | $3.168 \times 10^{-5}$ | 0.973 | 0.973 |
| **C2** | 0.972 | $3.598 \times 10^{-5}$ | 0.972 | 0.972 |
| **C3** | 0.969 | $3.367 \times 10^{-5}$ | 0.969 | 0.969 |
| **C4** | 0.961 | $2.958 \times 10^{-5}$ | 0.961 | 0.961 |
| **C5** | 0.958 | $5.550 \times 10^{-5}$ | 0.958 | 0.958 |
| **C6** | 0.952 | $3.237 \times 10^{-5}$ | 0.952 | 0.952 |

C1–C6 denotes Combination 1 – Combination 6, respectively.

**Conclusions of statistical analysis for subject 2 and stimulus intensity 120% of rMT**

When the results of Dunn's post–hoc test and estimated means are combined, it can be noticed that estimated mean values of the classification accuracy for combinations 1, 2 and 3 are close to each other and distributions of their accuracies do not differ statistically significantly from each other but differ from all other combinations' accuracy distributions.

Results for statistical analysis were calculated using significance level $\alpha = 0.05$. Statistically significant results are indicated by **.

**Shapiro–Wilk normality test**

| | W | p-value |
|---|---|---|
| **C1** | 0.945 | < 0.001** |
| **C2** | 0.931 | < 0.001** |
| **C3** | 0.886 | < 0.001** |
| **C4** | 0.887 | < 0.001** |
| **C5** | 0.935 | < 0.001** |
| **C6** | 0.948 | < 0.001** |

C1–C6 denotes Combination 1 – Combination 6, respectively.

| **Levene (Brown–Forsythe variation) homogeneity** | **W** | **p-value (small-False)** |
|---|---|---|
| | 2.886 | 0.014** |

| **Kruskal-Wallis** | **Degrees of freedom** | **H** | **p-value** |
|---|---|---|---|
| | 5 | 139.669 | < 0.001** |

**Dunn's post–hoc test**

| | C1 | C2 | C3 | C4 | C5 | C6 |
|---|---|---|---|---|---|---|
| **C1** | 1 | 0.034** | < 0.001** | < 0.001** | < 0.001** | < 0.001** |
| **C2** | | 1 | 0.011** | < 0.001** | < 0.001** | < 0.001** |
| **C3** | | | 1 | 0.052 | 0.017** | < 0.001** |
| **C4** | | | | 1 | 1 | 1 |
| **C5** | | | | | 1 | 1 |
| **C6** | | | | | | 1 |

C1–C6 denotes Combination 1 – Combination 6, respectively.

Pairwise comparisons using Dunn's test indicated for subject 3 that combination 1 accuracies were significantly different from those of all other combinations 2 ($p = 0.034$), 3 ($p < 0.001$), 4 ($p < 0.001$), 5 ($p < 0.001$) and 6 ($p < 0.001$). Combination 2 accuracies were also significantly different from those of all other combinations 1 ($p = 0.034$), 3 ($p = 0.011$), 4 ($p < 0.001$), 5 ($p < 0.001$) and 6 ($p < 0.001$). Combination 3 accuracies were significantly different from those of combinations 1 ($p < 0.001$), 2 ($p = 0.011$), 5 ($p = 0.017$) and 6 ($p < 0.001$). Combination 4 accuracies were significantly different from those of combinations 1 ($p < 0.001$) and 2 ($p < 0.001$). Combination 5 accuracies were significantly different from those of combinations 1 ($p < 0.001$), 2 ($p < 0.001$) and 3 ($p = 0.017$). Combination 6 accuracies were significantly different from those of combinations 1 ($p < 0.001$), 2 ($p < 0.001$) and 3 ($p < 0.001$). No other differences were statistically significant.

**Estimated mean test accuracies, their confidence intervals (lower -, upper +) and standard deviations for each selected combination**

| | Mean test accuracy | Standard deviation | Confidence interval - | Confidence interval + |
|---|---|---|---|---|
| **C1** | 0.657 | $9.745 \times 10^{-5}$ | 0.657 | 0.657 |
| **C2** | 0.644 | $7.100 \times 10^{-5}$ | 0.644 | 0.644 |
| **C3** | 0.630 | $8.738 \times 10^{-5}$ | 0.630 | 0.630 |
| **C4** | 0.623 | $5.813 \times 10^{-5}$ | 0.623 | 0.623 |
| **C5** | 0.620 | $7.398 \times 10^{-5}$ | 0.620 | 0.620 |
| **C6** | 0.620 | $8.172 \times 10^{-5}$ | 0.619 | 0.620 |

C1–C6 denotes Combination 1 – Combination 6, respectively.

**Conclusions of statistical analysis for subject 3 and stimulus intensity 120% of rMT**

When the results of Dunn's post–hoc test and estimated means are combined, it can be noticed that estimated mean value of the classification accuracy for combination 1 differs quite clearly from others and distribution of accuracy for combination 1 is statistically significantly different from all others.

Results for statistical analysis were calculated using significance level $\alpha = 0.05$. Statistically significant results are indicated by **.

**Shapiro–Wilk normality test**

| | W | p-value |
|---|---|---|
| **C1** | 0.200 | < 0.001** |
| **C2** | 0.624 | < 0.001** |
| **C3** | 0.575 | < 0.001** |
| **C4** | 0.718 | < 0.001** |
| **C5** | 0.656 | < 0.001** |
| **C6** | 0.556 | < 0.001** |

C1–C6 denotes Combination 1 – Combination 6, respectively.

| **Levene (Brown–Forsythe variation) homogeneity** | **W** | **p-value (small-False)** |
|---|---|---|
| | 7.583 | < 0.001** |

| **Kruskal-Wallis** | **Degrees of freedom** | **H** | **p-value** |
|---|---|---|---|
| | 5 | 366.206 | < 0.001** |

**Dunn's post–hoc test**

| | C1 | C2 | C3 | C4 | C5 | C6 |
|---|---|---|---|---|---|---|
| **C1** | 1 | < 0.001** | < 0.001** | < 0.001** | < 0.001** | < 0.001** |
| **C2** | | 1 | < 0.001** | < 0.001** | < 0.001** | < 0.001** |
| **C3** | | | 1 | 0.311 | < 0.001** | < 0.001** |
| **C4** | | | | 1 | 0.002** | < 0.001** |
| **C5** | | | | | 1 | 0.311 |
| **C6** | | | | | | 1 |

C1–C6 denotes Combination 1 – Combination 6, respectively.

Pairwise comparisons using Dunn's test indicated for subject 4 that combination 1 accuracies were significantly different from those of all other combinations 2 ($p = 0.034$), 3 ($p < 0.001$), 4 ($p < 0.001$), 5 ($p < 0.001$) and 6 ($p < 0.001$). Combination 2 accuracies were also significantly different from those of all other combinations 1 ($p < 0.001$), 3 ($p < 0.001$), 4 ($p < 0.001$), 5 ($p < 0.001$) and 6 ($p < 0.001$). Combination 3 accuracies were significantly different from those of combinations 1 ($p < 0.001$), 2 ($p < 0.001$), 5 ($p < 0.001$) and 6 ($p < 0.001$). Combination 4 accuracies were significantly different from those of combinations 1 ($p < 0.001$), 2 ($p < 0.001$), 5 ($p = 0.002$) and 6 ($p < 0.001$). Combination 5 accuracies were significantly different from those of combinations 1 ($p < 0.001$), 2 ($p < 0.001$), 3 ($p < 0.001$) and 4 ($p = 0.002$). Combination 6 accuracies were significantly different from those of combinations 1 ($p < 0.001$), 2 ($p < 0.001$), 3 ($p < 0.001$) and 4 ($p < 0.001$). No other differences were statistically significant.

**Estimated mean test accuracies, their confidence intervals (lower -, upper +) and standard deviations for each selected combination**

| | Mean test accuracy | Standard deviation | Confidence interval - | Confidence interval + |
|---|---|---|---|---|
| **C1** | 0.998 | $2.801 \times 10^{-5}$ | 0.998 | 0.998 |
| **C2** | 0.988 | $4.242 \times 10^{-5}$ | 0.988 | 0.988 |
| **C3** | 0.975 | $4.620 \times 10^{-5}$ | 0.975 | 0.975 |
| **C4** | 0.973 | $3.482 \times 10^{-5}$ | 0.973 | 0.973 |
| **C5** | 0.966 | $3.156 \times 10^{-5}$ | 0.966 | 0.966 |
| **C6** | 0.963 | $2.574 \times 10^{-5}$ | 0.963 | 0.963 |

C1–C6 denotes Combination 1 – Combination 6, respectively.

**Conclusions of statistical analysis for subject 4 and stimulus intensity 120% of rMT**

When the results of Dunn's post–hoc test and estimated means are combined, it can be noticed that estimated mean value of the classification accuracy for combination 1 differs quite clearly from others and distribution of accuracy for combination 1 is statistically significantly different from all others.

Results for statistical analysis were calculated using significance level $\alpha = 0.05$. Statistically significant results are indicated by **.

**Shapiro–Wilk normality test**

| | W | p-value |
|---|---|---|
| **C1** | 0.593 | < 0.001** |
| **C2** | 0.123 | < 0.001** |
| **C3** | 0.870 | < 0.001** |
| **C4** | 0.500 | < 0.001** |
| **C5** | 0.667 | < 0.001** |
| **C6** | 0.605 | < 0.001** |

C1–C6 denotes Combination 1 – Combination 6, respectively.

| **Levene (Brown–Forsythe variation) homogeneity** | **W** | **p-value** |
|---|---|---|
| | 16.309 | < 0.001** |

| **Kruskal-Wallis** | **Degrees of freedom** | **H** | **p-value** |
|---|---|---|---|
| | 5 | 272.683 | < 0.001** |

**Dunn's post–hoc test**

| | C1 | C2 | C3 | C4 | C5 | C6 |
|---|---|---|---|---|---|---|
| **C1** | 1 | 0.011** | < 0.001** | < 0.001** | < 0.001** | < 0.001** |
| **C2** | | 1 | 0.011** | 0.029** | < 0.001** | < 0.001** |
| **C3** | | | 1 | 1 | < 0.001** | < 0.001** |
| **C4** | | | | 1 | < 0.001** | < 0.001** |
| **C5** | | | | | 1 | 1 |
| **C6** | | | | | | 1 |

C1–C6 denotes Combination 1 – Combination 6, respectively.

Pairwise comparisons using Dunn's test indicated for subject 5 that combination 1 accuracies were significantly different from those of all other combinations 2 ($p = 0.011$), 3 ($p < 0.001$), 4 ($p < 0.001$), 5 ($p < 0.001$) and 6 ($p < 0.001$). Combination 2 accuracies were also significantly different from those of all other combinations 1 ($p = 0.011$), 3 ($p = 0.011$), 4 ($p = 0.029$), 5 ($p < 0.001$) and 6 ($p < 0.001$). Combination 3 accuracies were significantly different from those of combinations 1 ($p < 0.001$), 2 ($p = 0.011$), 5 ($p < 0.001$) and 6 ($p < 0.001$). Combination 4 accuracies were significantly different from those of combinations 1 ($p < 0.001$), 2 ($p = 0.029$), 5 ($p < 0.001$) and 6 ($p < 0.001$). Combination 5 accuracies were significantly different from those of combinations 1 ($p < 0.001$), 2 ($p < 0.001$), 3 ($p < 0.001$) and 4 ($p = 0.002$). Combination 6 accuracies were significantly different from those of combinations 1 ($p < 0.001$), 2 ($p < 0.001$), 3 ($p < 0.001$) and 4 ($p < 0.001$). No other differences were statistically significant.

**Estimated mean test accuracies, their confidence intervals (lower -, upper +) and standard deviations for each selected combination**

| | Mean test accuracy | Standard deviation | Confidence interval - | Confidence interval + |
|---|---|---|---|---|
| **C1** | 0.987 | $2.907 \times 10^{-5}$ | 0.986 | 0.987 |
| **C2** | 0.980 | $8.879 \times 10^{-5}$ | 0.980 | 0.980 |
| **C3** | 0.974 | $5.987 \times 10^{-5}$ | 0.973 | 0.974 |
| **C4** | 0.973 | $4.753 \times 10^{-5}$ | 0.973 | 0.974 |
| **C5** | 0.962 | $3.205 \times 10^{-5}$ | 0.962 | 0.962 |
| **C6** | 0.961 | $2.962 \times 10^{-5}$ | 0.961 | 0.961 |

C1–C6 denotes Combination 1 – Combination 6, respectively.

**Conclusions of statistical analysis for subject 5 and stimulus intensity 120% of rMT**

When the results of Dunn's post–hoc test and estimated means are combined, it can be noticed that estimated mean value of the classification accuracy for combination 1 differs from others and distribution of accuracy for combination 1 is statistically significantly different from all others.

Results for statistical analysis were calculated using significance level $\alpha = 0.05$. Statistically significant results are indicated by **.

**Shapiro–Wilk normality test**

| | W | p-value |
|---|---|---|
| **C1** | 0.761 | < 0.001** |
| **C2** | 0.874 | < 0.001** |
| **C3** | 0.928 | < 0.001** |
| **C4** | 0.891 | < 0.001** |
| **C5** | 0.881 | < 0.001** |
| **C6** | 0.926 | < 0.001** |

C1–C6 denotes Combination 1 – Combination 6, respectively.

| **Levene (Brown–Forsythe variation) homogeneity** | **W** | **p-value** |
|---|---|---|
| | 8.045 | < 0.001** |

| **Kruskal-Wallis** | **Degrees of freedom** | **H** | **p-value** |
|---|---|---|---|
| | 5 | 181.170 | < 0.001** |

**Dunn's post–hoc test**

| | C1 | C2 | C3 | C4 | C5 | C6 |
|---|---|---|---|---|---|---|
| **C1** | 1 | 0.769 | 0.054 | < 0.001** | < 0.001** | < 0.001** |
| **C2** | | 1 | 0.114 | < 0.001** | < 0.001** | < 0.001** |
| **C3** | | | 1 | < 0.001** | < 0.001** | < 0.001** |
| **C4** | | | | 1 | 0.114 | 0.019** |
| **C5** | | | | | 1 | 0.769 |
| **C6** | | | | | | 1 |

C1–C6 denotes Combination 1 – Combination 6, respectively.

Pairwise comparisons using Dunn's test indicated for subject 6 that combination 1 accuracies were significantly different from those of combinations 4 ($p < 0.001$), 5 ($p < 0.001$) and 6 ($p < 0.001$). Combination 2 accuracies were significantly different from those of combinations 4 ($p < 0.001$), 5 ($p < 0.001$) and 6 ($p < 0.001$). Combination 3 accuracies were significantly different from those of combinations 4 ($p < 0.001$), 5 ($p < 0.001$) and 6 ($p < 0.001$). Combination 4 accuracies were significantly different from those of combinations 1 ($p < 0.001$), 2 ($p < 0.001$), 3 ($p < 0.001$) and 6 ($p = 0.019$). Combination 5 accuracies were significantly different from those of combinations 1 ($p < 0.001$), 2 ($p < 0.001$) and 3 ($p < 0.001$). Combination 6 accuracies were significantly different from those of combinations 1 ($p < 0.001$), 2 ($p < 0.001$), 3 ($p < 0.001$) and 4 ($p = 0.019$). No other differences were statistically significant.

**Estimated mean test accuracies, their confidence intervals (lower -, upper +) and standard deviations for each selected combination**

| | Mean test accuracy | Standard deviation | Confidence interval - | Confidence interval + |
|---|---|---|---|---|
| **C1** | 0.910 | $4.043 \times 10^{-5}$ | 0.910 | 0.910 |
| **C2** | 0.909 | $6.126 \times 10^{-5}$ | 0.909 | 0.910 |
| **C3** | 0.903 | $7.845 \times 10^{-5}$ | 0.902 | 0.903 |
| **C4** | 0.888 | $6.356 \times 10^{-5}$ | 0.888 | 0.888 |
| **C5** | 0.881 | $5.646 \times 10^{-5}$ | 0.881 | 0.882 |
| **C6** | 0.876 | $8.103 \times 10^{-5}$ | 0.876 | 0.876 |

C1–C6 denotes Combination 1 – Combination 6, respectively.

**Conclusions of statistical analysis for subject 6 and stimulus intensity 120% of rMT**

When the results of Dunn's post–hoc test and estimated means are combined, it can be noticed that estimated mean values of the classification accuracy for combinations 1, 2 and 3 are quite close to each other and their distributions of accuracy do not differ from each other statistically significantly. However, distributions of accuracy of all of them differ from all others, i.e., combinations 4, 5 and 6, statistically significantly.

Results for statistical analysis were calculated using significance level $\alpha = 0.05$. Statistically significant results are indicated by **.

**Shapiro–Wilk normality test**

| | W | p-value |
|---|---|---|
| **C1** | 0.905 | < 0.001** |
| **C2** | 0.792 | < 0.001** |
| **C3** | 0.792 | < 0.001** |
| **C4** | 0.888 | < 0.001** |
| **C5** | 0.896 | < 0.001** |
| **C6** | 0.854 | < 0.001** |

C1–C6 denotes Combination 1 – Combination 6, respectively.

| **Levene (Brown–Forsythe variation) homogeneity** | **W** | **p-value** |
|---|---|---|
| | 12.120 | < 0.001** |

| **Kruskal-Wallis** | **Degrees of freedom** | **H** | **p-value** |
|---|---|---|---|
| | 5 | 127.657 | < 0.001** |

**Dunn's post–hoc test**

| | C1 | C2 | C3 | C4 | C5 | C6 |
|---|---|---|---|---|---|---|
| **C1** | 1 | < 0.001** | < 0.001** | < 0.001** | < 0.001** | < 0.001** |
| **C2** | | 1 | 0.979 | 0.944 | 0.979 | 0.039** |
| **C3** | | | 1 | 1 | 1 | 0.914 |
| **C4** | | | | 1 | 1 | 0.979 |
| **C5** | | | | | 1 | 0.908 |
| **C6** | | | | | | 1 |

C1–C6 denotes Combination 1 – Combination 6, respectively.

Pairwise comparisons using Dunn's test indicated for subject 7 that combination 1 accuracies were significantly different from those of all other combinations 2 ($p < 0.001$), 3 ($p < 0.001$), 4 ($p < 0.001$), 5 ($p < 0.001$) and 6 ($p < 0.001$). Combination 2 accuracies were significantly different from those of combinations 1 ($p < 0.001$) and 6 ($p = 0.039$). Combination 3 accuracies were significantly different from those of combination 1 ($p < 0.001$). Combination 4 accuracies were significantly different from those of combination 1 ($p < 0.001$). Combination 5 accuracies were significantly different from those of combination 1 ($p < 0.001$). Combination 6 accuracies were significantly different from those of combinations 1 ($p < 0.001$) and 2 ($p < 0.039$). No other differences were statistically significant.

**Estimated mean test accuracies, their confidence intervals (lower -, upper +) and standard deviations for each selected combination**

| | Mean test accuracy | Standard deviation | Confidence interval - | Confidence interval + |
|---|---|---|---|---|
| **C1** | 0.868 | $7.003 \times 10^{-5}$ | 0.868 | 0.868 |
| **C2** | 0.843 | $4.322 \times 10^{-5}$ | 0.843 | 0.843 |
| **C3** | 0.840 | $4.843 \times 10^{-5}$ | 0.840 | 0.840 |
| **C4** | 0.840 | $5.675 \times 10^{-5}$ | 0.839 | 0.840 |
| **C5** | 0.837 | $9.030 \times 10^{-5}$ | 0.837 | 0.837 |
| **C6** | 0.836 | $6.111 \times 10^{-5}$ | 0.835 | 0.836 |

C1–C6 denotes Combination 1 – Combination 6, respectively.

**Conclusions of statistical analysis for subject 7 and stimulus intensity 120% of rMT**

When the results of Dunn's post–hoc test and estimated means are combined, it can be noticed that estimated mean values of the classification accuracy for combination 1 differ quite clearly from all others and distribution of accuracy for combination 1 differs from all other distributions statistically significantly. Distributions for other combinations do not differ from each other statistically significantly, except distributions of combinations 2 and 6.